PB192333

DEVELOPMENT OF MARK I RADIOMETRIC THERMASONDE ™ AND SIMULATION AND EXPERIMENTAL STUDIES FOR PASSIVELY PROBING TEMPERATURE STRUCTURE WITHIN THE FIRST MILE OF THE ATMOSPHERE

by

W. D. Mount, A. C. Anway,
C. V. Wick, and C. M. Maloy

Sperry Rand Research Center
Sudbury, Massachusetts

and

R. Wilt

Sperry Microwave Electronics Division
Clearwater, Florida

FINAL REPORT
Contract No. PH22–68–22

Period Covered: 1968 April 1 to 1969 September 21

Project Officer: C. R. Hosler

Prepared for

METEOROLOGY DIVISION
NATIONAL AIR POLLUTION CONTROL ADMINISTRATION
RALEIGH, NORTH CAROLINA 27609

Reproduced by the
CLEARINGHOUSE
for Federal Scientific & Technical
Information Springfield Va. 22151

SPERRY RAND RESEARCH CENTER
SUDBURY, MASSACHUSETTS 01776

SRRC–CR–70–6

DEVELOPMENT OF MARK I RADIOMETRIC THERMASONDE ™ AND SIMULATION AND EXPERIMENTAL STUDIES FOR PASSIVELY PROBING TEMPERATURE STRUCTURE WITHIN THE FIRST MILE OF THE ATMOSPHERE

by

W. D. Mount, A. C. Anway,
C. V. Wick, and C. M. Maloy

Sperry Rand Research Center
Sudbury, Massachusetts

and

R. Wilt

Sperry Microwave Electronics Division
Clearwater, Florida

FINAL REPORT
Contract No. PH22–68–22

Period Covered: 1968 April 1 to 1969 September 21

Project Officer: C. R. Hosler

Prepared for

METEOROLOGY DIVISION
NATIONAL AIR POLLUTION CONTROL ADMINISTRATION
RALEIGH, NORTH CAROLINA 27609

ABSTRACT

Background material on theoretical and practical aspects of the use of millimeter wave radiometric equipment for remote probing is presented. Specifications for development of the Mark I Radiometric THERMASONDE™ are listed and performance characteristics are described. The paper, "Use of Millimeter Wave Radiometry to Remotely Measure Atmospheric Stability," presented at the Symposium on Advances in Instrumentation for Air Pollution Control, which describes work accomplished under this contract is given as Appendix I of this report. Simulated and experimental radiometric results are presented and discussed for climatological and equipment effects in the observing of lapse, ground-based, and elevated inversions. A nonlinear nomogram was developed to correct for radiometric smoothing of intensity and height of ground-based inversions. Different observing modes and signal processing techniques appear to assist in the interpretation of radiometric soundings for use in detecting elevated inversions.

TABLE OF CONTENTS

Section		Page
1	INTRODUCTION	1
2	MARK I RADIOMETRIC THERMASONDE™	3
	References	25
3	DISCUSSIONS OF COMPUTER SIMULATION AND EXPERIMENTAL RESULTS	26
4	CONCLUSIONS	66
	Appendix I - Use of Millimeter Wave Radiometry to Remotely Measure Atmospheric Stability	I-1
	Appendix II - Development of Applicable Height Concept	II-1

TABLE OF CONTENTS

Section		Page
1	INTRODUCTION	1
2	MARK I RADIOMETRIC THERMASONDE™	3
	References	25
3	DISCUSSIONS OF COMPUTER SIMULATION AND EXPERIMENTAL RESULTS	26
4	CONCLUSIONS	66
	Appendix I - Use of Millimeter Wave Radiometry to Remotely Measure Atmospheric Stability	I-1
	Appendix II - Development of Applicable Height Concept	II-1

LIST OF ILLUSTRATIONS

Figure	Description	Page
1	Diagram of a null balancing Dicke Radiometer, front end	10
2	Three-terminal coupling device	13
3	Block diagram of a null balance Dicke-type radiometer	16
4	Radiometric THERMASONDE™, Mark I, rear view	17
5	Radiometric THERMASONDE™, Mark I, front view	18
6	Operating controls of the Radiometric THERMASONDE™, Mark I	19
7	Applicable heights and radiometric temperatures versus elevation angle at Cincinnati, winter season, for frequencies of 54, 54.5, and 55 GHz	27
8	Pressure altitude effect on applicable height versus elevation angle between Cincinnati and Salt Lake City in the winter season	30
9	Seasonal effects on applicable height versus elevation angle for Salt Lake City	32
10	Synoptic pressure effects on applicable height versus elevation angle in the autumn season for Clearwater, Florida	33
11	Comparison of actual temperature profiles and computer simulated radiometric profiles for a lapse and ground-based inversion	35
12	Comparison of actual temperature profiles and computed radiometric profiles for a low strong and high weak ground-based inversion	37
13	Comparison of actual temperature profiles and computed radiometric profiles for ground-based inversions with the same heights but different intensities	38
14	Nomogram for translating null balance radiometric data at 54.5 GHz to obtain height and intensity of ground-based inversions. This relationship was derived for a station pressure of 1000 mb	41

LIST OF ILLUSTRATIONS - Cont'd

Figure	Description	Page
15	Comparison of actual temperature profiles and computer simulated radiometric profiles for elevated inversions	42
16	Comparison of calculated brightness temperatures versus frequency and corresponding applicable heights for a lapse, ground inversion and two elevated inversion temperature profiles	44
17	Results of a computational simulation of the effects of different angle scan rates on the radiometric record of a lapse profile	47
18	Comparison of a series of upward angle scans, Sudbury, Massachusetts, 1969 August 26, where three successive scans are made at a fixed rate (4°/min) and one each at a different rate (1.8, 3.8, and 8.2°/min)	49
19	Computer simulation of the effects of angle scanning on the radiometric record during a ground inversion	50
20	Simulation of the effects of different frequencies and angle scan rates on the radiometric record of a ground inversion	52
21	Experimentally observed effects of angle scan rate on ground inversions	53
22	Computer simulated up-down angle scans of a lapse profile	56
23	Computer simulated up-down angle scans of two elevated inversion profiles	57
24	Comparison of observed down-up radiometric scans with on-site and USWB RAOB data and helicopter data, Salt Lake City, 1500 MST, 1968 November 19. The curves with arrows indicate the direction of the angle scan at 4°/min and radiometric temperature output. The line connected by circles is the helicopter sounding. The solid line and dash-dot line are the on-site and Weather Bureau RAOB	59
25	Comparison of observed up-down radiometric scans with on-site and USWB RAOB data and helicopter data, Salt Lake City, 0800 MST, 1968 November 20. The curves with	

LIST OF ILLUSTRATIONS - Cont'd

Figure	Description	Page
	arrows indicate the direction of the angle scan at 3.5°/min and radiometric temperature output. The line connected by circles is the helicopter sounding. The solid line and dash-dot line are the on-site and Weather Bureau RAOB.	61
26	Comparison of observed up-down radiometric scan with on-site and USWB RAOB data and helicopter data, Salt Lake City, 0800 MST, 1968 November 21. The curves with arrows indicate the direction of the angle scan at 3.5°/min and radiometric temperature output. The line connected by circles is the helicopter sounding. The solid line and dash-dot line are the on-site and Weather Bureau RAOB.	62
27	Comparison of observed up-down radiometric scan with on-site and USWB RAOB data and helicopter data, Salt Lake City, 1200 MST, 1968 November 21. The curves with arrows indicate the direction of the angle scan at 3.5°/min and radiometric temperature output. The line connected by circles is the helicopter sounding. The solid line and dash-dot line are the on-site and Weather Bureau RAOB.	64
28	Comparison of observed radiometric scan with on-site and USWB RAOB data and helicopter data, Salt Lake City 1100 MST 1968 November 20.	65

BLANK PAGE

SECTION I

INTRODUCTION

This Final Report covers work during the time period 1968 April 1 to 1969 September 21 under Contract No. PH-22-68-22 with the National Air Pollution Control Administration.

Previously* it was shown that ground-based millimeter wave radiometers could be used to passively measure radiation from oxygen molecules and derive low level air temperature profiles with accuracies approaching that attainable with radiosondes. These passive radiometric techniques can provide this information without requiring highly trained personnel or the loss of expendable packages. Also, without producing a physical hazard, these techniques can provide real time representative observations of atmospheric stability conditions.

The previous experimental observations were taken at one location (Oklahoma City, Oklahoma) where a 1500-foot instrumented tower was available. Therefore the computer-simulated and experimental results and techniques developed applied only to summer and fall meteorological conditions at this one location. We know that more atmosphere exists above sea level than above mountain stations, consequently the surface pressure depends upon the station height above sea level. Also, the station surface pressure changes due to the migration of cyclones and anticyclones. Since pressure changes produce a change in the attenuation of radiation emitted by oxygen moledules, it is reasonable to expect a pressure altitude and seasonal effect on the height to which remote temperature observations would be applicable for stations in continental U.S.A.

Passive methods of remote probing automatically introduce a smoothing of existing temperature discontinuities. There is smoothing due to equipment

*Contract No. PH-86-67-76, National Air Pollution Control Administration, Final Report, "Investigation of the Capabilities of Millimeter Wave Radiometers for Remotely Measuring Temperature Profiles Pertinent to Air Pollution."

factors (such as beam width, bandwidth, and integration time) and smoothing due to our inability to analytically extract all the information contained within the radiometric signals. During temperature inversion conditions, for example, the maximum observed radiometric temperature is always less than that actually existing at the top of the inversion. The previous results showed that for ground-based inversions it is not unusual to have radiometric temperature increases equal to half the increase that actually exists in the atmosphere. These smoothing effects have systematic characteristics which could be incorporated into the data processing technique for translating radiometric data into observations of air temperature as a function of height.

One objective of this investigation was to develop a specialized version of Sperry Rand's research radiometer for air pollution control requirements. Such a radiometer, the Radiometric THERMASONDE™, was constructed with sufficient sensitivity and stability to permit further assessment of the capabilities of microwave radiometry for the measurement of atmospheric vertical temperature profiles. The second objective was to conduct simulation and experimental investigations of seasonal, pressure altitude, and smoothing effects on the ability to remotely measure the low level air temperature profiles pertinent to air pollution. Work on the Mark I THERMASONDE™ was accomplished at the Sperry Microwave Electronics Division, Clearwater, Florida, and the simulation and experimental investigations were conducted by the Sperry Rand Research Center.

Section 2 of this report covers the theory and hardware aspects of the millimeter wave radiometer--the Mark I Radiometric THERMASONDE™. Section 3 contains discussions of simulation and experimental results, and the conclusions are presented in Section 4. Appendix I contains a paper on "Use of Millimeter Wave Radiometry to Remotely Measure Atmospheric Stability" presented at the symposium sponsored by the National Air Pollution Control Administration on Advances in Instrumentation for Air Pollution Control, 1969 May 26-28. Readers without prior knowledge in passive millimeter wave probing would probably find it worthwhile to first read the background material in this Appendix. The applicable height concept is developed and presented in Appendix II. This technique allows for a table look-up approach for on-site translation from radiometric to temperature profile information.

SECTION 2

MARK I RADIOMETRIC THERMASONDE™

1. INTRODUCTION

The objective of this program was to develop a specialized radiometer for measurement of atmospheric brightness temperature in the oxygen absorption band to be used for determining vertical temperature profiles in the lower atmosphere.

Work on this contract was started on 1968 April 1 and the National Air Pollution Control Administration accepted delivery of the equipment at Clearwater on 1969 February 6.

This section covers the Mark I specifications and description, basic radiometer theory, calibration methods, and operating techniques.

2. BACKGROUND INFORMATION

2.1 Scope - This section contains the basic specifications upon which the equipment design was based, some basic theory of radiometry pertinent to the design, and microwave design concepts peculiar to radiometers.

It will be noted that the specification refers to Microwave Radiometer, Mark I. The name was later changed to provide a functional description of intended usage. Specifications are given as incorporated in the initial contract.

2.2 Specification for Microwave Radiometer Mark I

2.2.1 General - This radiometer will be designed for the measurement of atmospheric brightness temperature in the oxygen absorption frequency band. It will be portable, and designed for outdoor and field use and operate from external primary power.

2.2.2 Operating Center Frequency - The radiometer will be fix-tuned at a frequency of 54.5 GHz.

2.2.3 Radio Frequency Bandwidth - In order to keep frequency smearing to a practical minimum, the 3-dB RF bandwidth will be restricted to 500 MHz or less. The RF bandwidth will be centered on the RF center frequency.

2.2.4 Intermediate Frequency Bandwidth - The 3-dB bandwidth will be at least 100 MHz.

2.2.5 Sensitivity - The minimum detectable temperature difference (ΔT_{min}) of the radiometer will be 0.26°K when the integration time is 60 seconds. The design goal sensitivity will be 0.13°K.

2.2.5.1 Integration times of 4, 30, and 60 seconds will be provided by switching. The 4-second integration time will be used for test purposes only.

2.2.6 Calibration - The radiometer will be calibrated for manual null balance measurement of atmospheric brightness temperature at a local oscillator frequency of 54.5 GHz.

2.2.6.1 The radiometer will be calibrated for source temperatures from 200°K to 320°K. A calibration chart will be provided which gives brightness temperatures versus readout on the balance control at balance.

2.2.7 Antenna - The antenna will have a beamwidth of approximately 2.5 degrees. Polarization will be horizontal in order to provide minimum sidelobes in elevation. The entire antenna will be enclosed in a temperature controlled chamber (with low-loss radome window) for control of antenna loss temperature.

2.2.8 Microwave Circuitry - The microwave circuitry will be that necessary for a null balance, Dicke-type superheterodyne radiometer.

2.2.8.1 Local oscillator input will be provided from a high reliability klystron operating at the lowest voltages practical in this frequency range. Operating conditions will be so chosen as to provide maximum frequency stability and tube lifetime. Local oscillator power level to the mixer will be adjustable by means of an attenuator. A micrometer type frequency meter will be provided for checking the local oscillator frequency.

2.2.8.2 Balancing noise will be provided from a gas discharge noise generator through a directional coupler and stable attenuator. Sufficient noise will be available to balance brightness (antenna beam) temperatures down to at least 200°K.

2.2.8.3 A Dicke-type modulator with stable reference temperature will be included. Switching frequency will be one half the power line frequency for optimum rejection of line-induced noise.

2.2.8.4 Between the modulator and the mixer a high isolation ferrite isolator will be included to insure stable calibration.

2.2.8.5 The mixer will be of the balanced type with frequency range and noise figure required to provide the characteristics specified in 2.2.8.2 through 2.2.8.5. This mixer will not normally require adjustment in the field.

2.2.9 Electronic Circuitry - Solid state components will be used wherever practical. Critical electronic circuitry will be temperature controlled.

2.2.10 Packaging - This radiometer will be designed for protability. All electronic components will be packaged in no more than two units.

2.2.10.1 The receiver package will be approximately 14 x 11 x 22 inches overall and will weigh less than 100 pounds. It will contain all microwave and electronic circuits and circuit power supplies. The klystron and noise tube power supplies may be contained in a separate package. The receiver package will be weatherproofed and critical components temperature-controlled for expected extremes of ambient temperature. Design value maximum ambient is +35°C with full sunlight, minimum ambient is -25°C with darkness. An indicator that proper operating temperature has been established will be provided. The receiver package will be designed for exclusion of radiant and conducted radio frequency interference and the power line filtered for protection against line transients and noise.

2.2.10.2 All normal operating controls and indicators will be accessible and/or visible without opening the receiver case. Operating controls and indicators will be kept to the minimum consistent with good design and operating practice. Indicators will be illuminated, as required, for nighttime operation. All normal operating controls will be conveniently arranged in one area.

2.2.11 Remote Readout

2.2.11.1 A connection for remote readout and recording of integrated signal output will be provided. Output impedance will be 1 kilohm or less and the scale factor will be at least 10 millivolts per degree Kelvin.

2.2.11.2 A connection for readout of elevation-angle incremental travel will be provided. Output will be a contact closure at angle increments of 5° or less.

2.2.12 Input Power - The radiometer will operate from nominal single phase 115 volt, 60 Hz power.

2.2.13 Cables - A three-wire power cable 25 feet long will be provided. Cable between receiver package and power supply, if separate, will be of equal length.

2.2.14 Pedestal - The receiver package will be mounted on and readily demountable from a tripod-pedesta' assembly. This assembly will provide adjustments, capabilities and readouts as follows:

- Leveling screws or jacks and bubble levels
- Manual adjustment of elevation over azimuth
- Constant rate motor drive adjustment of elevation over azimuth, approximately 2 degrees per minute (Note: This specification was changed by retrofitting a gear change to provide a 4-degree-per-minute rate.)

2.2.15 Finish - The receiver will be finished in gloss white epoxy enamel.

2.3 Background Theory

2.3.1 Introduction - The technology of microwave radiometry is concerned with the detection and measurement of extremely low-level microwave energy. This energy is radiated by all matter, including certain gases, which are above the temperature of absolute zero. It is well known that red-hot materials give off both visible light energy and heat energy that can be seen and felt at a distance, and that even materials which are not hot enough to show visible signs of heat can still radiate enough heat to be felt at some distance. What is not generally realized is that red-hot objects radiate energy over an extremely broad frequency spectrum, from very low frequencies to frequencies well above visible light, and that even objects which are cold to the touch still radiate energy in the infrared and lower frequency ranges. Most of this energy is concentrated in the infrared band, however, the concern here is with the energy in the microwave frequency spectrum. At frequencies below about 100 GHz, the power radiated by a material having a total emissive surface (defined as a black body) can be computed from the simple equation (Ref. 1, Eq. 13)

$$P = \frac{2kT\Delta f}{\lambda^2} \text{ watts per square meter per unit solid angle} \qquad (1)$$

where k is Boltzman's constant, equal to 1.38×10^{-23} joules per Kelvin,
T is the thermometric temperature in Kelvin,
Δf is the bandwidth in Hertz, and
λ is the wavelength in meters.

Most naturally occurring materials (including water, ice, and metals) do not have totally emissive surfaces and do not, therefore, radiate in exact accordance with Eq. (1); however, if these materials are defined as gray bodies and T is the apparent (or radiometric) temperature of the material as would be measured with an antenna of zero beamwidth, Eq. (1) will give the radiated power.

The power received by an antenna from a surface or object within its beam is (Ref. 1, Eq. 20)

$$P = \frac{kT\Delta f}{4\pi} \int_{\Omega} G(\theta,\phi)\, d\Omega \qquad (2)$$

where $G(\theta\phi)$ = power gain of antenna in direction θ,ϕ with respect to an isotropic antenna and Ω = solid angle subtended by the object at the antenna.

When the antenna is pointed into the atmosphere and the operating frequency is within the oxygen absorption band, where a signal transmitted would be totally absorbed within a few kilometers of range, and no interfering objects are within the antenna beam at closer range, the antenna beam may be considered to be immersed in a black body enclosure. If the antenna beam can be considered to be inside a black body enclosure, then the value of the integral in Eq. (2) becomes simply 4π and

$$P = kT\Delta f \quad . \qquad (3)$$

In the case of the atmosphere, however, total absorption does not occur at a fixed distance in range and the temperature T is itself an integral of absorption over distance. The antenna receives a power proportional to the complex integral relating atmospheric temperature and absorption in the direction the antenna beam is pointed.

The radiometer is required to provide an accurate measurement of this effective temperature.

2.3.2 Radiometer Sensitivity and Other Factors - The sensitivity of a microwave radiometer is defined in terms of the "minimum detectable mean input level increment." Specifically, this refers to a change in input temperature which produces an output deflection increment just equal to the standard deviation of the output fluctuations about the mean deflection. In engineering terms, the minimum detectable temperature input change (ΔT_{min}) is one which produces an output change equal to the rms noise output. The equation for radiometer sensitivity (Ref. 2) is

$$\Delta T_{min} = \frac{M\, T_{es}}{\sqrt{\tau B}} \sqrt{1 + \frac{(I\zeta)^2}{\tau B}} \qquad (4)$$

where M = modulation factor determined by receiver type

T_{es} = effective system input noise temperature

B = predetection bandwidth of the system

τ = post detection integration time

I = fractional rms variation due to instability alone, and

ζ = instability reduction factor.

The terms are further defined as follows:

For a dc (total power) radiometer: $\zeta = 1$ and $T_{es} = T + T_{er}$.

For a Dicke modulated signal radiometer:

$$\zeta = \frac{T - T_R}{T + T_{er}} \quad \text{and} \quad T_{es} = T_{er} + \frac{T + T_R}{2} \qquad (5)$$

where T = signal temperature into the Dicke switch

T_R = the reference temperature in a switched radiometer

and T_{er} = effective receiver noise temperature .

Also, $T_{er} = (F-1)T_o$

where F = receiving system noise figure (single or double sideband as appropriate)

and $T_o = 290K$.

The instability factor I is difficult to compute for a real system, but should always be kept to an absolute minimum. Perhaps the most notable fact is that if either I or ζ can be made equal to zero, then ΔT_{min} will be a minimum according to Eq. (4). In a dc radiometer, ζ is always equal to unity so that whatever receiver instabilities exist will show up at the output. In the Dicke radiometer, if $T - T_r = 0$, or is at least very small relative to $T + T_{er}$, then ζ will equal or approach zero and instabilities will have negligible effect.

In a Dicke-type radiometer, measuring temperatures in the 25°C (298 K) range with a 55°C (328 K) reference temperature, $T - T_R$ will be about 30 K. Assuming F = 14 db or 25 to 1, then $\zeta = \frac{298 - 328}{298 + (25-1)290} = \frac{30}{7258} = 0.0041$. This is a major improvement over a DC radiometer having $\zeta = 1$ and the same instability factor I. In order to reduce the effect of instability even further, the technique of null balancing was devised. A diagram of a null balancing Dicke radiometer front end is shown in Fig. 1. Operation of the circuit is simple: A calibrated noise temperature T'_N is added to the signal temperature T_s so that the total signal temperature into the signal port of the Dicke switch or chopper is exactly equal to the internal reference temperature T_R . The differential temperature output from the chopper $T - T_R$ becomes zero, and this reduces the instability reduction factor ζ to zero. The diagram shows the practical means of adding calibrated noise to accomplish null balance. High temperature noise T_N is provided by a stable gas-discharge noise generator with a temperature output of about 18,000 K. A precision attenuator is used to control the magnitude of this signal reaching a directional coupler in the signal line. In the Mark I, this coupler is about 20 dB which means that it is possible to add about 186 K to the signal while the signal loss in the coupler, due to coupling, is only about 1%. The signal temperature at null is determined from calibration giving T_s in terms of attenuator setting at balance.

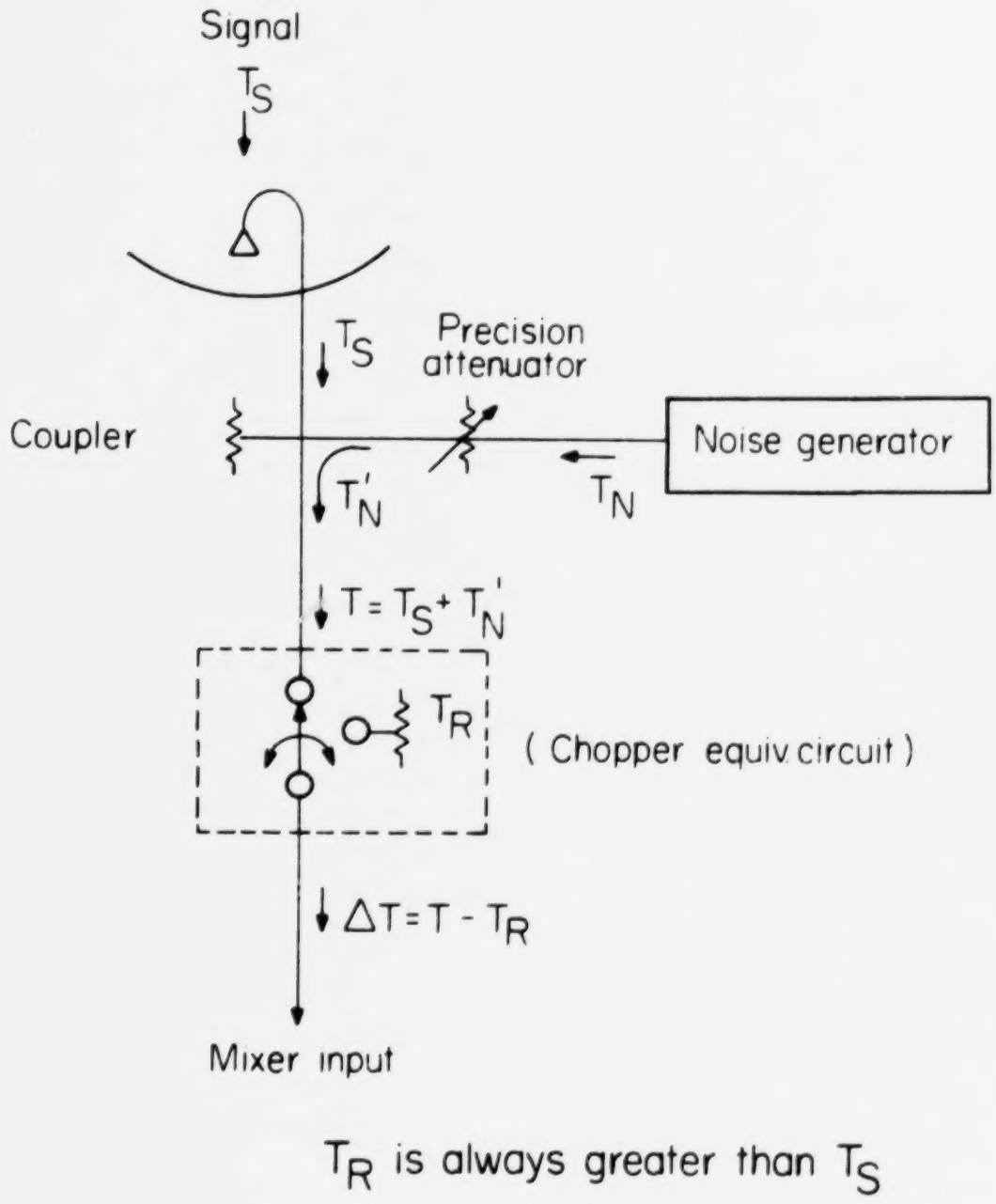

FIG. 1 Diagram of a null balancing Dicke radiometer, front end.

The preceding discussion illustrates why a Dicke radiometer with null balancing front end was chosen for the Mark I Radiometric THERMASONDE™, which is intended for precise measurement of temperatures and extremely small temperature differences: to reduce the effects of instrument instability on measurement accuracy.

2.3.3 Practical Radiometer Relations - Equation (4) was presented to show the basic form of the sensitivity equation and show the instability relation; however, this is not the form ordinarily used in engineering computations. If pains are taken so that instability is negligible and T is very nearly equal to $T_o = 290$ K (which is normally the case), then the sensitivity of the radiometer is given very nearly by

$$\Delta T_{min} = KFT_o / \sqrt{B\tau} \qquad (6)$$

where K = a radiometer constant depending upon radiometer type and related to modulation and filter factors,

and F, τ, T_o and B are as stated previously. It should, perhaps, be pointed out that B is the equivalent rectangular bandwidth of the receiver and not the common half-power bandwidth. B is defined mathematically as one half the self convolution of the power transfer characteristics of the reception filters. In practice, B for any receiver may be found by measuring the power frequency response of the receiver up through the video detector and computing

$$B = \frac{\left(\sum_{k=1}^{n} A_k \right)^2 \Delta f}{\sum_{k=1}^{n} \left(A_k \right)^2} \qquad (7)$$

where A_k = normalized power gain at frequency K

Δf = frequency interval of measurement

and n = number of samples.

2.3.4 Radiometer Noise Figure - The computation of overall noise figure of a radiometer which has significant losses ahead of the receiver must include those losses. In the 54 and 55 GHz band, the waveguide is very small and relatively lossy*; therefore, these losses must be considered.

The noise figure of any series arrangement of system components is computed according to the relation

$$F_s = F_1 + \frac{F_2 - 1}{G_1} \cdots + \frac{F_n - 1}{G_{n-1}}$$

where F_s = system noise figure

F_1 = noise figure of first component

F_2 = noise figure of second component

F_n = noise figure of last component

G_1 = gain of first component

and G_{n-1} = gain of next to last component.

The noise figures and gains of amplifiers and mixers are well understood from common definitions. The noise figure of any lossy component in the signal path can be computed (Ref. 3) as

$$F = 1 + \frac{T}{290}(L-1) \qquad (8)$$

where T = thermodynamic temperature of component, Kelvin

L = loss ratio

290 = standard reference temperature for noise figure, 290 Kelvin. The gain of such a component is just the reciprocal of the loss factor.

The noise figure of a device which couples energy from an auxiliary line

*The theoretical minimum loss is about 0.52 dB per foot and practical loss is somewhat greater.

into the signal line, such as a directional coupler as shown in Fig. 2, can be computed very closely as

$$F = 1 + \frac{T}{T_i} \frac{(L-1)}{(1-t_c)} + \frac{T_s}{T_i} \left(\frac{t_c}{1-t_c} \right) \tag{9}$$

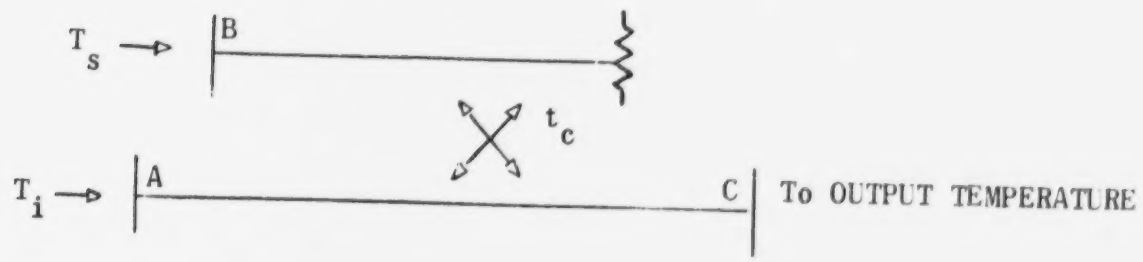

Note: Ohmic losses from Port A to C and Port B to C are both assumed equal to L

FIG. 2 Three-terminal coupling device.

where T_i = input signal temperature to signal line, assumed 290 K by convention

T_s = input signal temperature at secondary line

t_c = coupling transmission coefficient between lines

L = ohmic loss factor from either input port to single output port, and

T = thermodynamic temperature of device.

2.3.5 Lossy Component Temperatures - Another matter of great importance in radiometer design for accurate temperature measurements is the stability of temperature contribution due to lossy components in the signal path. A lossy signal path not only reduces the amplitude of signal transmitted but adds a noise component proportional to its loss and temperature. Since this is true, both the loss and temperature of all system components must be stable to prescribed limits. Losses can normally be made stable without great difficulty; however, where the system is to operate over a wide range of temperature environments, the effects of changes in temperature of lossy components must be carefully evaluated and, if necessary, the temperature

controlled.

For a system such as described in this report the evaluation is very complex, although the basic method is simple as may be shown by a rudimentary example. The output temperature at port C of the device shown in Fig. 2 is very nearly

$$T_o = \frac{T_i}{L}(1-t_c) + \frac{T_s t_c}{L} + T\left(1-\frac{1}{L}\right) \tag{10}$$

and the output temperature of a simple lossy component such as a waveguide section is

$$T_o = \frac{T_i}{L} + \left(1-\frac{1}{L}\right)T \tag{11}$$

where T_i is now taken as the input signal temperature and T_s, t_c, and L are assumed to be stable constants.

T_o can change only if T_i or T change, but T_i is the signal which can and will be variable. So far as changes in environment are concerned, only a change in T will cause an error in T_o. The magnitude of the change in T_o with a change in T is

$$\Delta T_o = \Delta T\left(1-\frac{1}{L}\right) \tag{12}$$

In practice it is impossible to hold ΔT to zero over a wide ambient range; therefore, a maximum permissible error in measure ΔT_o, is assigned to the component, the value of L is estimated, and the equation is solved for the permissible variation in T. This variation is then the temperature range within which T must be controlled. In those cases where T cannot be controlled, such as the radome, ΔT_o is assigned from the system error budget, the ambient temperature range is assigned to ΔT, and the maximum permissible loss L is computed.

The various equations given were used in the design and analysis of the

3. RADIOMETRIC THERMASONDE™ DESCRIPTION

3.1 General Information - The Radiometric THERMASONDE™, Mark I, Sperry Part Number X2689420, is designed for the measuring of atmospheric brightness temperature in the oxygen absorption band and from this, the vertical temperature profile. It is tunable over the 54 and 55 GHz frequency range. It consists of two units: the radiometer proper and the pedestal and yoke assembly.

The radiometer is of the null balance Dicke-type employing a mechanical modulator or chopper (see Fig. 3 block diagram). Null balance is achieved by adding calibrated noise (from a gas discharge tube) to the antenna signal. Because of the use of the mechanical chopper and because of the rather high waveguide losses in this band, the entire microwave assembly is temperature controlled to maintain calibration accuracy.

The radiometer output is a DC voltage, either positive or negative, depending upon whether the sum of antenna and noise injection temperatures is greater or less than the chopper card temperature. Output scale factor is at least 25 millivolts per Kelvin difference at all frequencies within the band.

The radiometer is calibrated for null balance operation. A calibration chart is provided with the radiometer, giving brightness temperature as a function of attenuation to balance at 54.5 GHz. The radiometer operates from a 105 to 125 VAC, 60 Hz power line.

3.2 Equipment Illustrations - Figure 4 shows the Radiometric THERMASONDE™ set up and ready for operation except for external cable connections to remote recorder and power line. Figure 5 is a view of the opposite side showing the radome window on the end of the case and the cooling vents on the bottom of the case. Figure 6 shows all of the normal operating controls for the equipment, including those normally concealed by the L. O. ADJUSTMENTS cover.

3.3 Signal Channel Functioning - From Fig. 3, noise signals received by the antenna (E1) pass through the directional coupler (DC1) to the wave-

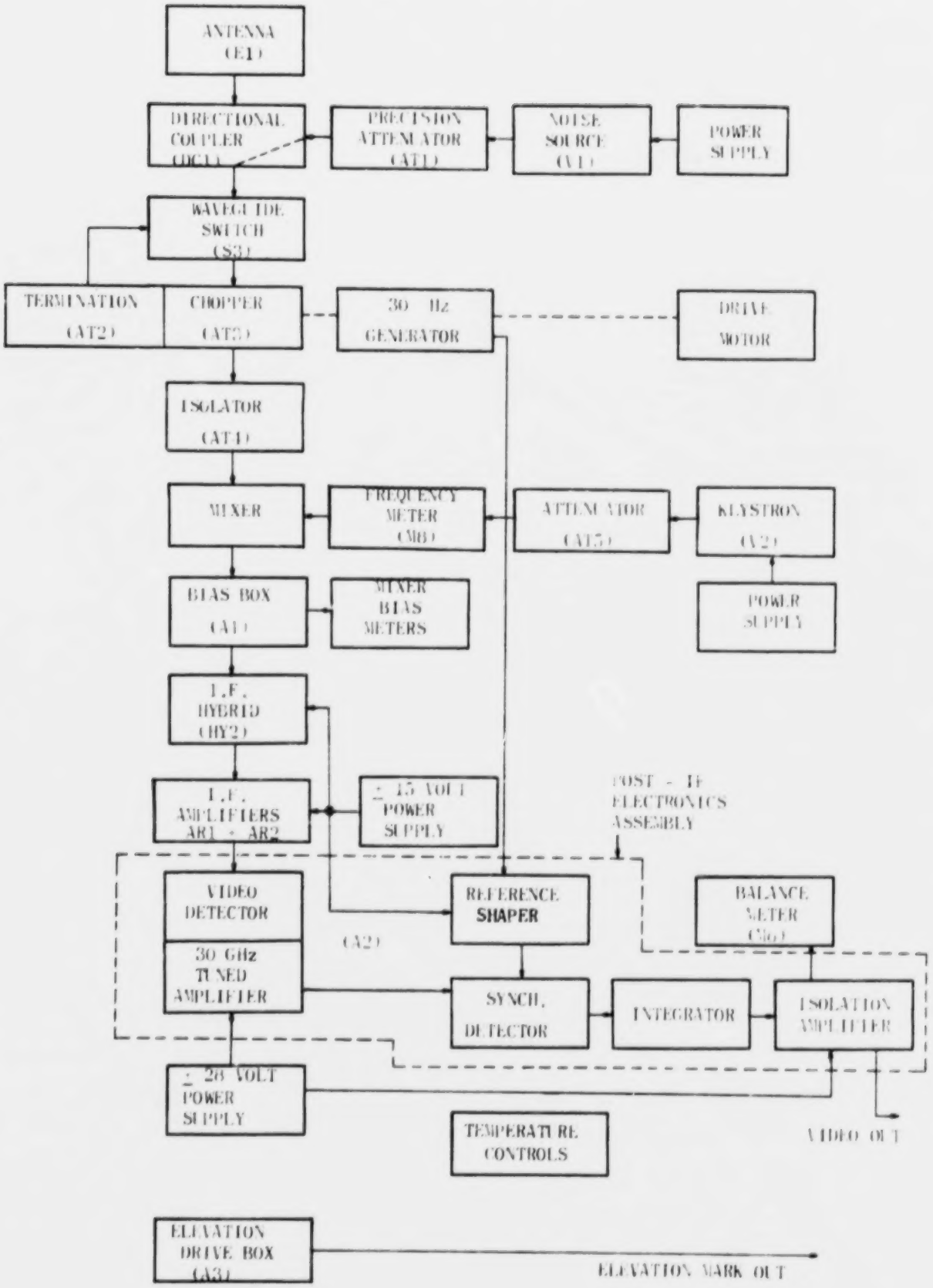

FIG. 3 Block diagram of a null balance Dicke-type radiometer.

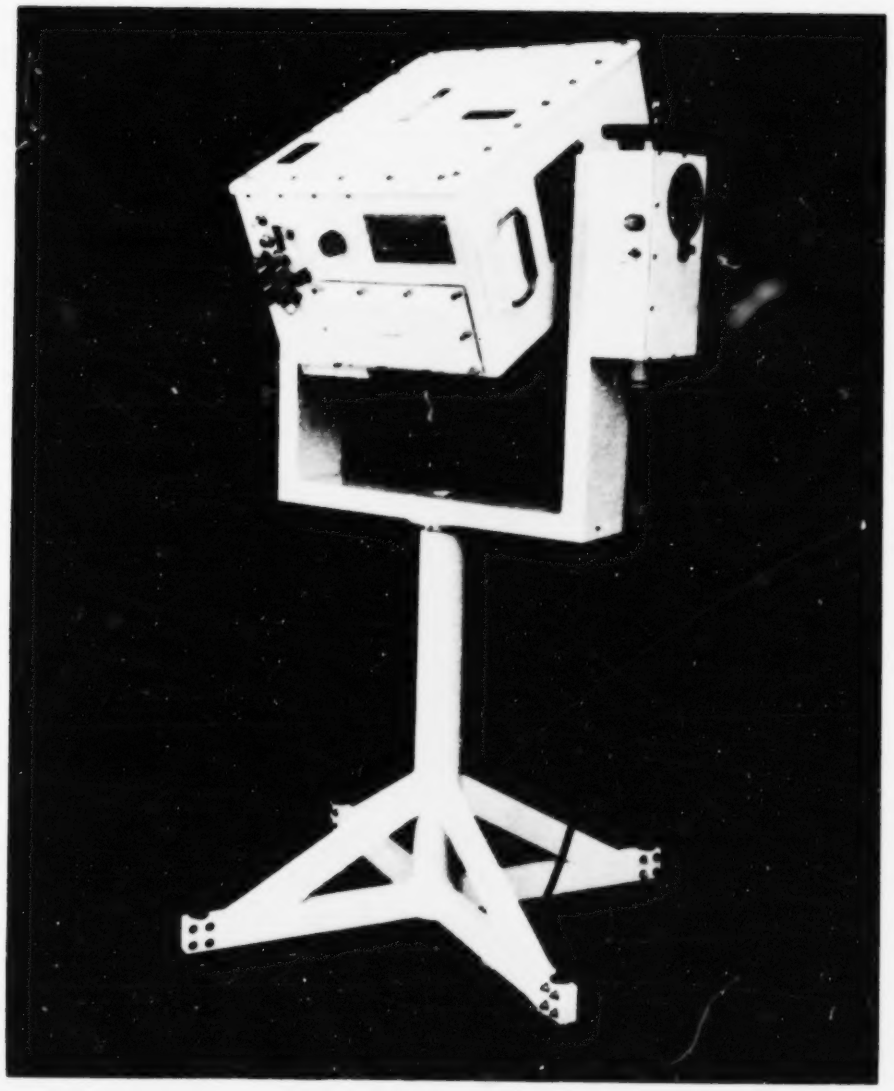

FIG. 4 Radiometric THERMASONDE™, Mark I, rear view.

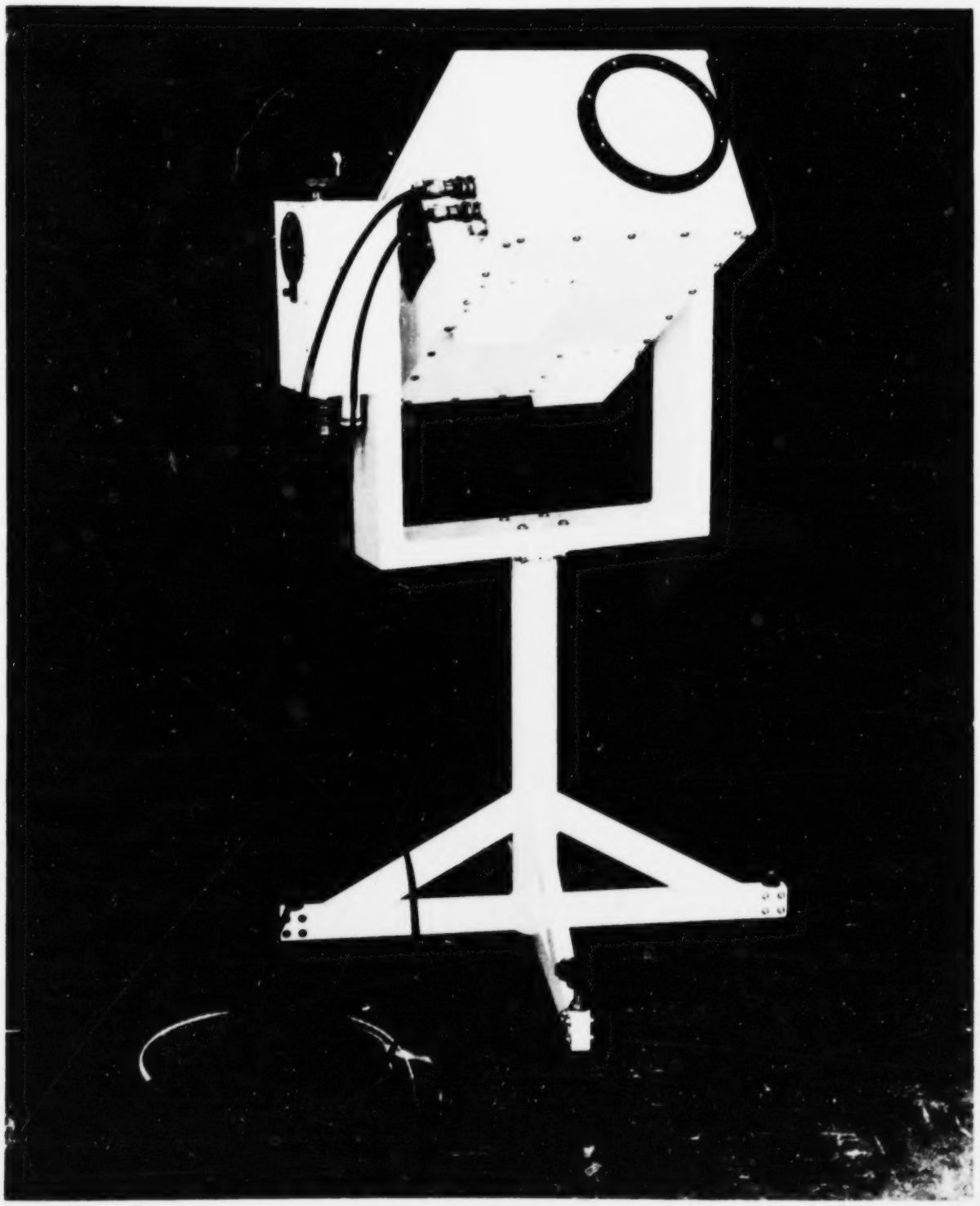

FIG. 5 Radiometric THERMASONDE™, Mark I, front view.

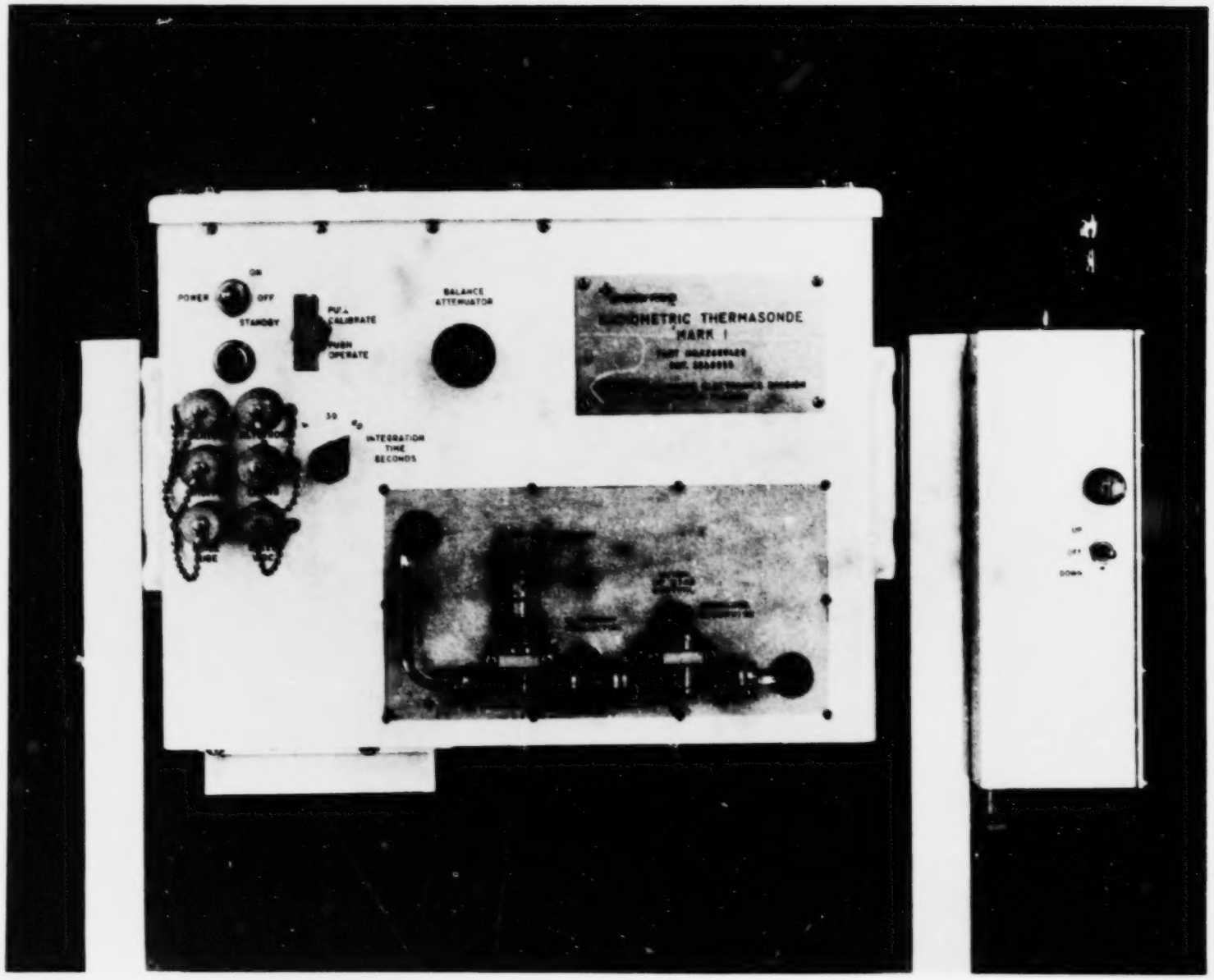

FIG. 6 Operating controls of the Radiometric THERMASONDE^{TM}, Mark I.

guide switch (S3). When this switch is in the OPERATE position, this signal proceeds on through the switch to the chopper (AT3). The chopper is on an ON-OFF attenuator with high OFF attenuation such that when it is OFF the signal entering the isolator is the thermal noise (temperature) generated by the attenuator card. As the chopper card rotates at 1800 rpm, the isolator input alternates at 30 Hz between the chopper card noise temperature and the noise temperature output from the waveguide switch (S3). The noise temperature from the directional coupler consists of the antenna signal plus noise purposely injected into the signal line from the noise source (V1). The amplitude of injected noise is controlled by a balance attenuator (AT1). The purpose of noise injection is to make the antenna signal plus injected noise equal to the noise generated by the chopper card so that the isolator input signal is a constant and the radiometer becomes a null-indicating device of maximum accuracy and sensitivity. When the waveguide switch is in the CALIBRATE position, a different signal - that from a matched waveguide load (AT2) at the same temperature as the chopper - is fed through S3 to the chopper to provide an equal chopper output, whether the chopper is ON or OFF. From the chopper, signals proceed through the isolator (AT4), whose purpose is to prevent impedance variations in the chopper and signal lines from creating spurious signals due to reflection of local oscillator signal and noise back to the mixer. From the isolator the signal goes to the balanced mixer, which consists of the hybrid (HY2) and two crystal holders with mixer crystals where the signal is heterodyned with the local oscillator signal to convert the signal to the intermediate frequency band.

The bias box (A1) provides DC bias required for operation of the mixer.

The local oscillator (L.O.) signal is provided by the klystron oscillator (V2) through the level-set attenuator (AT5).

The frequency meter (M8) in the L.O. line permits checking of L.O. frequency.

The IF signals from the crystals are recombined in the IF hybrid (HY2) and amplified by the IF amplifier (AR1 and AR2). Then the IF signal is fed to the post-IF electronics assembly (A2). The electronics assembly

contains a video detector, a 30 Hertz tuned amplifier, a reference shaper circuit (which receives a 30 Hertz synchronizing sinewave from the generator on the chopper), a synchronous detector, an integrator, and an output amplifier. The output from the electronics board is a DC voltage whose amplitude and polarity depend upon the difference in signal temperature into the mixer as the chopper card rotates. This DC voltage is connected to the data output jack for recording and also to the balance indicator meter (M6). This meter is provided with a voltage and current limiting device to give adequate sensitivity while preventing damage to the meter when the unbalance is large.

3.4 Achieved Specifications - All of the specifications delineated in Paragraph 2.2 of this section were achieved, except that weight was 101½ pounds instead of the specified 100 pounds.

4. CALIBRATION METHODS AND RESULTS

4.1 Introduction - Calibration of the Radiometric THERMASONDE™ consists of determining what setting of the balance attenuator corresponds to each antenna beam brightness temperature when the THERMASONDE™ is operated in the null balance mode. This calibration proceeded in two stages:

First, the antenna was removed and the receiver calibrated for antenna output port temperature to produce a curve of antenna calibration temperature versus dB-to-balance (balance attenuator readout at balance).

Second, measurements were made which permitted converting this curve into a calibration curve of antenna beam brightness temperature versus dB-to-balance. This conversion amounts to correcting the original curve for losses in the antenna and radome. It also corrects for some systematic errors in the original curve.

4.2 Apparatus Used - The apparatus used in calibrating the receiver was, in effect, a matched termination whose temperature was variable from below 200 Kelvin to above 320 Kelvin. The critical part of the apparatus was a waveguide assembly consisting of a matched termination, a waveguide thermal isolator with vapor seal windows, a precision rotary-vane attenuator, and two waveguide sections. One waveguide section extended from the receiver input port inside the Mark I through a dummy radome to the precision attenuator outside. The other section connected between the thermal isolator and the

termination. The purpose of the thermal isolator was to thermally isolate the termination temperature from the precision attenuator; the windows prevented atmospheric moisture from entering the termination or the isolator.

The insertion loss of all components was very carefully measured and the components assembled using O-ring seals on all joints between the termination and the attenuator. Thermocouples were attached to each part of the calibration assembly so that component temperatures could be measured with a thermocouple bridge.

4.3 Calibration - The antenna and radome were removed from the THERMASONDE™ and replaced with the calibration waveguide assembly and the dummy radome.

The termination was immersed in various temperature baths including boiling liquid nitrogen, ice water, hot water, and various temperatures of warm water. The bath temperatures and the precision attenuator setting were then varied to provide receiver input temperatures throughout the calibration range. The balance attenuator was adjusted to provide a null output at each temperature. The exact input temperatures were then determined by measuring the bath and individual calibration component temperatures, noting precision attenuator setting, and computing the input temperature using an equation based on Eq. (11) (Para. 2.3.5). When a sufficient number of points were obtained, the curve of antenna temperature versus dB-to-balance was plotted. The normal antenna and radome were then replaced in the THERMASONDE™.

Correction for antenna and radome loss is best done outdoors, so the unit was moved to the antenna range. Here the unit was warmed up and a null balance measurement of brightness temperature was made. For this measurement the antenna was pointed at zero-degree elevation toward a wooded area some thousand feet away across a grassy field, on a cool overcast day. The weather and siting conditions practically insured that the true brightness temperature observed by the antenna would be equal to the local ambient temperature which was measured with a thermocouple bridge. At the time of the measurement the temperature of the shroud around the antenna was also measured.

The effective antenna transmission coefficient t_a was computed as

$$t_a = (T_c - T_a) / (T_s - T_a)$$

where T_c = antenna temperature as determined from the calibration chart at balance

T_a = measured antenna shroud temperature, and

T_s = measured signal (i.e., local ambient temperature).

The results of the first test gave $t_a = 0.803$; however, it was later found that some small errors had been made in the measurement. Additional checks were made and the most probable value of t_a was determined to be 0.81. It should perhaps be noted that the precise value of t_a is very hard to determine but the ambient (brightness) temperature, T_s , and the dB-to-balance for that temperature represent a true point on the final brightness temperature calibration curve. The only reason for computing t_a is to make it possible to correct the antenna temperature curve for brightness temperatures not available to direct measurement at 0-degrees elevation. If the value of t_a determined by this procedure is in error, it will show up as an increasing discrepancy in the final curve at points increasingly removed from the measured point.

Following the determination of t_a , temperatures were taken from the original calibration curve and their equivalent brightness temperatures were computed according to the relation

$$T_s = \left[(T_c - T_a)/t_a \right] + T_a$$

where T_s is the brightness temperature corresponding to the dB-to-balance for the antenna temperature T_c taken from the original curve.

Enough such temperatures were computed to plot the final curve of brightness temperature versus dB-to-balance. The original T_s point, from which t_a was computed, fell on the new curve--as it must if the computations are properly made.

The final calibration curve provided in the Handbook of Instructions for

the Radiometric THERMASONDE™ gives brightness temperatures from 189.5 to 322 Kelvin corresponding to attenuator readout digital dial settings (at balance) from 000 to 452. Points on this curve are estimated to be in error by no more than 1°C plus 3% of the difference between the true brightness temperature and 300 Kelvin (about 4.3 K maximum at brightness temperature of 190 K).

5. OPERATING AND MEASURING TECHNIQUES

5.1 Operation - Preparing the Mark I for making measurements consists of setting up the equipment in the desired location, connecting the output to any suitable recorder, connecting to the power line and turning on the power. After waiting for the unit to reach its stable operating temperature, the klystron frequency and the various monitor meters should be checked to make sure the equipment is on frequency and functioning properly.

If measurements are to be made on a regular schedule at one location, the Mark I power switch should be left in the STANDBY position when not in use. This will keep the temperature controls in operation and the waiting time after switching to the ON position will normally be less than ten minutes.

5.2 Measurement Methods - The basic measurement method utilizes the null balance technique alone to measure absolute brightness temperatures. To use this method, the true system zero is first found by pulling the CALIBRATE knob out and observing the final reading on the balance indicator. The unit is then pointed at the desired elevation and azimuth, the CALIBRATE knob pushed in, and the balance attenuator control adjusted until the balance indicator reads exactly as it did with the CALIBRATE knob out. Once balance is achieved, the brightness temperature is determined from the attenuator readout number and the calibration chart which gives brightness temperature versus digital dial reading at balance. The procedure is repeated for all elevation angles of interest.

A second measurement technique provides for continuous measurement of brightness temperature versus antenna elevation angle. For maximum measurement accuracy, the following procedure is recommended:

- Point unit at a convenient azimuth
- Set elevation manually to 0 degrees
- Find temperature at this elevation by the null balance technique
- Start paper drive on auxiliary recorder
- Place toggle switch on elevation drive box in UP position
- Wait 22 1/2 minutes for elevation scan to be completed, then turn elevation drive off
- Find temperature at the final elevation by null balance technique
- Since the output is linear, all temperatures for angles between 0 and 90 degrees can be found by linear interpolation of the chart recording between the two known end-point temperatures.

REFERENCES

1. Harris, D. B., "Microwave Radiometry," Microwave Journal V. 3, No. 4, April 1960 and V. 3, No. 5, May 1960.

2. Colvin, R. S., "A Study of Radio Astronomy Receivers," Stanford Radio Astronomy Institute, Publication No. 18A, AD-268503.

3. Strum, P. D., "Considerations in High Sensitivity Microwave Radiometry," Proc. IRE, V. 46, No. 1, January 1958.

SECTION 3

DISCUSSIONS OF COMPUTER SIMULATION AND EXPERIMENTAL RESULTS

1. APPLICABLE HEIGHTS

1.1 General - It has been assumed for discussion in this section that the reader has some familiarity with passive probing techniques. Appendix I provides background information and a review of the results available at the time the paper was submitted. Appendix II contains the development of the applicable height concept. Applicable heights were generated using a computer simulation of millimeter wave radiative transfer in the atmosphere. They were obtained for use in conducting experimental programs at Clearwater, Florida; Sudbury, Massachusetts; Cincinnati, Ohio; and Salt Lake City, Utah; where the station elevations are about 10, 200, 1000, and 5000 feet, respectively. They were derived from upper air temperature soundings selected from the nearest radiosonde station, categorized according to season, and averaged to give a smooth lapse temperature profile from the surface up to 10 mb. For the winter season, the Salt Lake City soundings showed a ground-based inversion in the mean; however, this was smoothed to give a lapse profile so that no ambiquity would exist in deriving applicable heights. For each location, season, frequency, and elevation angle, the computed applicable heights were for a null balance operation, which assumes that absolute brightness temperature observations are made at discrete elevation angles.

1.2 Frequency Effect - Figure 7 presents radiometric brightness temperatures computed from a mean Cincinnati winter profile as a function of frequency and elevation angle. The scale on the left-hand side of this figure represents the height in the atmosphere where the computed brightness temperature equals the air temperature of the mean winter profile. Thus for a fixed surface pressure and mean winter profile, the curves in Fig. 7 represent the applicable height of radiometric observations under lapse conditions. It can be seen at 90 degrees elevation angle that as frequency decreases the depth of penetration (or applicable height) increases from 1.4 to 2.8 km for 55, 54.5, and 54 GHz, respectively.

Nearly a linear curve represents the translation function at 55 GHz be-

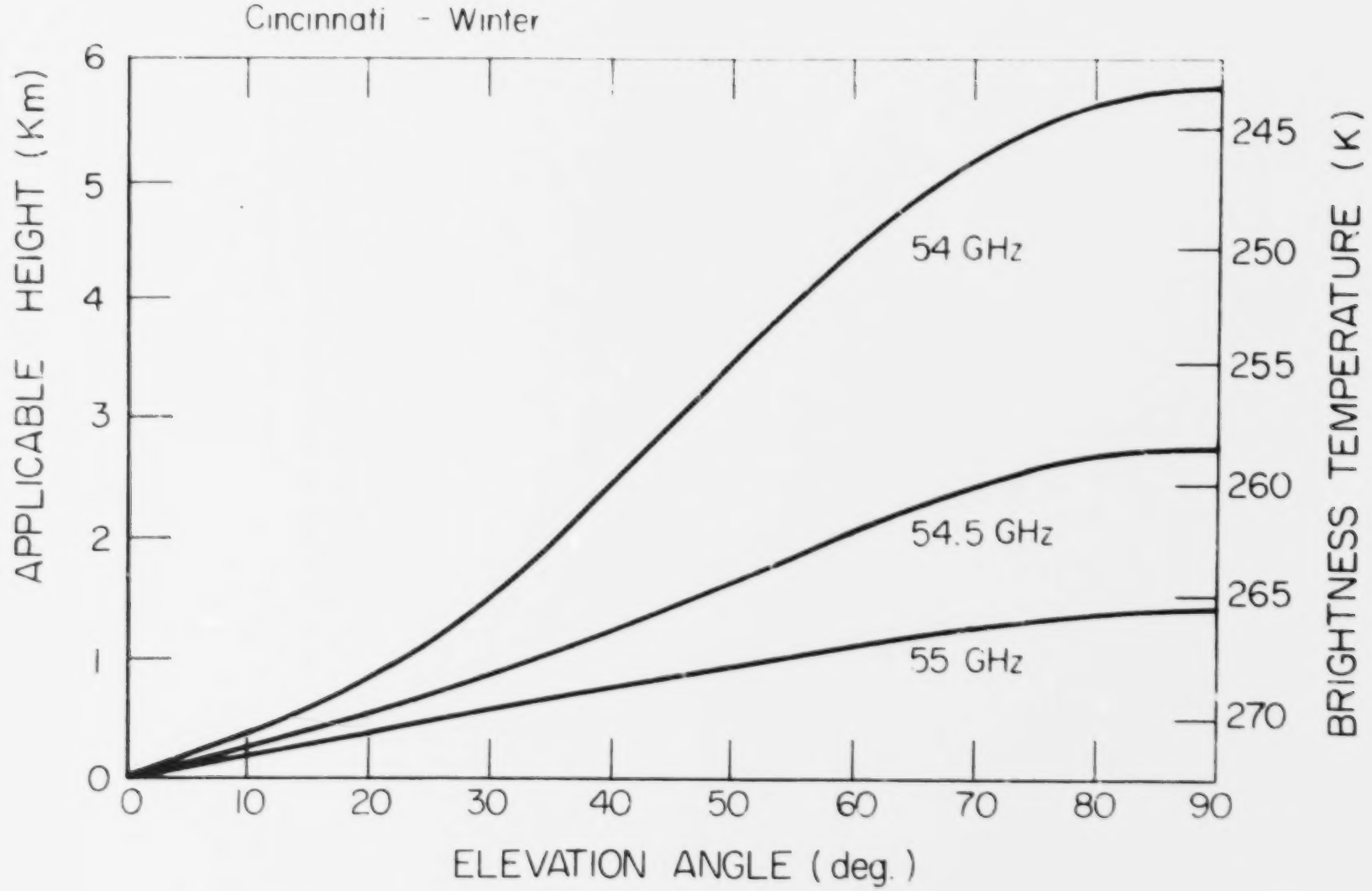

FIG. 7 Applicable heights and radiometric temperatures vs elevation angle at Cincinnati, winter season, for frequencies of 54, 54.5, and 55 GHz.

tween elevation angle and applicable height. As frequency decreases, the translation functions become more S-shaped and little or no change in applicable height is found between 80 and 90 degrees elevation angle. Stated another way, radiometric brightness temperatures are nearly the same from 80 to 90 degrees elevation angle; therefore little new information is obtained in this region. This means that observations taken in a null balance mode need not be taken at uniform angle increments, allowing a complete sounding between 0 and 90 degrees to be completed more rapidly.

If, however, the radiometer is operated in a non-null balance mode giving relative temperature measurements as the antenna scans at a constant rate from the horizontal to the vertical, then this S-shaped effect is somewhat modified. In practice, the radiometer has a circuit that filters its output signal over time to reduce not only the noise internal to the equipment but the unwanted short-term atmospheric fluctuations as well. Thus when the antenna is scanning, the filter (or integrator) affects the output signal in a manner depending upon the brightness temperature gradient, antenna scan rate, operating frequency, and filter time constant. For example, consider a lapse profile. As the antenna scans from horizontal to vertical, the warmer temperatures initially sensed at lower elevation angles are delayed in passing through the integrator and some percentage of these warmer temperatures is outputted at higher elevation angles. Thus the brightness temperatures at any angle are warmer than those obtained if null balanced observations are made at the same indicated angle. The reverse is true when scanning down from the vertical--colder brightness temperatures sensed at higher elevation angles are displayed at lower angles and the indicated radiometric profile is colder than that obtained in a null balance mode of operation. Computer simulation and experimental results of this effect are discussed at greater length later in this report. At this point it is sufficient to state that the S-shape relation between angle and applicable height or brightness temperature is such that the output response of the filter is non-uniform with angle, being a maximum around 50 degrees and diminishing to almost nothing at zero and 90 degrees. Furthermore, this effect is more pronounced at the lower frequencies. Operationally, this means signal processing techniques for translating radiometric

data into air temperature profiles must consider the way in which radiometric observations are taken.

1.3 Pressure Altitude Effect - Radiation emanating from an oxygen molecule is attenuated exponentially in proportion to the density of intervening molecules. Since the atmosphere is a gaseous fluid, the pressure decreases logarithmically as height increases above sea level. The ideal gas law states that for the same air temperature if the pressure is higher so is the density. Thus sea-level stations have a higher surface pressure (and, therefore, a higher density of oxygen molecules immediately above the ground) than, for instance, stations one mile above sea level. Hence, at a station high above sea level it is possible to detect radiation originating from higher levels in the atmosphere. Consequently, for given lapse conditions and a fixed frequency, brightness temperatures are colder and the heights at which they apply are higher than for a sea-level station. This effect is illustrated in Fig. 8 in which the applicable height (brightness temperature) curves for Cincinnati and Salt Lake City are presented for the same season, frequency, and elevation angles. These computations were made for lapse conditions in which the surface temperatures were the same at these two stations, but the surface pressure was representative for each location for the winter season. Since Salt Lake City is almost a mile high, its surface pressure is on the order of 870 mb; Cincinnati has a higher surface pressure of around 970 mb. Figure 8 shows that this 100 mb surface pressure differential is by no means insignificant. Notice that this effect becomes more pronounced as the elevation angle increases. As shown, this pressure altitude effect represents a difference of about 3/4 of a kilometer in applicable height between these two stations. Locations having a greater pressure altitude differential have a greater applicable height (or brightness temperature) differential, and the lower the frequency the more pronounced this effect is. Thus all techniques for translating radiometric data into measures of air temperature as a function of height must take the pressure altitude effect into consideration.

1.4 Seasonal Effects - Just as there is a pressure altitude effect, there is also at any location a seasonal variation in the surface pressure and temperature profile which, in turn, effects the density and vertical distribution of oxygen molecules. The seasonal effects for Salt Lake City at

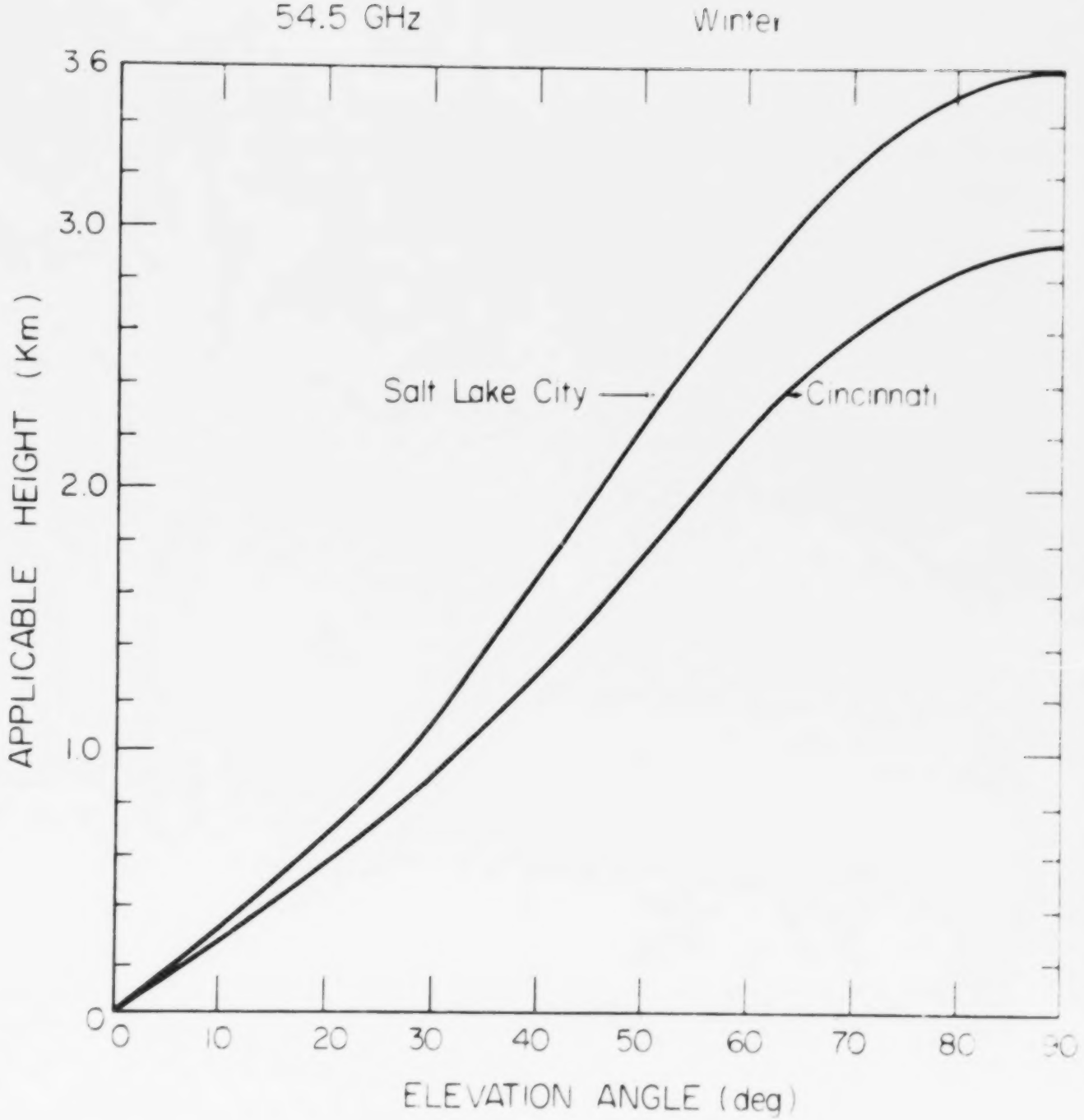

FIG. 8 Pressure altitude effect on applicable height vs elevation angle between Cincinnati and Salt Lake City in the winter season.

54.5 GHz are illustrated graphically in Fig. 9 for autumn, winter, and summer conditions. The applicable height extremes between summer and winter are less than the pressure altitude effects but are, nevertheless, significant--about 1/2 kilometer at 54.5 GHz and 90° elevation angle. Each location has its own climatological conditions that effect the depth through which the radiation is sensed for any fixed frequency and elevation angle. It can also be seen from Fig. 9 that the seasonal effects become less pronounced at lower elevation angles and the differences become insignificant--in this case, for angles below about 30°. These results were obtained computationally, using a mean of several RAOB soundings representative of the seasonal upper air temperature profiles but having the same surface pressure. For colder mean virtual temperatures the thickness between mandatory pressure surfaces is smaller, such that at any fixed height above the surface the average air pressure is lower for winter than for summer conditions. Here again, the pressure term in the radiation equation and the difference in the seasonal gradient of the temperature profile is such that a winter radiometric observation applies at a greater height than that obtained during the summer. It can also be seen from Fig. 9 that the transitional months of autumn and spring need not be evenly divided between the extremes. In general, it can be stated that climatological seasonal variations of surface pressure and upper air profile can be used to infer the magnitude of these effects on the radiational characteristics of the atmosphere.

1.5 Synoptic Pressure Effects - Formation, movement, and decay of cyclones and anticyclones produce surface pressure variations which, likewise, have an effect upon the height at which a radiometric observation applies. Figure 10 presents computational results for a subtropical station where seasonal effects are less severe than for extratropical stations, but where surface pressure variations are still significant. Here the same upper air profile, typical of autumn at Clearwater, Florida, was used to compute radiometric brightness temperatures at a fixed frequency (54 GHz) and variable elevation angles and surface pressures. The plotted curves represent the height at which the brightness temperatures correspond with the input temperature profile. It can be seen that the difference in applicable height between surface pressures of 980 to 1020 mb, which is not at all extreme for this

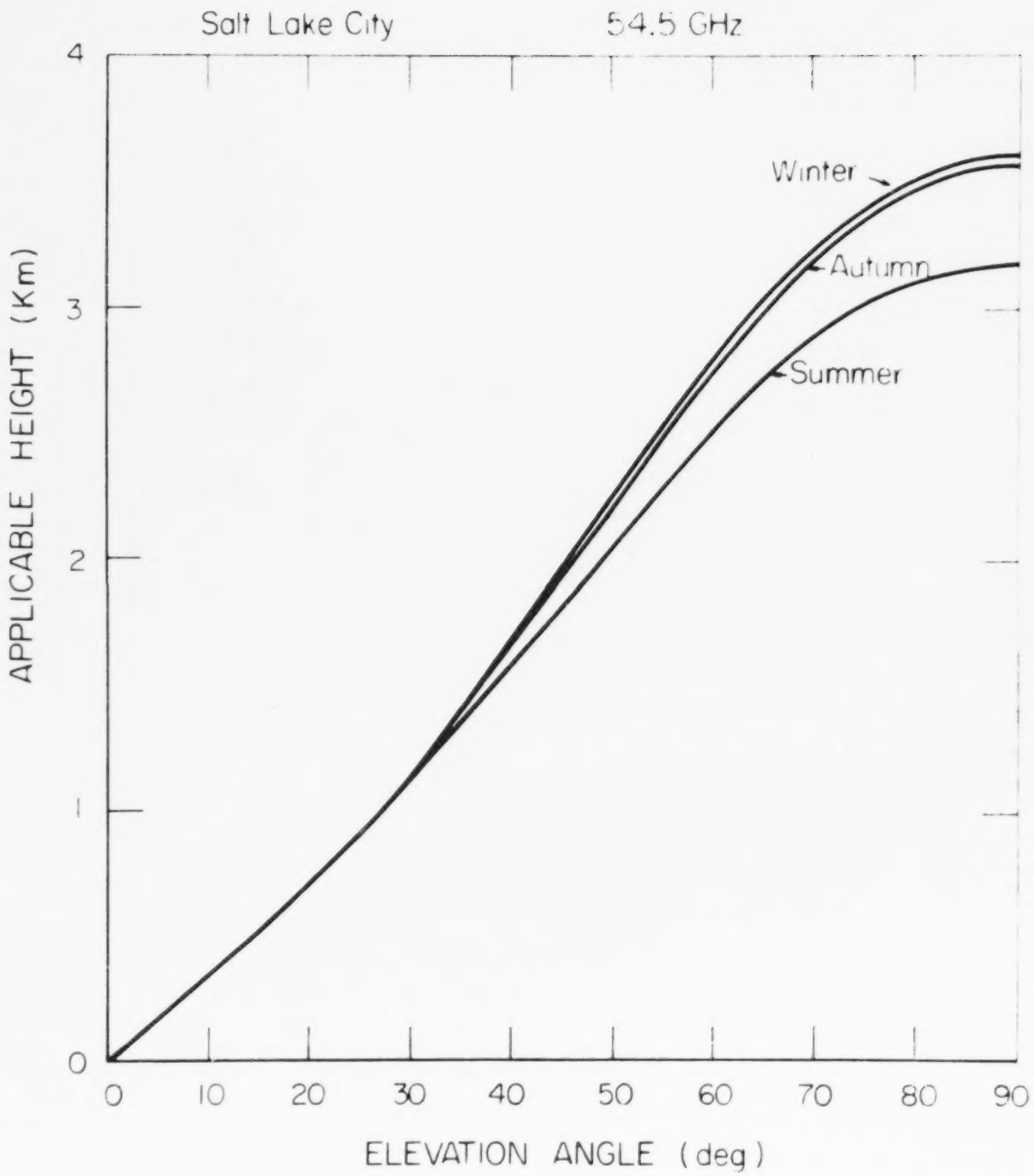

FIG. 9 Seasonal effects on applicable height vs elevation angle for Salt Lake City.

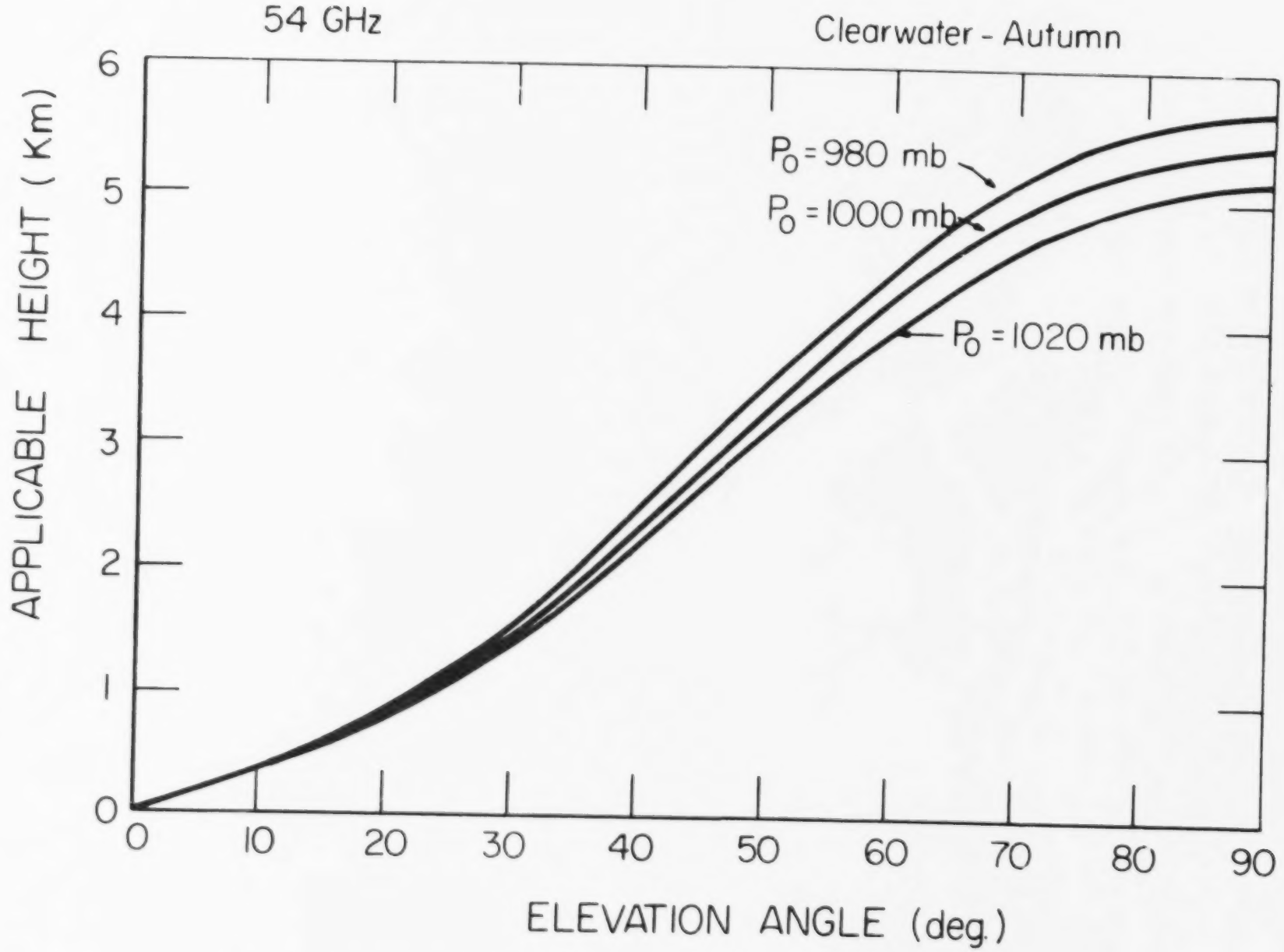

FIG. 10 Synoptic pressure effects on applicable height vs elevation angle in the autumn season for Clearwater, Florida.

location, is nearly 2.3 km at 54 GHz and 90° elevation angle. As in the seasonal effects, this difference becomes small for elevation angles below 30 degrees. Also, this effect becomes larger or smaller if the operating frequency is lower or higher, respectively. As shown by the 1000 mb curve in Fig. 10, a linear interpolation is possible for intermediate surface pressures. It is not at all unreasonable to have surface pressure variations of 40 mb at any one location, hence these effects should be accounted for in routine daily observations.

2. NULL BALANCE RADIOMETRIC SMOOTHING

2.1 General - A radiometric brightness temperature is a decreasing exponentially weighted mean of the air temperature beginning at the antenna and extending along its line of sight out to a distance beyond which additional contributions are negligible. As shown theoretically in Appendix II, the radiometric response to a change in air temperature at a remote point will always be less than the actual change. Further, the radiometric response to a given temperature change becomes smaller as the distance to that change increases and as the magnitude of the change decreases. Thus, it is more difficult to radiometrically detect small changes that occur at greater heights in the actual temperature profile. These radiometric smoothing effects will be discussed for ground-based and elevated inversions. A nomogram correction for height and intensity of ground inversions will be presented along with a multi-frequency approach to measuring elevated inversions. All these results are derived from computer simulation of a radiometer operating in a null balance mode. Realistic temperature profiles are used to represent "actual" conditions. Previously derived applicable heights for Clearwater, Florida, are used to plot computed brightness temperatures at a height corresponding to each frequency and elevation angle in order to obtain the "radiometer profile."

2.2 Smoothing of Ground-based Inversions - From the lapse case in Fig. 11 it can be seen that the applicable heights apply quite well in the first two-to-three kilometers. At the top of the radiometric profile (5.5 km) the brightness temperature is two and a half degrees warmer than the actual. This is also true for the low-level, ground-based inversion in the same figure. Since

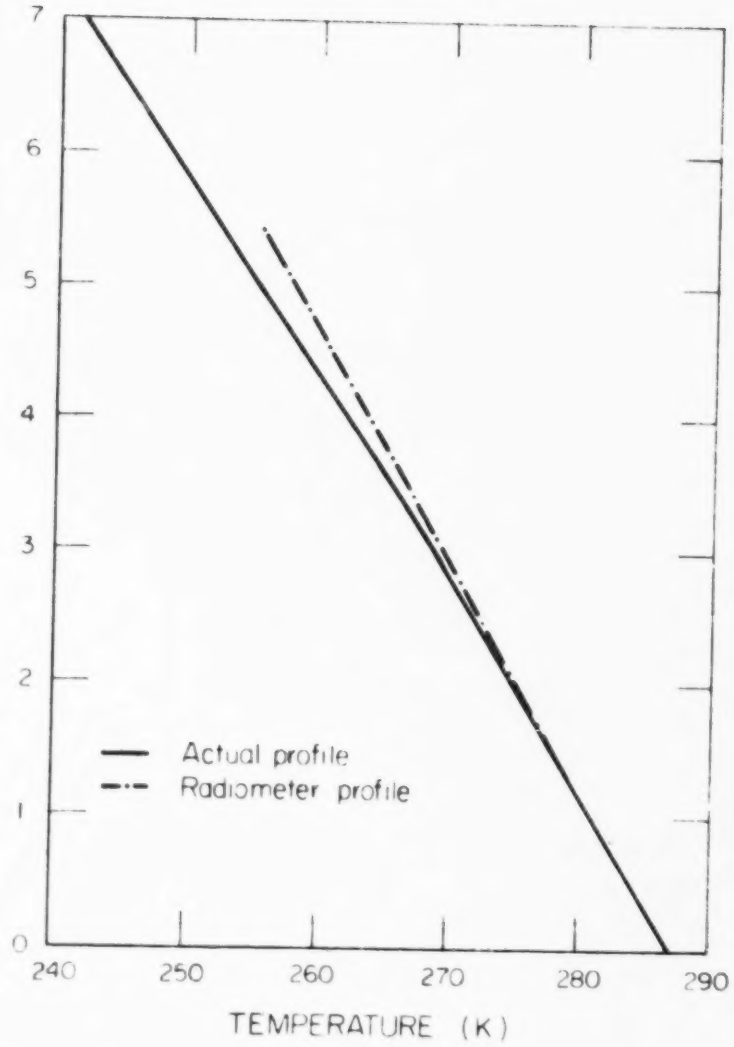

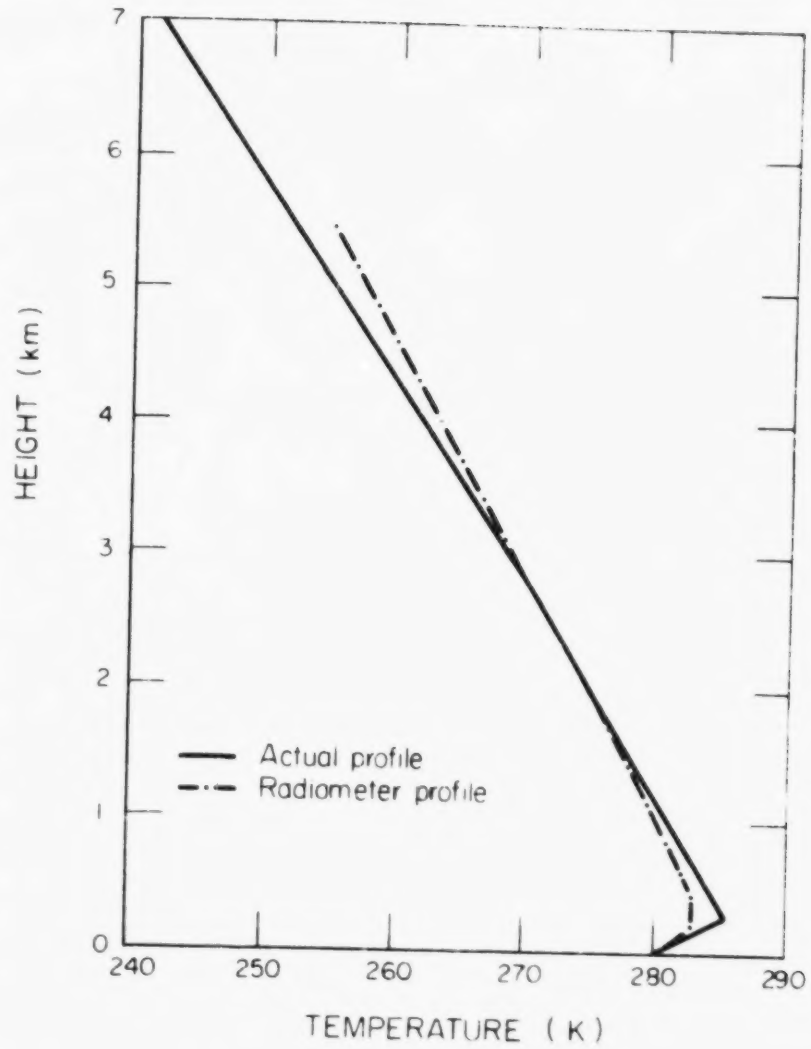

FIG. 11 Comparison of actual temperature profiles and computer simulated radiometric profiles for a lapse and ground-based inversion.

the interest here is on radiometric smoothing of ground inversions, the height axes are expanded in Figs. 12 and 13 to cover the range from 0 to 1.8 km so that the effects due to ground inversions can be amplified and better displayed. Also, only one of the radiometric profiles is plotted, although brightness temperatures were computed for 54, 54.5, and 55 GHz. The reason is that all three radiometric profiles fall very nearly on top of one another; the main difference is the height to which they extend. In other words, for every brightness temperature computed at one frequency and elevation angle, there exists a different frequency and angle combination that gives the same brightness temperature--provided, of course, that the temperature is within the range possible of measuring with both frequencies. In addition, those frequency and angle combinations having nearly the same brightness temperatures also have nearly the same applicable heights regardless of whether lapse, ground-based, or elevated inversions exist.

Figure 12 shows two ground-based inversions varying considerably in height and magnitude. The lowest inversion has a height of 0.05 km and magnitude of 5 C, whereas the other is nearly isothermal (±0.5 C) for half a kilometer. The computer-simulated radiometric profiles are typical of what is observed in practice. Note that for very low, intense, ground-based inversions, radiometric response to the temperature difference between the ground and the top of the inversion is about three quarters of the actual difference. Also, the height of the inversion suggested by that point on the radiometric profile that corresponds with the maximum radiometric deflection is higher than the actual height. However, for the weak but thick ground inversion, the radiometric response shows the beginning of the ground inversion; but that point indicating radiometric top of the inversion is considerably lower than the actual.

Figure 13 shows two profiles of ground-based inversions at the same height (0.5 km) but of two different intensities, namely 5 C and 10 C. The radiometric profile shows a response which is about half the actual intensity. Also, it can be seen that for thick ground-based inversions at the same height, the greater the intensity the more closely the radiometric height of the inversion corresponds with the actual height. Although a one-to-one correspon-

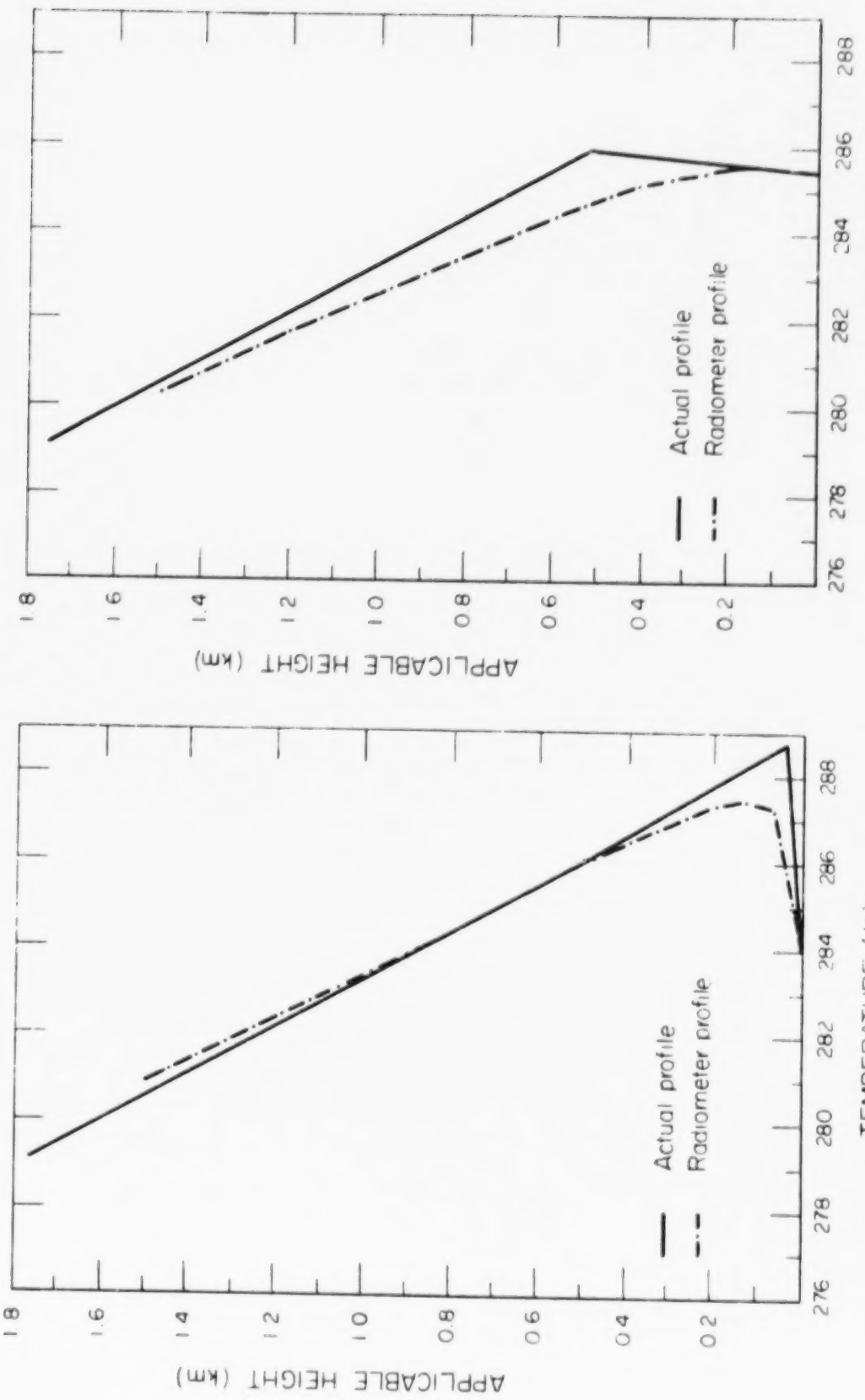

FIG. 12 Comparison of actual temperature profiles and computed radiometric profiles for a low strong and high weak ground-based inversion.

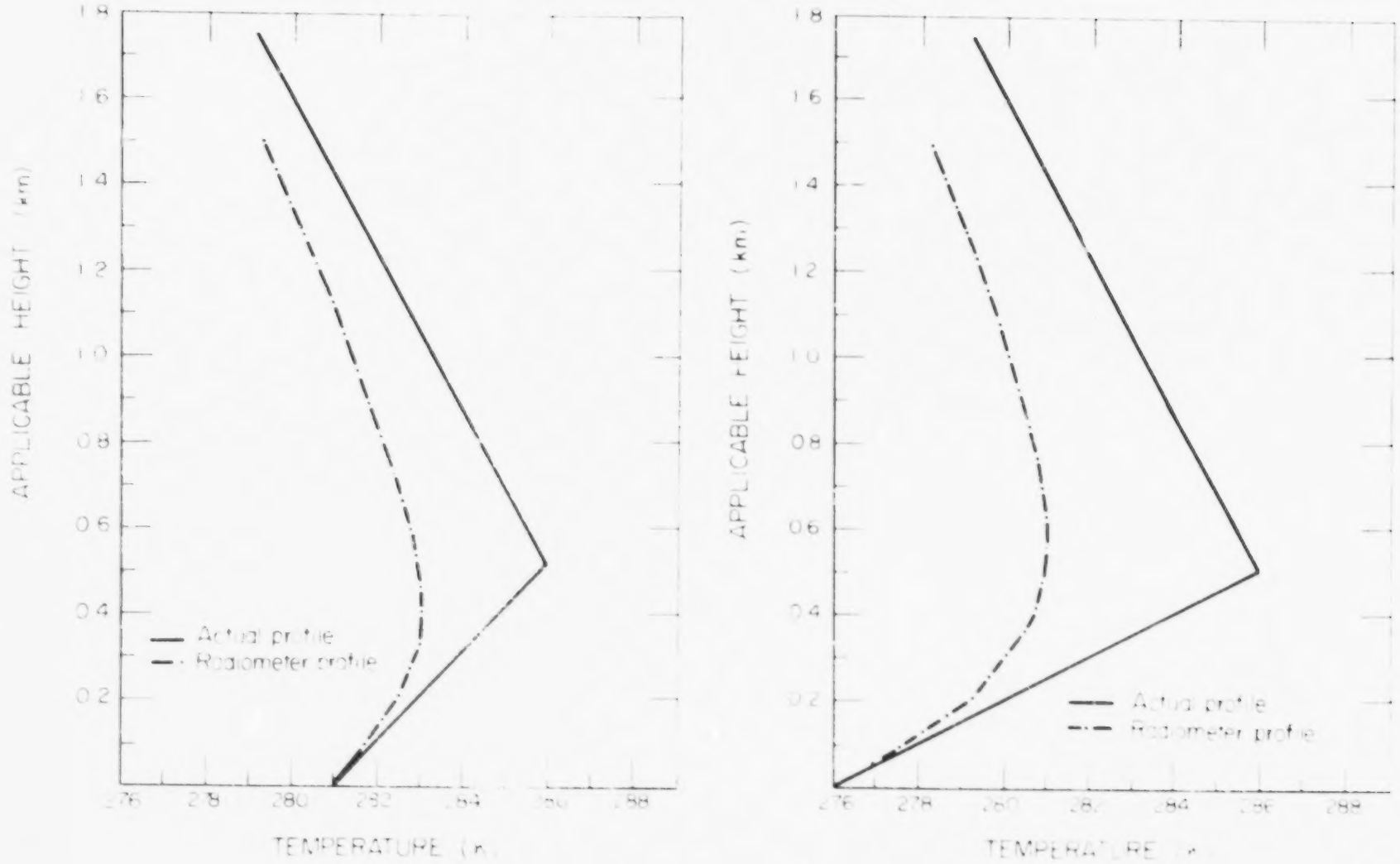

FIG. 13 Comparison of actual temperature profiles and computed radiometric profiles for ground-based inversions with the same heights but different intensities.

dence does not exist (and should not be expected to exist), there is sufficient systematic behavior that it should be possible to analytically account for this and obtain a more precise representation of the actual profiles.

2.3 Corrections for Ground-Based Inversion Smoothing - Computer simulations were used to derive the maximum brightness temperature and the antenna elevation angle where this occurred as a function of radiometric frequency and the height and intensity of ground-based inversions. A large number of computations had to be made in order to develop a reasonable sample of the different heights and intensities of ground-based inversions that can exist in the atmosphere. Upper and lower constraints were imposed, as follows:

1) The maximum and minimum intensities considered for each height of the ground inversions were 10 C and 5 C, respectively.

2) The lowest and highest top of the ground inversions considered for each intensity were 0.04 and 0.5 km, respectively. There were 11 different intensities and 13 different heights of ground-based inversions considered, giving a total of 143 ground-based temperature inversion cases. The brightness temperatures were computed in unit increments of elevation angle for every case and the computer selected and outputted the first angle where the brightness temperature had a maximum positive deflection with respect to that obtained at a zero-degree elevation angle. As often happens, there may be two or more brightness temperatures of equal value at successive angles. In the interest of eliminating this ambiguity of determining which angle should be used, the lowest elevation angle corresponding to maximum increase in brightness temperature was selected. For the weak ground inversions where the radiometric temperatures may only be isothermal before decreasing with increasing elevation angle, the angle corresponding with the topmost isothermal point was outputted.

Figure 14 shows the nomogram resulting from simulating null balance radiometric data for 143 ground-based inversion cases at 54.5 GHz. In all these cases the surface pressure was held constant at 1000 mb, so use of this nomogram at any particular location may require accounting for pressure altitude and/or surface pressure variations. At each intersecting point of maximum change in brightness temperature and corresponding elevation angle, the actual height and intensity of the ground inversion used in the computation was plotted. After

plotting the output from each case, a smoothed-line best fit was subjectively drawn to give isopleths of actual temperature intensity and height of ground inversions. Considering Fig. 14, if the maximum measured increase in brightness temperature were 2 C and occurred at an elevation angle of 7°, this would correspond with an actual inversion intensity of 4 C with the ground-based inversion top at 0.15 km. From the nomogram, it can be seen that the actual intensity of the inversion is always greater than that measured radiometrically. Likewise, the interrelationships are by no means linear. In general, the more intense the ground inversion, the less sensitive is the relationship to small errors in angle or brightness temperature. Weak ground-based inversions present the greatest difficulty. Not only is the increase of brightness temperature close to the noise level but, also, a small error in determining the appropriate elevation angle represents a large error in defining the top of the inversion. Recalling that these data were derived for a null balance mode of operation, it can be seen that many observations would be required at a large number of discrete angles to insure adequate angular coverage to provide the desired height resolution. All the experimental data gathered during ground inversions, however, were obtained while operating in a non-null balance continuous angle-scanning mode. The advantage of this is that a continuous trace of brightness temperature is obtained as a function of elevation angle at the sacrifice of introducing the effects due to the equipment integration circuit and unbalanced equipment noise. A verification of this nomogram is presented after the discussion of angle-scanning effects. At this point it is sufficient to say that the results are very good.

2.4 Null Balance Smoothing of Elevated Inversions - Computations of null balance radiometric brightness temperatures were made as a function of frequency and elevation angle for different elevated inversions. Elevated inversions of 5 C intensity were simulated with bases at 0.5, 1.0, and 1.5 km, each having a thickness of .25 km. The temperature profiles used in the computations, along with the derived radiometric profiles, are shown in Fig. 15. Again, results were identical when the brightness temperatures from many frequencies ranging between 53.5 to 60 GHz were translated to the applicable height corresponding to the appropriate elevation angle. Here again, the only difference was the depth of penetration as a function of frequency.

These analytical results are rather typical of the experimental results

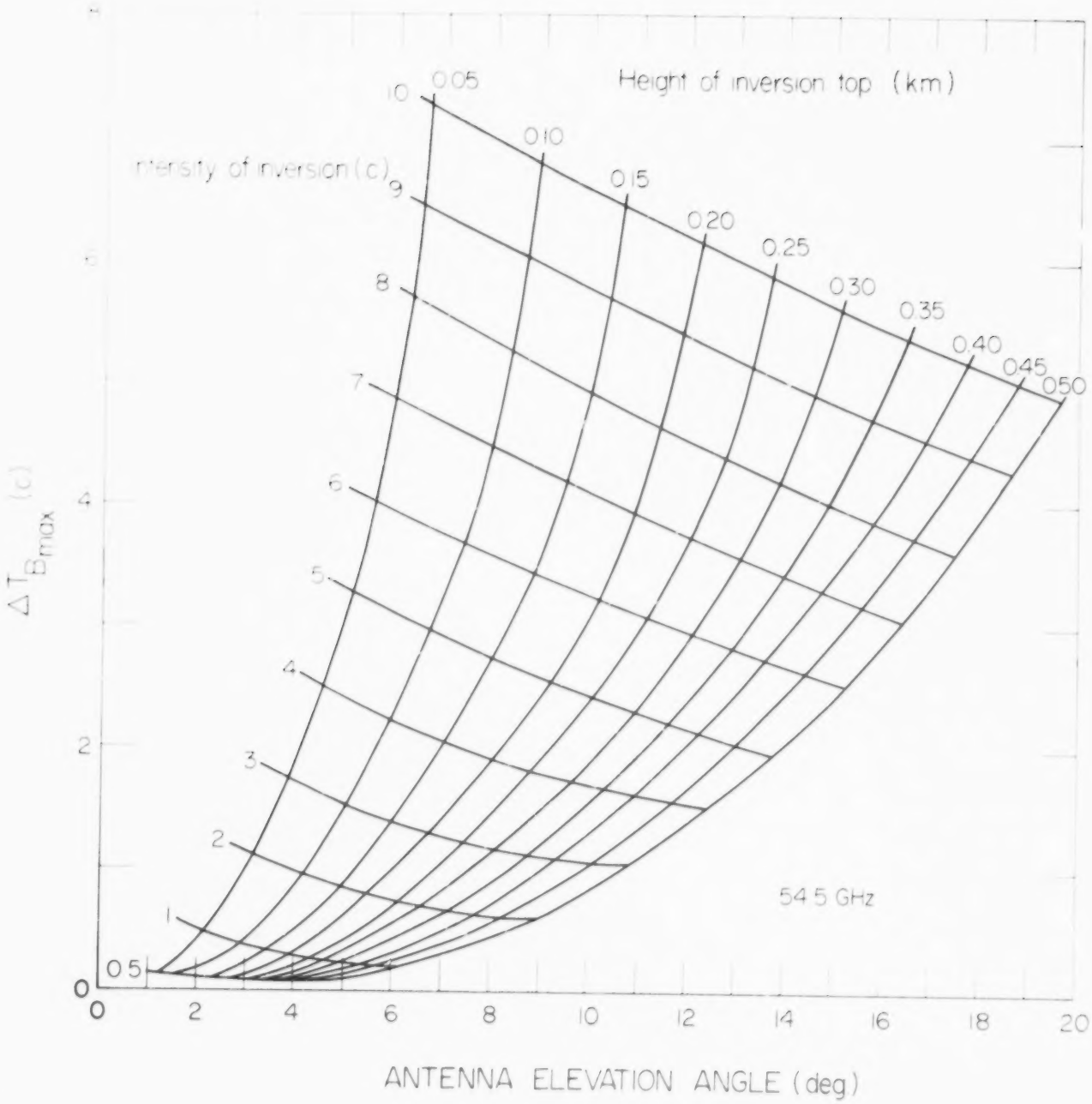

FIG. 14 Nomogram for translating null balance radiometric data at 54.5 GHz to obtain height and intensity of ground-based inversions. This relationship was derived for a station pressure of 1000 mb.

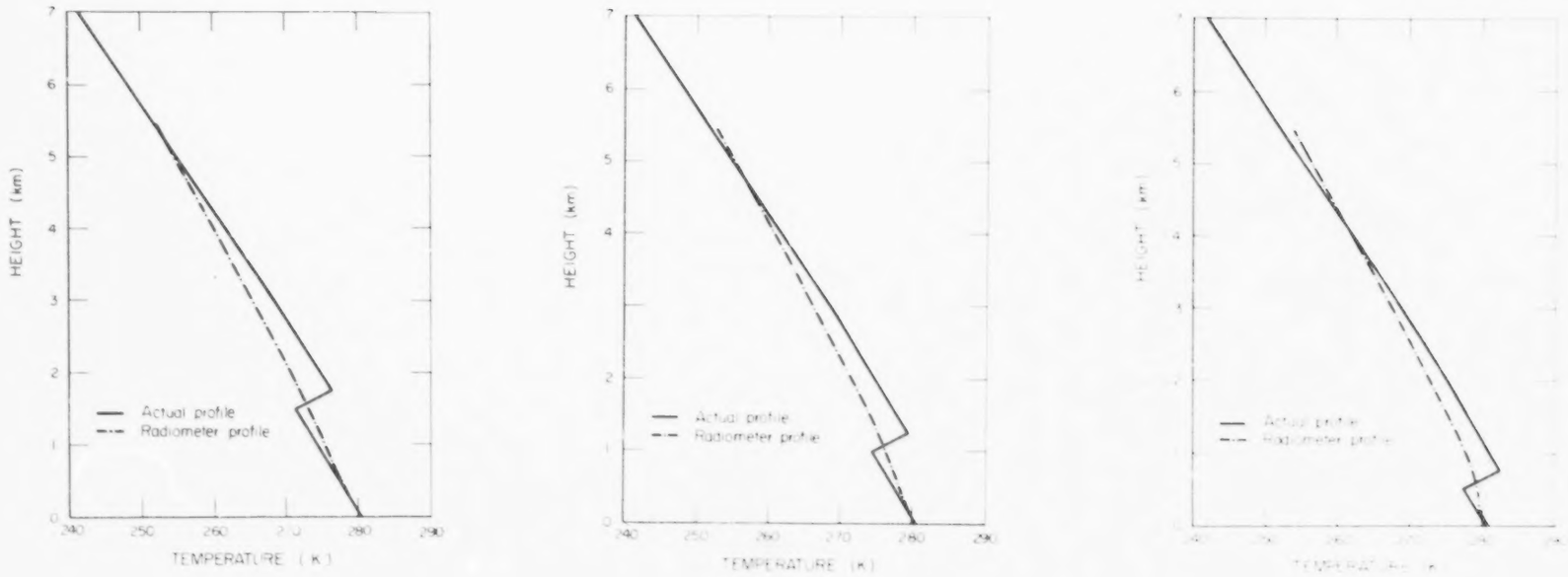

FIG. 15 Comparison of actual temperature profiles and computer simulated radiometric profiles for elevated inversions.

when analyzed using the applicable height translation scheme. That is, the radiometer operating at a fixed frequency and scanning in elevation angle shows the beginning of the lapse profile in the lowest layers; it then becomes more stable and smoothis out, but passes through the elevated inversion region in each case. The gradient changes in signal response decrease as the height of the elevated inversion increases. In practice, however, there appears to be more of a radiometric response than that obtained by the computer simulation. The simulated results also showed that at no single frequency did the brightness temperature increase with elevation angle for these particular cases. That is, although there was a change in slope of the brightness temperatures the slope never became positive, as it did in the actual profiles.

Another possible equipment mode of operation was investigated by computer simulation, namely, a vertically pointing antenna with null balance or absolute temperature measurements at many frequencies. These results are presented in Fig. 16 for lapse, ground-based, and elevated inversions. The intensity of all the inversions was 5 C, with the top of the ground inversion at .25 km, the base of the two elevated inversions at 0.5 and 1.5 km, and their corresponding tops at .75 and 1.75 km. Brightness temperature information was obtained for frequencies from 53.75 to 60 GHz; however, only the frequency range between 54.60 and 58.32 GHz showed the interesting character associated with the ground and elevated inversions. In fact, at the higher end of the band there was only 0.016 C difference in brightness temperatures between 58.32 and 60 GHz.

Figure 16 was constructed to depict as clearly as possible the differences in the character of the radiometric data obtained from the several different types of temperature profiles. Brightness temperatures were computed at each frequency for 90° elevation angle. If the brightness temperatures were plotted linearly as a function of frequency, the slope of the linear lapse profile would appear curved because depth of penetration is not linear with frequency. For this reason, the height at which the brightness temperature at each frequency corresponded to the air temperature of the lapse profile (i.e., the applicable height for that frequency at 90° elevation angle) was used to determine the point of the linear applicable height abscissa at which the computed brightness temperatures were plotted. Thus, the applicable height at

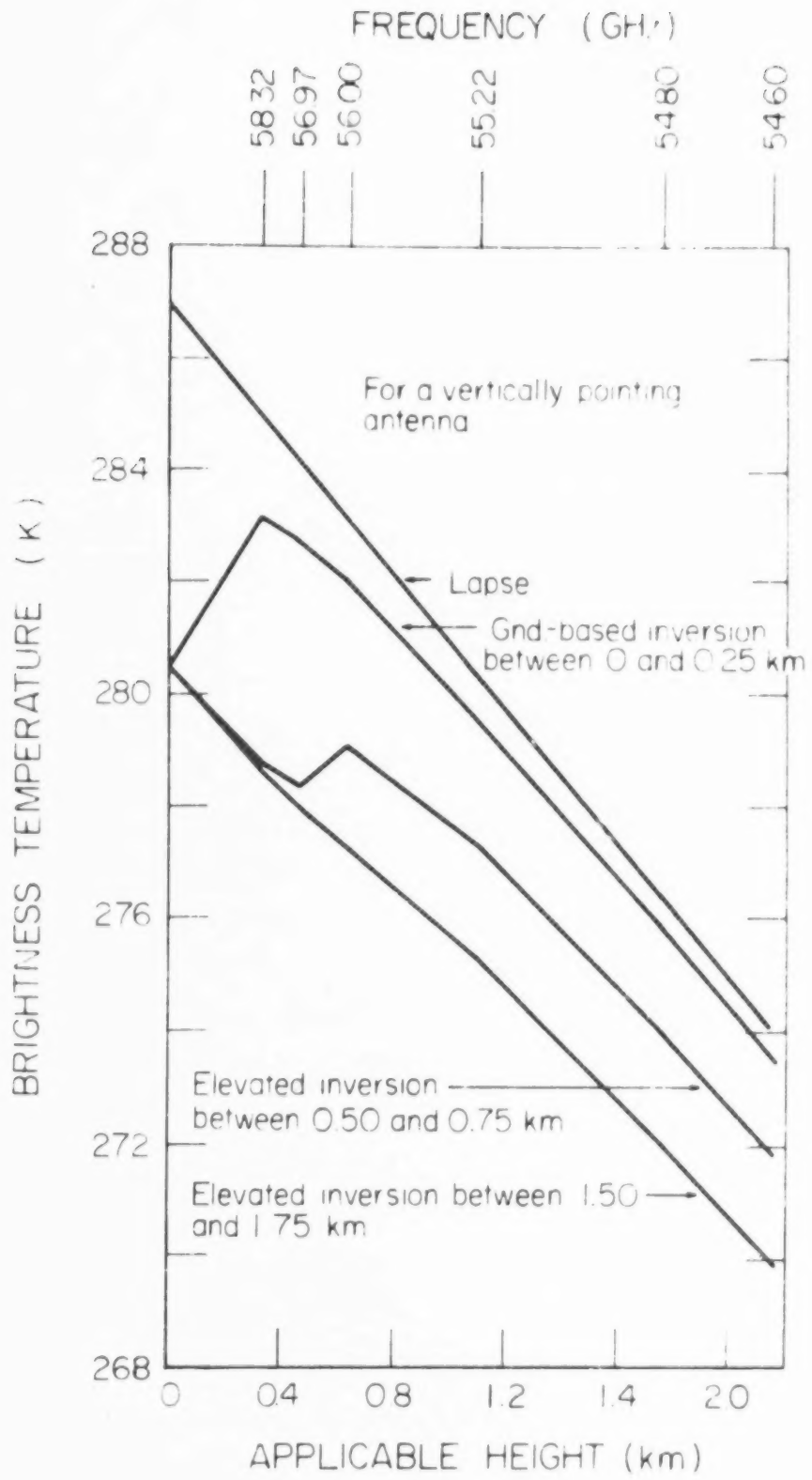

FIG. 16 Comparison of calculated brightness temperatures vs frequency and corresponding applicable heights for a lapse, ground inversion and two elevated inversion temperature profiles.

58.32 GHz and 90° elevation angle was 0.33 km and the computed brightness temperature at this frequency and elevation angle for each profile was plotted at that height. The same procedure was applied to the remaining five frequencies. No frequency yields a measure of the surface temperature for a vertically pointing antenna, but if the radiometer were pointed horizontally then a surface air temperature would be obtained--hence the actual surface air temperature is plotted at 0.0 km in Fig. 16.

The most striking features in Fig. 16 are associated with the inversion cases. There is no doubt that the ground inversion with a top at 0.25 km and the elevated inversion with base and top at 0.5 and 0.75 km are detected. In fact, it was only via the vertically pointing multi-frequency mode that the indicated temperature gradient was positive for the elevated inversion case. The magnitude of this analytically derived temperature increase was 0.7 C.

In contrast with the results for the ground-level and low-level elevated inversion case are the results for the higher-level elevated inversion. The radiometric profile for this case differs only slightly from that of the lapse case. Consequently, the problem of discriminating between a high elevated inversion and a lapse profile remains rather difficult.

From the results of this limited simulation experiment, it appears that the variable-frequency, fixed-angle mode shows considerable promise of being able to differentiate the characteristics of lapse, ground-based, and low-level elevated inversion profiles, and to do this with probably greater accuracy than achievable with the fixed-frequency variable angle mode. However, the equipment specifications and the operator skill required to implement this mode of operation are considerably more difficult to realize than those required for a fixed-frequency angle scan mode of operation--the most severe of these requirements being the accuracy of frequency calibration and its long-term stability.

3. ANTENNA ELEVATION ANGLE SCANNING EFFECTS

3.1 Simulated Angle Scanning of Lapse Profiles - Brightness temperatures computed from any given profile simulate measurements in the null balance mode of operation which is equivalent to a zero-degree-per-minute antenna scan rate.

This assumes that absolute brightness temperature observations are made at each frequency and/or elevation angle; however, the radiometer may be operated in a mode where the frequency is fixed and the antenna is scanned continuously from the horizontal to the vertical, or vice versa. Most of the experimental work reported here is for the angle scanning mode; therefore another computer program was written to simulate the temperature output from a radiometer operating at a fixed frequency, fixed time constant, and constant scan rate. The results obtained for a simulated scan from the horizontal to the vertical under lapse conditions for 54 and 54.5 GHz, 4- and 10-degrees-per-minute scale rates, and a one-minute integration time (30-second time constant) are presented in Fig. 17. The null balance results (zero-degrees-per-minute scan rate) are presented for comparison. It can be seen that the warmer brightness temperatures sensed at lower elevation angles are displayed by the filter circuit at higher elevation angles--the result being that the output temperatures are always warmer for a lapse profile than for those obtained via null balance. The temperatures differ by an amount proportional to the scan rate. There is also a frequency effect such that lower frequencies produce larger deviations. This is the result of brightness temperatures having a greater change with angle at lower frequencies; it can be seen that the effects at 54 GHz are about double those at 54.5 GHz. For any given frequency, the variable scan rate curves in Fig. 17 are common at the point where the scan begins, diverge rapidly, and maintain a fairly constant difference as angle changes from 10 to 80 degrees, and begin to converge at the top of the scan between 80 and 90 degrees. It is desirable to have a long-time constant to minimize equipment noise and a fast scan rate to minimize atmospheric variations during any particular sounding. However, if these parameters are too large, considerable distortion is introduced in the indicated brightness temperature. The computational results in Fig. 17 show that the indicated brightness temperatures are expected to differ from null balanced data by 1 K and 2 K at 4 and 10 degrees per minute, respectively, at 54 GHz. At 54.5 GHz and 4 degrees per minute, where most of the experimental data were gathered, the difference in brightness temperature amounted to 0.5 K.

3.2 Observed Effects of Scan Rate on Lapse Profiles - A sequence of experimental runs at one frequency (54.5 GHz) was made at Sudbury, Massachusetts,

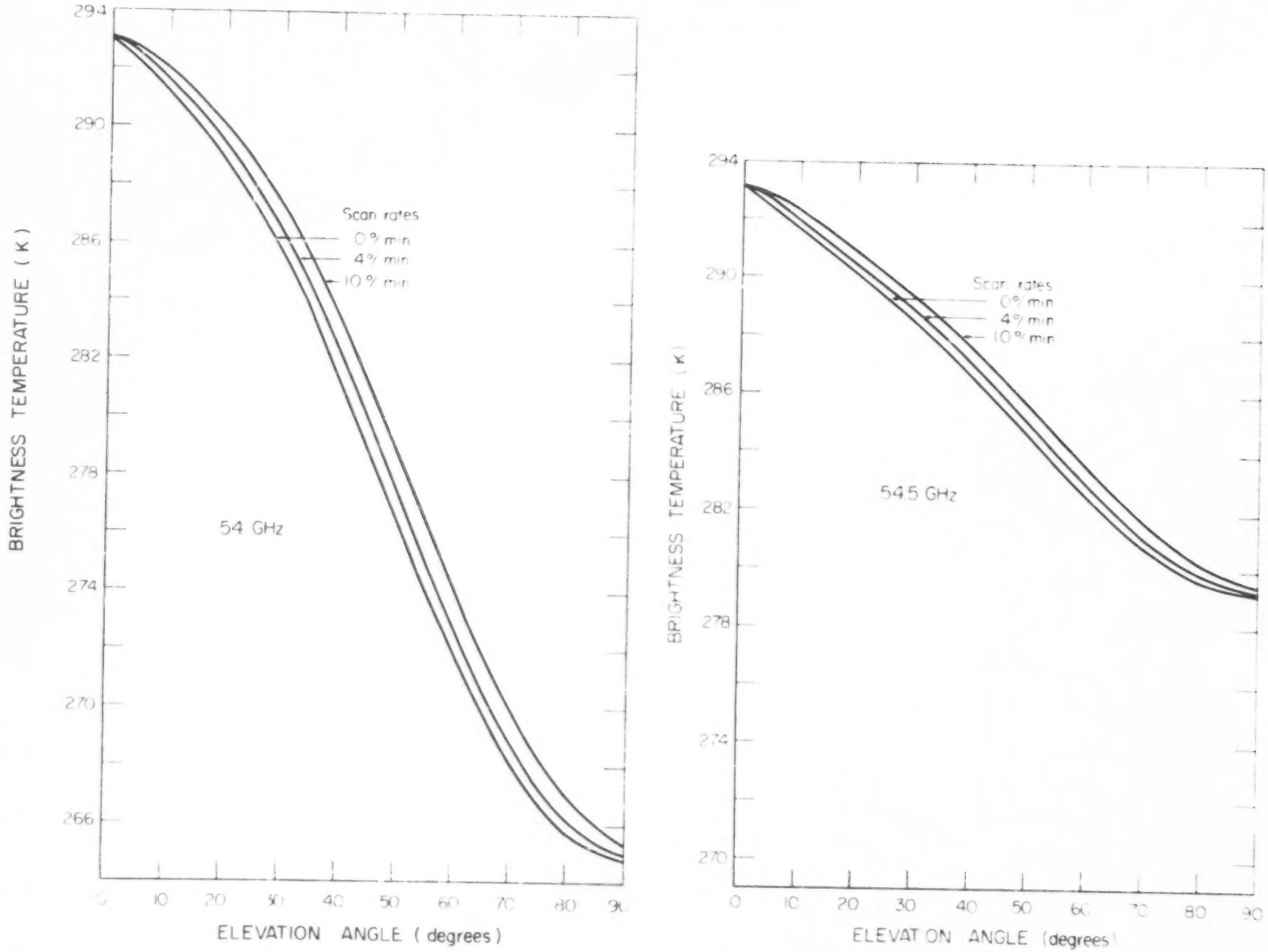

FIG. 17 Results of a computational simulation of the effects of different angle scan rates on the radiometric record of a lapse profile.

for upward scanning at the rate of 8.2, 3.8, and 1.8 per minute. An integration time of one minute was used for all runs. Later the same day, 1969 August 26, another sequence of three upward scans was completed over about the same time interval of 1½ hours. This time both the frequency (54.5 GHz) and the scan rate (4°/min) were held constant in order to observe variations due to equipment and atmospheric changes. These results along with a morning and afternoon on-site RAOB are presented in Fig. 18. In all cases the relative brightness temperatures were plotted such that the surface temperature corresponded with that from the RAOB nearest in time. The curves produced by the variable scan rate are consistent in the lower portion of the profile with computer-simulated results, being increasingly warmer than the RAOB as scan rate was increased. In this lower portion of the profile there is about 0.6 C difference between temperatures measured at 1.8 and 8.2 deg./min. The curves cross over in the mid-portion of the profile and reverse at the top, with the slowest scan temperatures being the warmest. Although the effects due to scan rate are detectable, their relative magnitudes were found to be small when compared with natural atmospheric and equipment variations as shown by the fixed scan rate curves in Fig. 18. Therefore, at this time it appears difficult to assess the extent to which the simulated results can be used to account for radiometric temperature differences obtained at variable scan rates. This is especially true when relative brightness temperatures measured over a 1½ hour time period have to be compared with a single RAOB.

3.3 Simulated Effects of Scan Rate on Ground Inversions - Again a one-minute integration time and scan rates of 0°/min., 4°/min., and 10°/min. were used to simulate what should be expected experimentally for ground-based inversion conditions. Brightness temperatures computed at 54.5 GHz on a ground-based inversion with a height of 0.42 km and intensity of 5 C are plotted as a function of elevation angle in Fig. 19. First, it can be seen that the maximum increase in brightness temperature occurs at higher elevation angles for higher scan rates. In other words, the radiometric response to the actual maximum air temperature is delayed by the filter circuit and displayed at higher angles for the faster scan rates. Second, the magnitude of the radiometric response decreases as the scan rate increases. Third, temperatures are always colder for higher scan rates for angles below that at the maximum radiometric tem-

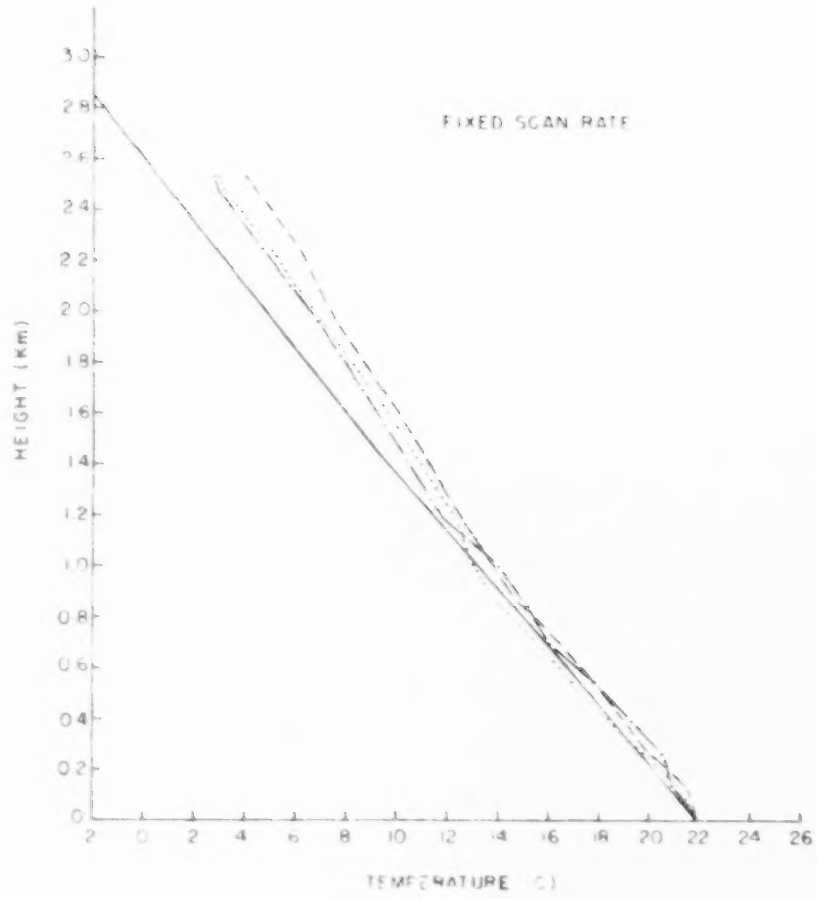

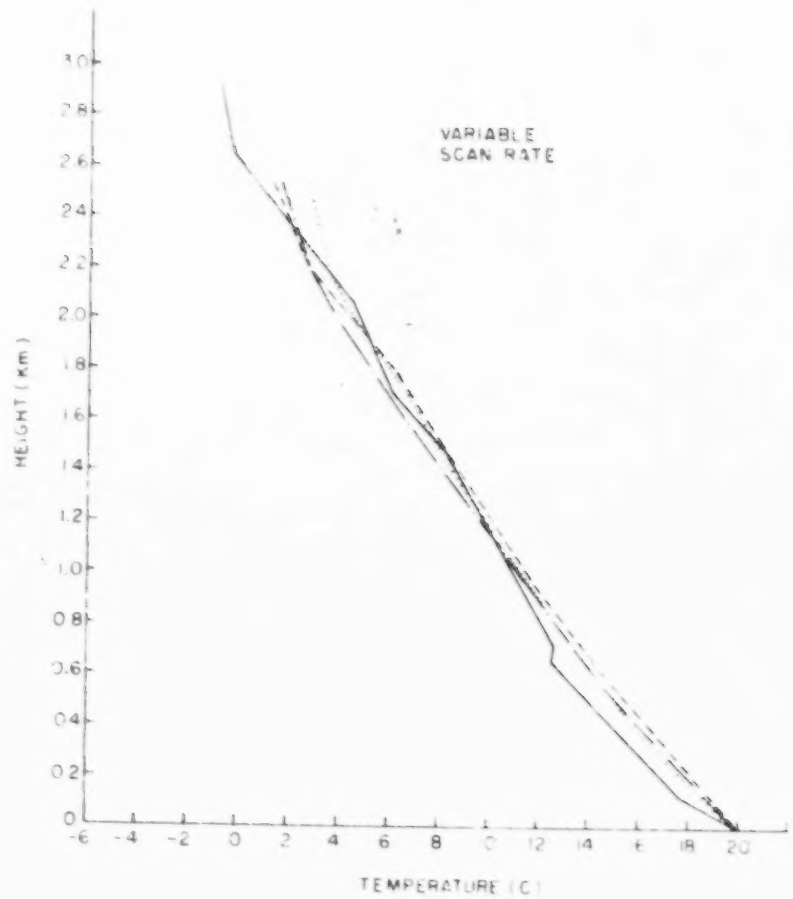

FIG. 18 Comparison of a series of upward angle scans, Sudbury, Massachusetts, 1969 August 26, where three successive scans are made at a fixed rate (4^{o}/min) and one each at a different rate (1.8, 3.8, and 8.2^{o}/min).

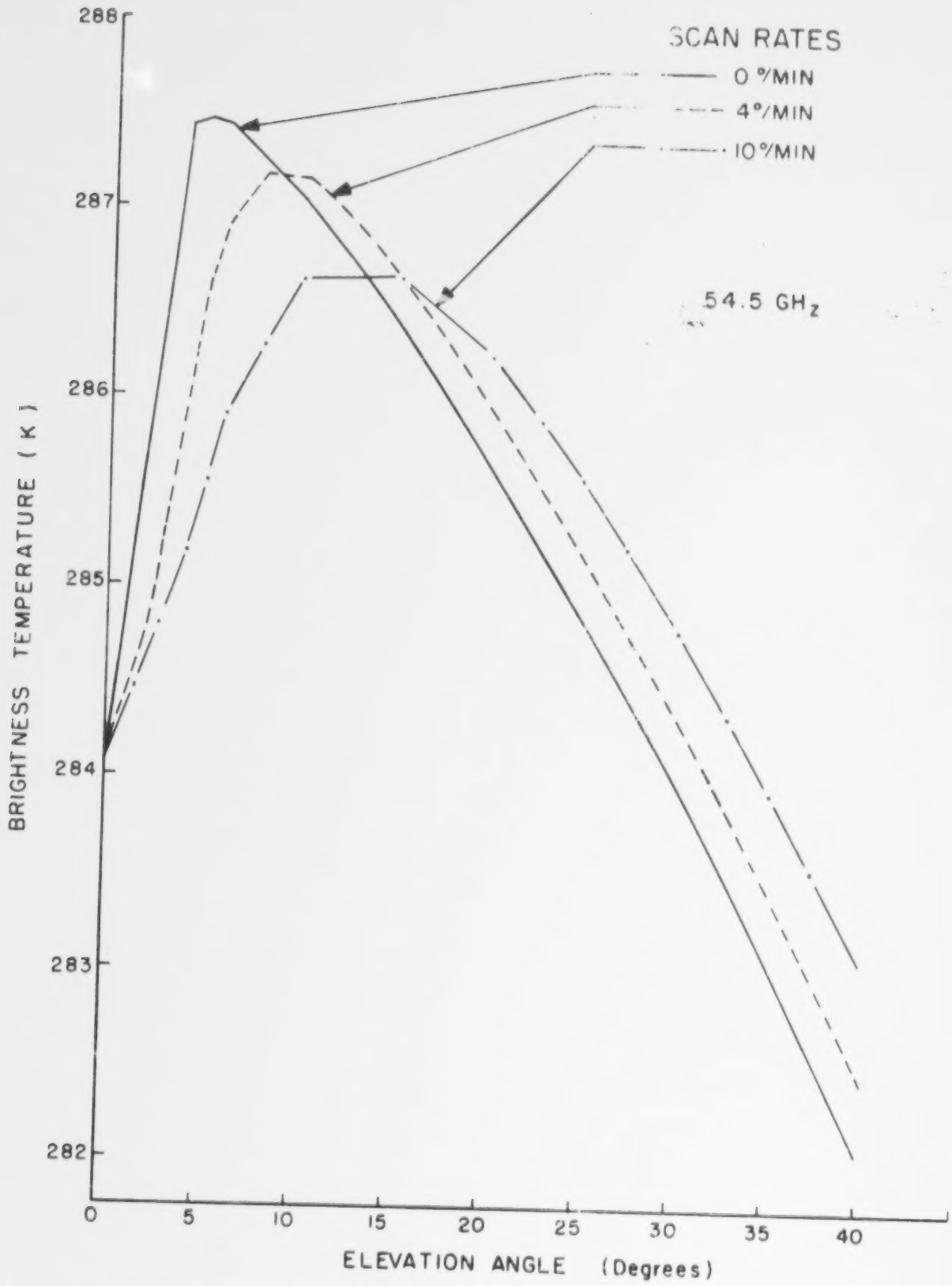

FIG. 19 Computer simulation of the effects of angle scanning on the radiometric record during a ground inversion.

perature, whereas the reverse is true for angles above the maximum point. Figure 20 shows the effects due to frequency and scan rate variations for a ground-based inversion with an intensity of 5 C and a height of 0.25 km. In this figure the brightness temperatures are plotted at the applicable heights that correspond with the various frequencies and elevation angles. Theoretically, the radiometric curves should be smooth, but the discrete angle computation accounts for their broken nature. In all cases, the curves were extended to only about 1.2 km in order to present the frequency and angle scan effects on the same scale and with sufficient amplification to distinguish salient features. It is easy to see from Fig. 20 that the lower the frequency the greater the dispersion among the curves. In all cases, the indicated radiometric height of the inversion increases as the scan rate increases--the difference between that for null balance and that for 10°/min. curves at 55 GHz being 0.12 and 0.3 km at 54 GHz. The results show that considerably different radiometric responses are obtained--for different scan rates and frequencies during ground-based inversions.

3.4 Observed Effects of Scan Rate on Ground Inversions - Figure 21 shows two different ground inversion cases where radiometric observations were taken at the same frequency (55 GHz) with consecutive runs made at different scan rates. Each scan is plotted to only 0.5 km, but from this height on up to 1.4 km the radiometric sounding progressively diverged with a maximum difference at the top ranging between 1.5 C and 3 C warmer than the observed profile. Observations on 1968 September 19 were made during the early evening, whereas those on the 20th were made during early morning hours. For each day, it can be seen that the height of the inversion is best defined by the 3 and 4°/min. scans and that the 10°/min. scans consistently depict too high an inversion. Both simulation and experimental data dictate that scan rate and frequency must be considered in order to properly interpret radiometric observations.

4. SCAN RATE AND NOMOGRAM VERIFICATION ON GROUND INVERSIONS

4.1 Results from Clearwater, Florida - Only ground inversions that existed at Clearwater, Florida, were considered in these analyses because both the nomogram and the scanning rate study were accomplished using surface pressures typical at sea level stations. Eight cases of ground inversions

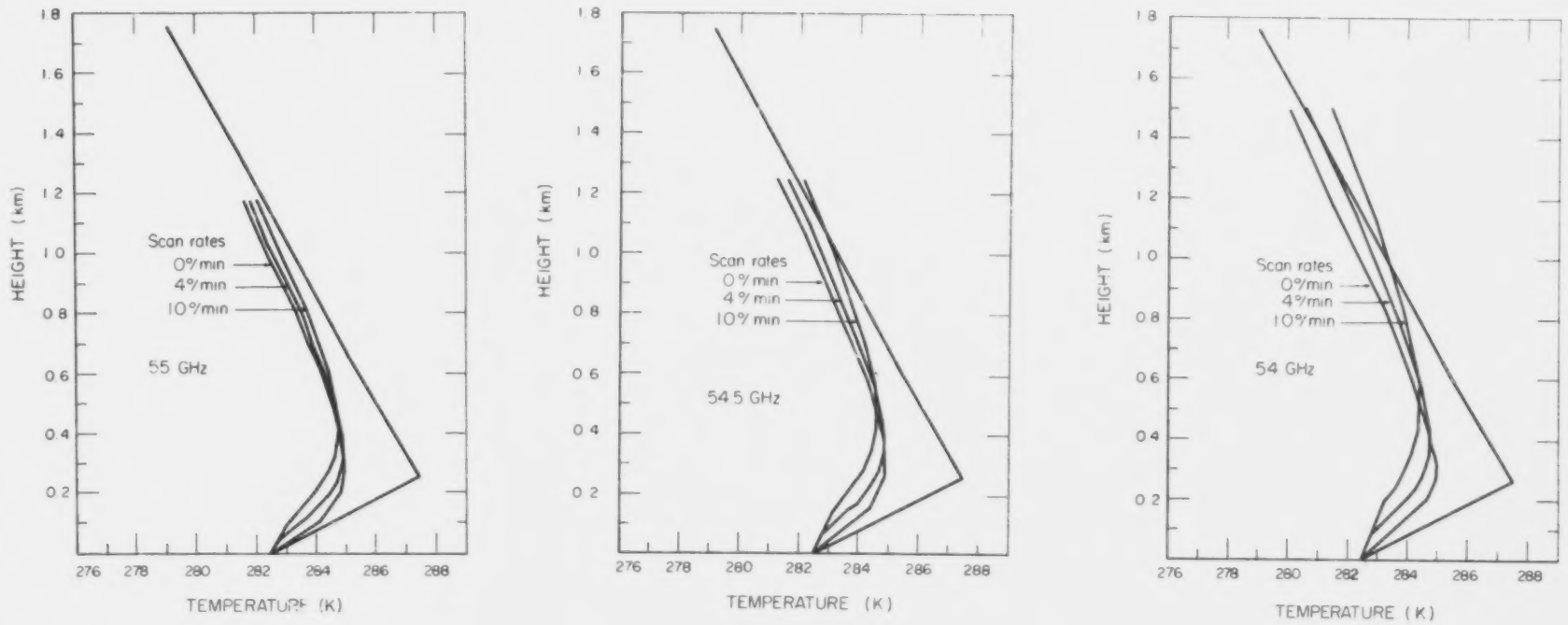

FIG. 20 Simulation of the effects of different frequencies and angle scan rates on the radiometric record of a ground inversion.

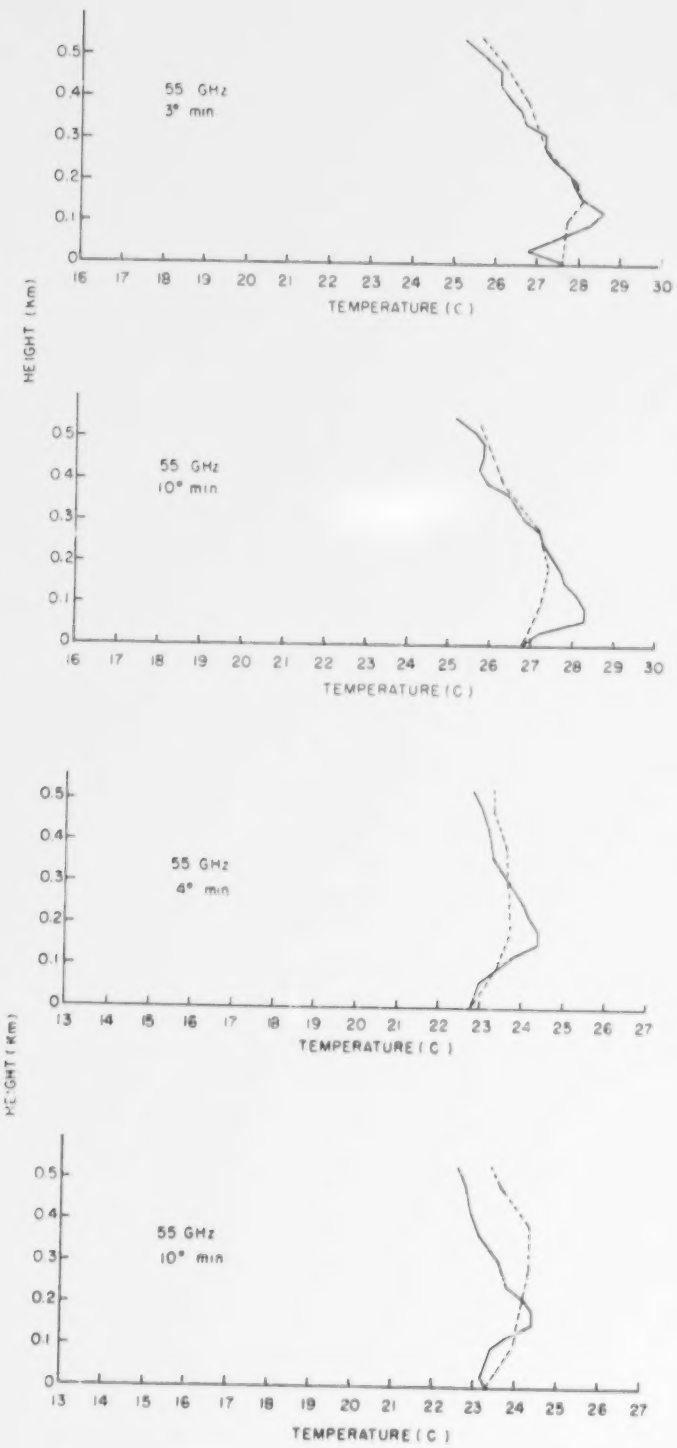

FIG. 21 Experimentally observed effects of angle scan rate on ground inversions.

ranging in height from 0.06 to 0.28 km and in intensity from 1.5 to 6.8 C constitute the data sample. Mostly helicopter soundings were available, but one case was verified with RAOB data. The height and intensity of the inversions were predicted three ways: 1) using the null balance derived applicable height concept, 2) correcting this by using the null balance derived nomogram, and 3) correcting for the scan rate and then using the nomogram. Two cases were observed at 54.5 GHz and the remainder at 55 GHz, with scan rates ranging between 2 and 10°/min. The observed intensity of the ground inversion was obtained by subtracting the surface measured temperature from the maximum positive temperature. The height of the inversion was taken at the point corresponding with the maximum temperature. In the analysis of the radiometric data the height of the top of the ground inversion was defined as that point in the scan where the maximum radiometric temperature first occurred. The results are summarized in Table I. Values shown in the table are averages (over the eight cases available) of differences between quantities predicted by each of the three radiometric techniques and similar quantities measured from direct sounding data. The particular quantities are intensity difference, absolute value of intensity difference, height difference and absolute value of height difference.

TABLE I

Ground-Based Inversion Prediction Quality
(Average Differences for Eight Cases)

Quantity	Method		
	Uncorrected Applicable Height	Applicable Height Plus Nomogram	Scan Corrected Applicable Height Plus Nomogram
Intensity Dif.	- 1.7 C	+ 0.5 C	- 0.2 C
Absolute Intensity Dif.	1.7 C	0.9 C	0.6 C
Height Dif.	+ 0.05 km	+ 0.12 km	- 0.03 km
Absolute Height Dif.	0.07 km	0.14 km	0.06 km

The best performance is realized when corrections are made for both the scan rate and non-linear relations presented in the nomogram.

5. ANGLE SCANNING DETECTION OF ELEVATED INVERSIONS

5.1 Computer Simulation Results - The computer program that simulated fixed-frequency angle scanning radiometric output was used to investigate the character of brightness temperature profiles for upward and downward scanning. Figure 22 shows what is analytically expected at a fixed-frequency (54.5 GHz) and integration time (60 seconds) scanning up and down at two rates (4 and 10 degrees per minute) under lapse conditions. It can be seen from Fig. 22 that at no time is there a crossover between the up and down scan profiles for lapse conditions. Also, the higher the scan rate the greater the separation between the radiometric profiles. In all cases the computer simulations do not include fluctuations in the radiometric profiles due to either equipment or atmospheric turbulence effects.

As previously shown, the filter circuit displaces and smooths temperature discontinuities such as ground and elevated inversions. The direction of the displacement and its magnitude are related to the degree of discontinuity and the direction from which it is scanned. For example, in ground-based inversions an upward scan indicates brightness temperatures that are colder than they would be if the radiometer were not scanning. On a downward scan, the warmer brightness temperatures are carried downward in elevation so that the outputted brightness temperatures are warmer than they would be if the radiometer were not angle scanning. The extent to which this effect can contribute to the detection of the existence of elevated inversions was investigated at only one frequency (54.5 GHz) and two scan rates, 4 and 10 degrees per minute for two elevated inversions based at 1.0 and 1.5 km.

Figure 23 shows the up-down scanning computer simulation results for 5 C-intensity elevated inversions. Notice that for the 1 km elevated inversions, the 10°/min. downward scan curve crosses over the upward scan trace slightly below the elevated inversion. At the slower scan rate no such crossover existed for this elevated inversion. Also, at the higher elevated inversion it is more difficult to obtain a discernible radiometric response. It can be seen at this one frequency and two scan rates that no clue as to the presence of the 1.5 km elevated inversion was obtained. The radiometric response that would be obtained at other frequencies and scan rates to interrogate these

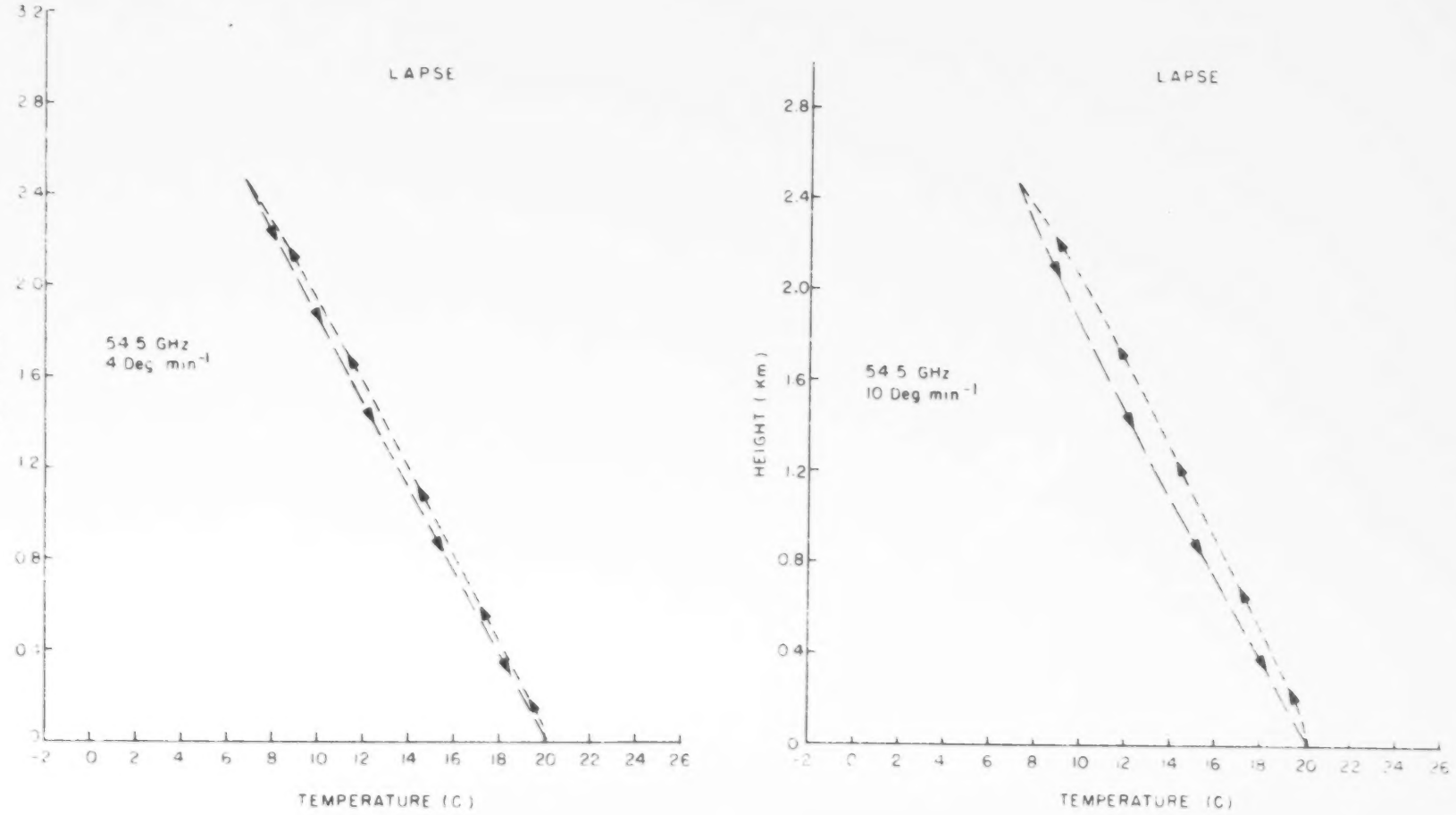

FIG. 22 Computer simulated up-down angle scans of a lapse profile.

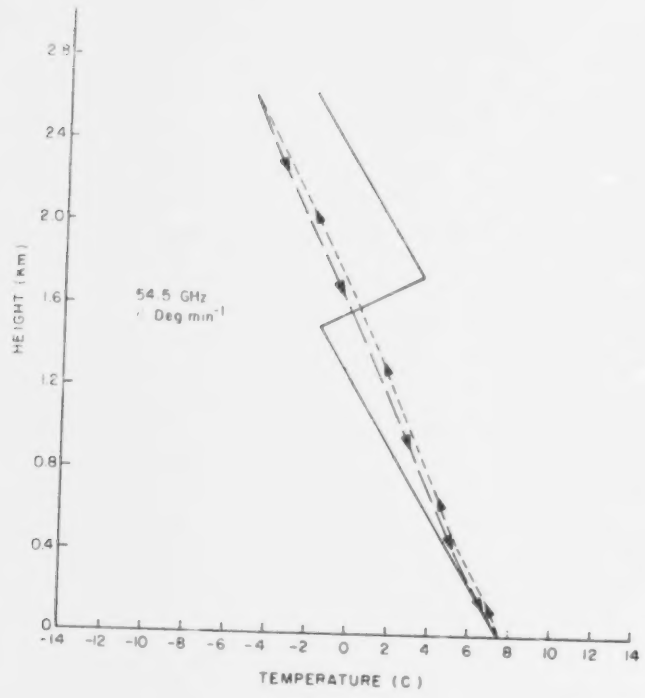

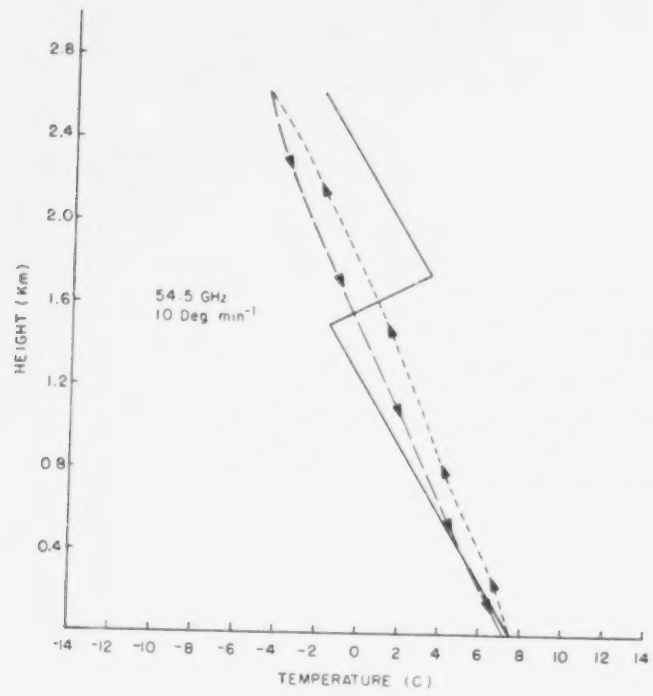

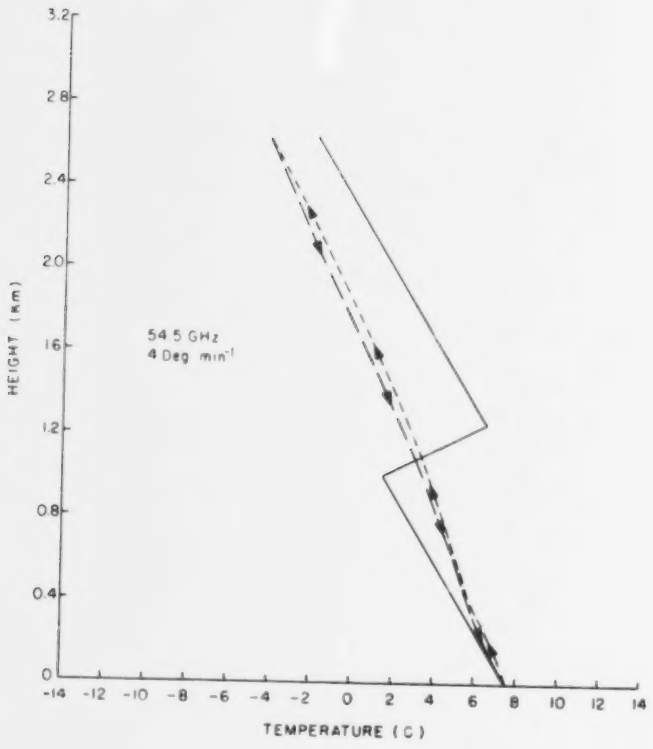

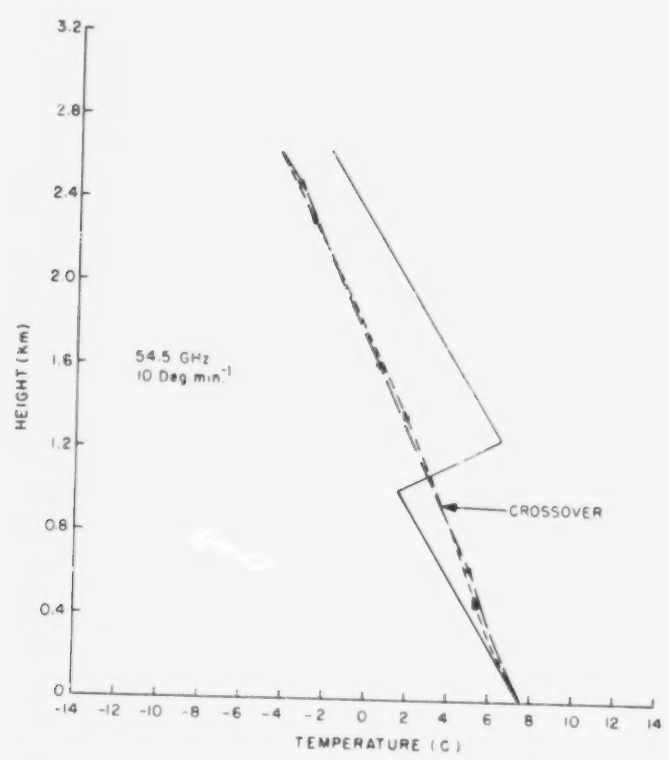

FIG. 23 Computer simulated up-down angle scans of two elevated inversion profiles.

atmospheric temperature discontinuities has yet to be investigated.

5.2 Experimental Detection of Elevated Inversions - After the computer simulated results showed the possibility of detecting the existence of elevated inversions, previously obtained experimental data were perused for elevated inversion cases having up-down or down-up scanning sequences. It is important to note the sequence of two successive scans, because these two scans have a different point in common (depending upon the sequence). An up-down scan (0-90-0) has a common point at 90°, whereas a down-up scan (90-0-90)has a common point at 0°. Several such runs were made at Salt Lake City during a dynamically produced elevated inversion situation lasting from 1968 November 19 to 21. Since there was only one case with a down-up scan, it will be discussed first and is shown in Fig. 24. Sequential observations at 55 GHz were made during the afternoon of November 19, first scanning from the vertical to the horizontal and then up again at a constant rate of 4 degrees per minute. The helicopter, on-site, and official Weather Bureau RAOBs each showed strong lapse conditions extending to 1.4 km. The helicopter did not attain the altitude to detect the elevated inversion. The official RAOB scheduled time of release was two hours after the on-site RAOB, helicopter, and radiometric runs. The on-site RAOB gives the base and top of the elevated inversion at 1.52 and 1.83 km, respectively. The down-up scans have a common point at the ground, and for the lapse profiles the two scans should not cross. However, it can be seen in Fig. 24 that the down-up radiometric profiles cross over in the vicinity of the elevated inversion, namely, at 1.76 km. These results are very encouraging to our efforts at developing a means for detecting the existence of elevated inversions. Given this information, the effectiveness of most data analysis schemes for translating radiometric to actual air temperature data could be greatly improved.

Early in the morning of 1968 November 20, during which time ground-based and elevated inversions existed, radiometric up-down scans at 55 GHz and 3.5 degrees per minute were made (see Fig. 25). The common point for all up-down scans was taken at 80-degrees elevation angle. The official Weather Bureau RAOB schedule time was three hours earlier than the on-site observations. The on-site RAOB signal was very noisy from the surface to 0.4 km, so this is where

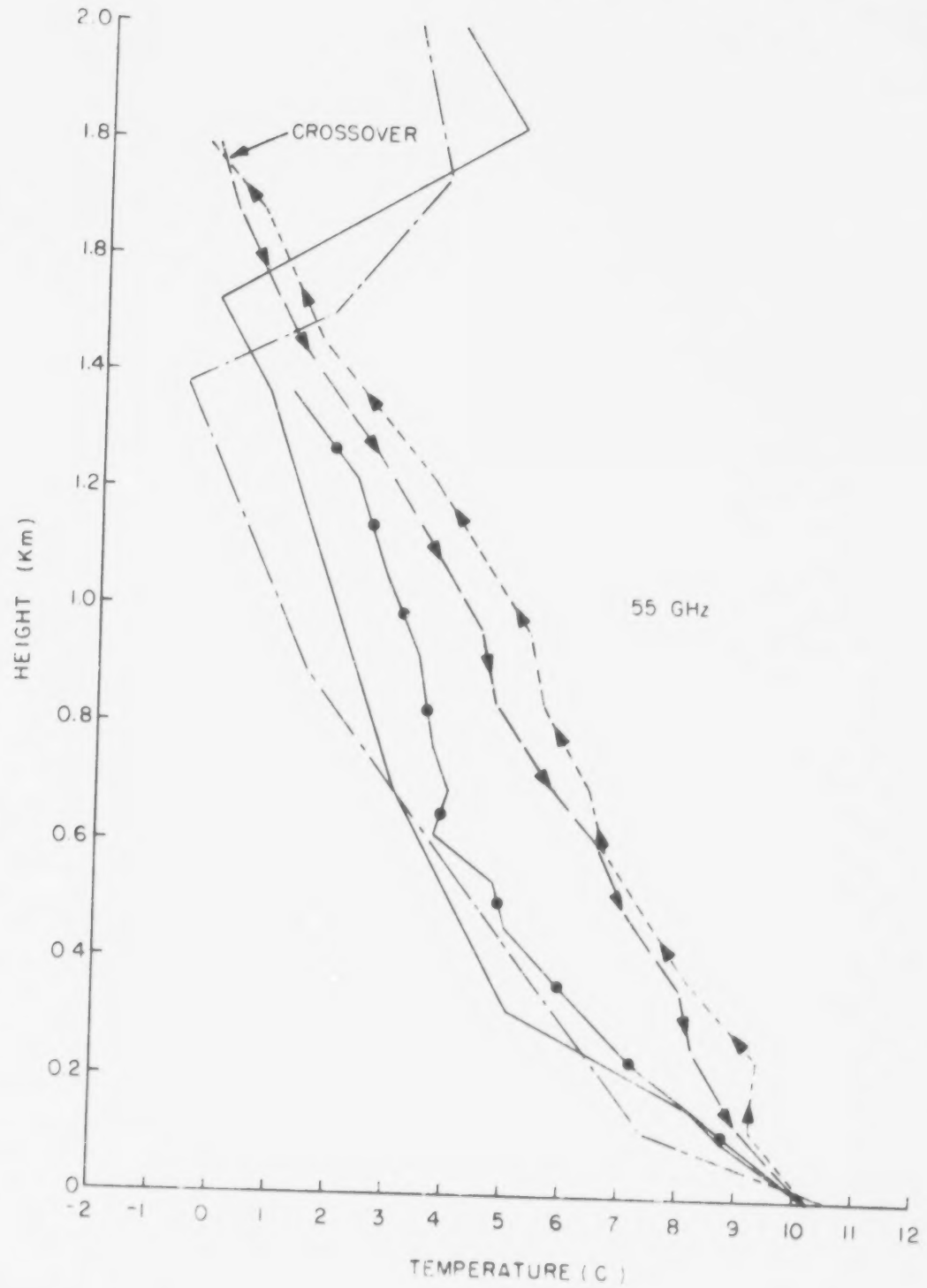

FIG. 24 Comparison of observed down-up radiometric scans with on-site and USWB RAOB data and helicopter data, Salt Lake City, 1500 MST, 1968 November 19. The curves with arrows indicate the direction of the angle scan at 4^{o}/min and radiometric temperature output. The line connected by circles is the helicopter sounding. The solid line and dash-dot line are the on-site and Weather Bureau RAOB.

the first reliable data point was plotted. The helicopter and USWB RAOB indicated the height of the ground inversion to be at 0.25 and 0.46 km, respectively, with the base and top of the elevated inversion ranging between 0.9 and 1.0 for the base and 1.2 and 1.85 km for the top. The radiometric data had one crossover at 1.4 km associated with the elevated inversion and one crossover at 0.45 km associated with the ground-based inversion. The lower crossover point can be distinguished as being due to a ground-based inversion, since the upward scan dictates the presence of a ground-based inversion; under these conditions a crossover occurs between the two scans. A other case such as this is presented in Fig. 26, where the up scan shows a deep ground-based inversion with the down scan crossover occurring at 1.5 and again at 1.0 km. Light fog was present and the morning surface air temperature was rapidly increasing such that by the time the helicopter took off (one hour after starting the up scan), the surface temperature rose over 2 C. The USWB RAOB and helicopter show the inversion top at 1.13 and 1.22 km.

Figure 27 shows an up-down scan at 55 GHz and 3.5 degrees per minute on an elevated inversion having a low base and high top. The on-site RAOB gave the base of the elevated inversion as 0.2 km, whereas the radiometric up scan shows it at 0.12 km. The first helicopter data point was at 0.15 km. Above the base of the inversion secondary increases are indicated to be at 0.33 and 0.68 km by the RAOB and only at 0.6 km by the helicopter, while the radiometric up scan shows it at 0.4 km. The top of the elevated inversion is given at 1.22 km by the helicopter, whereas the RAOB indicated an isothermal maximum between 1.15 to 1.45 km. The radiometric crossover occurred at 1.46 km.

The only case observed at 54.5 GHz is presented in Fig. 28 with up-down scans at 3.5 degrees per minute. The calibration of the on-site RAOB is questionable; it appears to be consistently cold by 2.5 C, yet it depicts the same atmospheric structure as the helicopter sounding. The upward scan shows the low-level lapse condition extended to 0.1 km, whereas the RAOB and helicopter indicate that it extends to 0.2 km. Above this point the radiometer as well as the RAOB and helicopter indicate a slight inversion, then an isothermal region above which the upward scan smooths out the region at the top of the

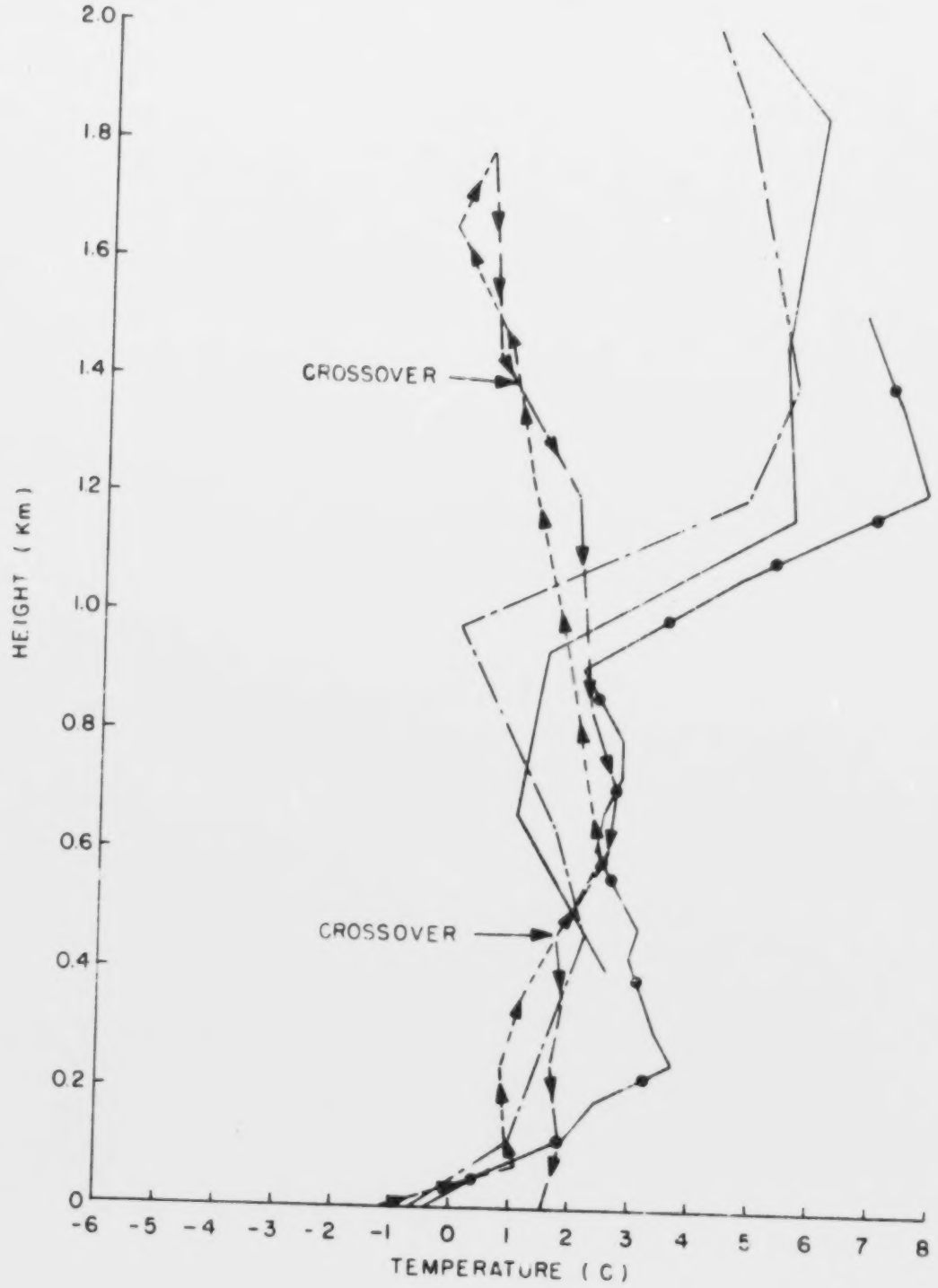

FIG. 25 Comparison of observed up-down radiometric scans with on-site and USWB RAOB data and helicopter data, Salt Lake City, 0800 MST, 1968 November 20. The curves with arrows indicate the direction of the angle scan at 3.5^{o}/min and radiometric temperature output. The line connected by circles is the helicopter sounding. The solid line and dash-dot line are the on-site and Weather Bureau RAOB.

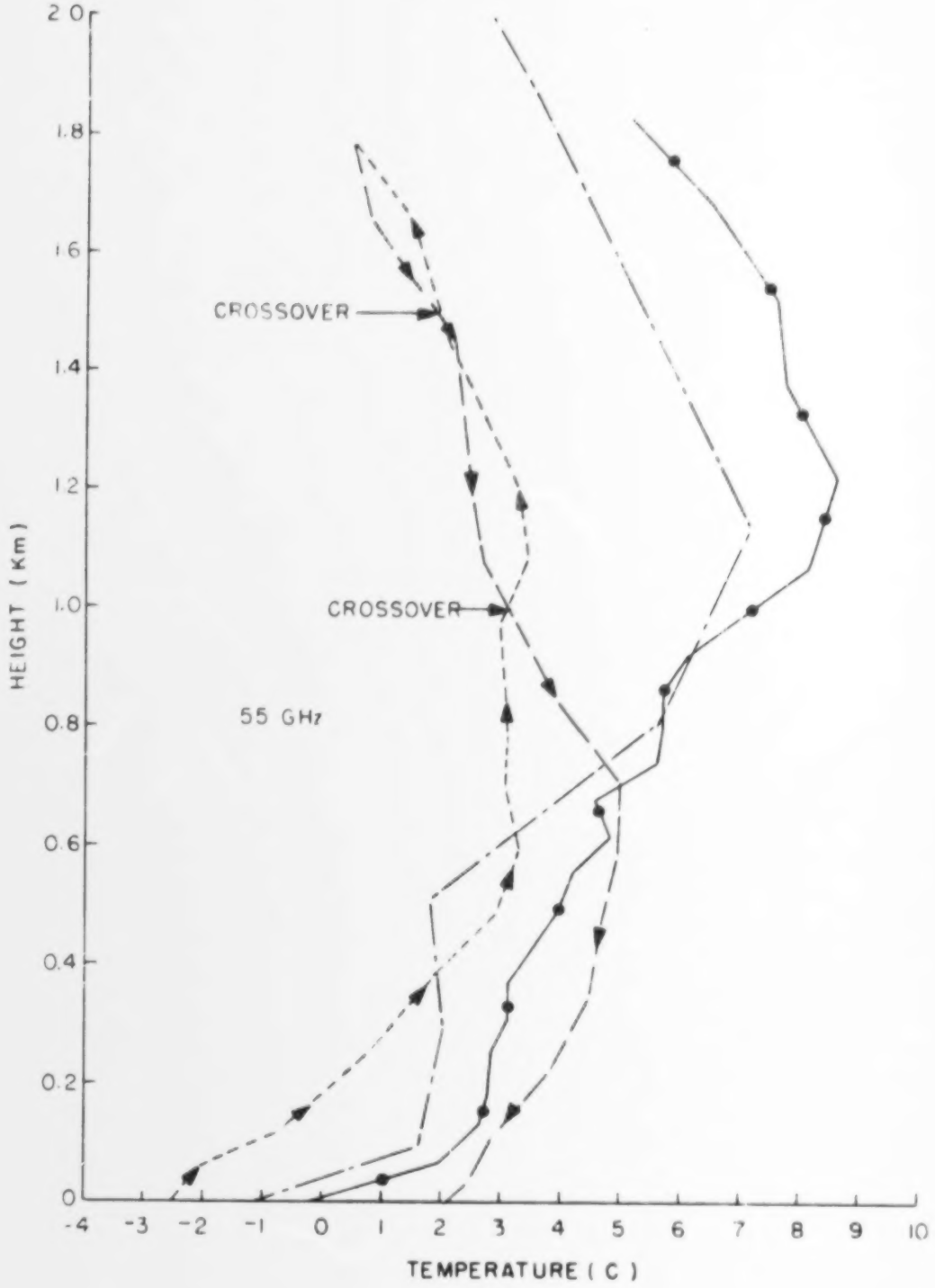

FIG. 26 Comparison of observed up-down radiometric scan with on-site and USWB RAOB data and helicopter data, Salt Lake City, 0803 MST, 1968 November 21. The curves with arrows indicate the direction of the angle scan at 3.5^{o}/min and radiometric temperature output. The line connected by circles is the helicopter sounding. The solid line and dash-dot line are the on-site and Weather Bureau RAOB.

inversion. Both the helicopter and RAOB indicate two peaks in the top of the elevated inversion located at 1.37 and 1.68 km, with the up-down radiometric crossover indicating 1.4 km.

The most striking feature of these fixed-frequency, up-down scan runs is that for the observed cases available they seem to provide a means for looking at radiometric data which is very useful and perhaps necessary for better interpreting the radiometric observations and for specifying not only ground-based inversions but also elevated inversions.

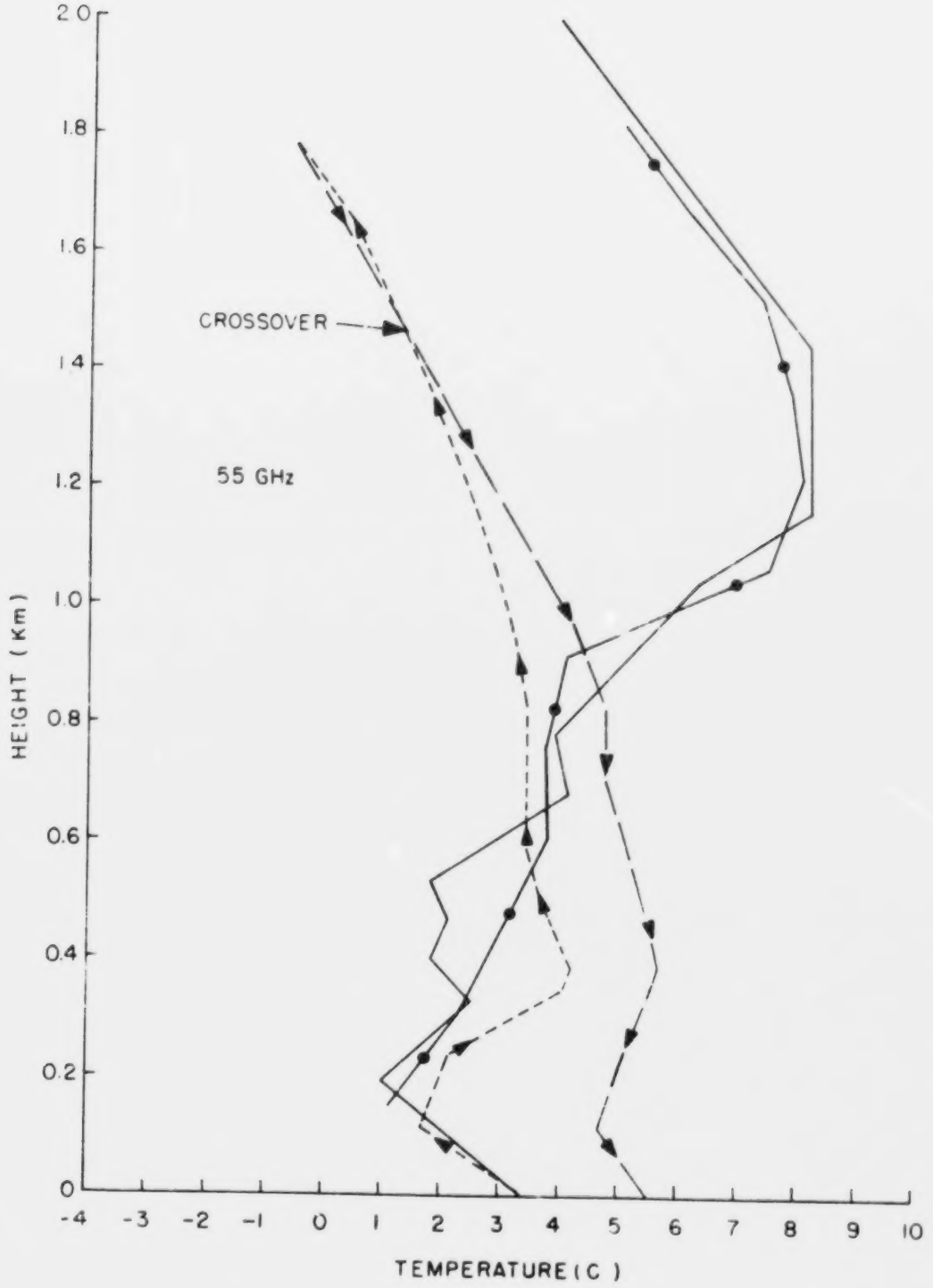

FIG. 27 Comparison of observed up-down radiometric scan with on-site and USWB RAOB data and helicopter data, Salt Lake City, 1200 MST, 1968 November 21. The curves with arrows indicate the direction of the angle scan at 3.5°/min and radiometric temperature output. The line connected by circles is the helicopter sounding. The solid line and dash-dot line are the on-site and Weather Bureau RAOB.

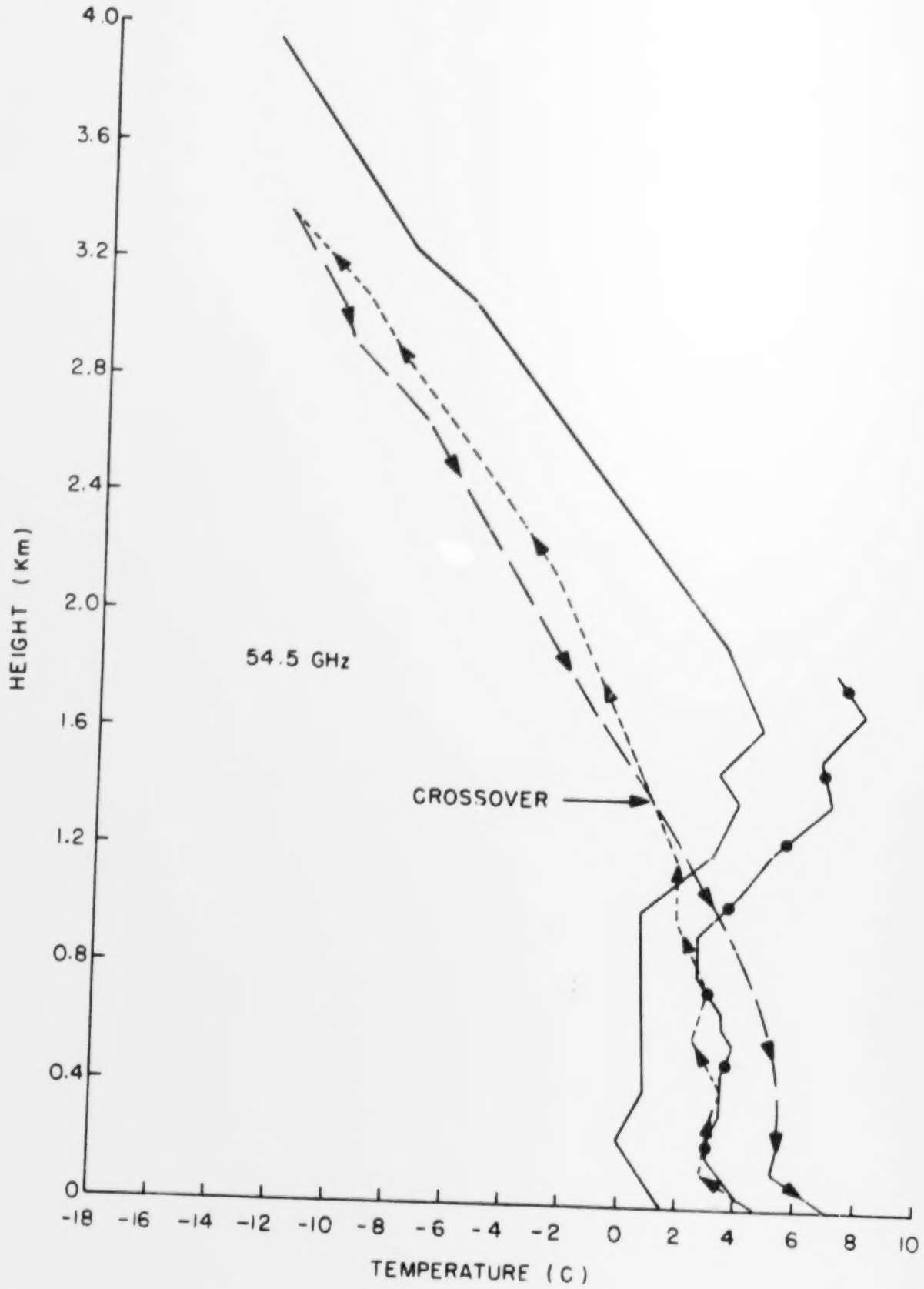

FIG. 28 Comparison of observed radiometric scan with on-site and USWB RAOB data and helicopter data, Salt Lake City 1100 MST 1968 November 20.

SECTION 4

CONCLUSIONS

1. The development program for the Mark I Radiometric THERMASONDE™ either met or exceeded the design goals, with the exception that the package was overweight by one and one-half pounds.
2. Comparisons between Sperry Rand's Mark 0 and National Air Pollution Control Administration's Mark I THERMASONDES™ showed increased short- and long-time stability, sensitivity, and overall performance of the Mark I for its design frequency range of 54 to 55 GHz.
3. Pressure altitude, seasonal, frequency, and synoptic pressure variations play a significant role in passive radiometric derivation of the air temperature profile.
4. Null balance or absolute radiometric temperature observations produce a smoothing of temperature discontinuities such as ground and elevated inversions because of the physics governing passive probing techniques. The burden of extracting this information is placed upon the data analysis procedures for the chosen mode of observation.
5. Lapse profiles are defined quite nicely.
6. Simulation of a vertically pointing variable frequency radiometer shows a clear indication of lapse, ground-based, or elevated inversion conditions to 0.5 km. The indication of a 5-C elevated inversion at 1.5 km is difficult to distinguish from that of a lapse profile.
7. Often atmospheric and/or equipment fluctuations over a relatively short time period (1½ hours) are sufficient to negate an attempt to have a well controlled experiment in the field, such as investigating the effects due to fixed-frequency multiple-angle scan rates. Nevertheless, both simulation and field experiments indicate the smoothing and displacement effects which occur for fixed-frequency continuous-angle scans under ground-based inversion conditions.
8. It appears that radiometric profiles can be adjusted to yield height and intensity of ground-based inversions by properly incorporating scan rate and nonlinear relations between maximum increase in brightness temperature and the angle at which this occurred. A verification at one location showed

the average absolute magnitude of the difference between direct and remote observations to be 0.6 C in intensity and 0.06 km in height for eight ground-based inversion cases.

9. Experimental results showed that by operating in a fixed-frequency angle scanning mode, sequential up and down scans provide valuable information for detecting the existence of elevated inversions as high at 1.8 km.

APPENDIX I

USE OF MILLIMETER WAVE RADIOMETRY TO REMOTELY MEASURE ATMOSPHERIC STABILITY

APPENDIX I

USE OF MILLIMETER WAVE RADIOMETRY TO REMOTELY MEASURE ATMOSPHERIC STABILITY*

by

Wayne D. Mount
Sperry Rand Research Center
Sudbury, Mass.

ABSTRACT

Thermal radiation emitted and absorbed by oxygen molecules is discussed to show it is possible to use a ground-based sensitive receiver to indirectly measure the low-level temperature profile. The Radiometric THERMASONDE™ equipment is described briefly, and computer simulation and experimental results are presented for unstable, neutral, and stable weather conditions.

Atmospheric stability plays an important role in the transport of heat, momentum, water vapor, and pollutants in the air-ground and air-sea interface. To measure these meteorological conditions directly with available instrumentation requires either very tall towers, instrumented aircraft, tethered balloons, or an expendable balloon-borne radiosonde. These existing methods either present a physical hazard to aircraft operations, are expensive in materials and trained manpower, have tremendous data reduction and processing problems, cannot provide continuous vertical sounding, are immobile, or are not very sensitive to the conditions important to the transport mechanisms in the lowest layers of the atmosphere. For these reasons it would be highly desirable to have a ground-based device which overcomes these limitations yet provides a reliable measure of the low-level temperature structure.

Over the past several years we have developed techniques to detect and analyze radiation coming from oxygen molecules in the atmosphere. The equip-

---

*Paper presented in Cincinnati at the Symposium on Advances in Instrumentation for Air Pollution Control, 1969 May 26, 27, 28, Department of Health, Education and Welfare.

ment, which we call a Radiometric THERMASONDE™, is a sensitive radio receiver that operates in the millimeter wave region of the electromagnetic spectrum and passively detects thermal radiation emitted by oxygen molecules. The amount of thermal power received by a radiometer is proportional to a weighted mean temperature of the ambient air molecules. The oxygen molecules are continuously radiating, but the distance through the atmosphere that this radiation can travel is a function of the atmospheric absorption characteristics. Figure 1 shows the frequency and altitude dependence of atmospheric oxygen absorption. Note that there are two peaks--one that occurs at about 60 GHz, or 5 mm in wave length, and one that occurs at 120 GHz. We will focus our attention in the frequency region from 50 to 60 GHz. It can be seen that the atmospheric attenuation increases sharply from 50 to 60 GHz. This means that a sensitive receiver, tuned to 60 GHz with its antenna pointed vertically, detects radiation coming from only those molecules nearest the antenna. The reason for this is that the radiation from those molecules at higher levels in the atmosphere is absorbed by the intervening molecules and reradiated in proportion to the temperature of these lower molecules. This effect will be discussed in greater detail, but before doing so let us look at another significant effect. It can also be seen from Fig. 1 that the value of the absorption coefficient at any frequency decreases as the height above the the surface increases. That is to say, at lower pressures in the atmosphere the absorption coefficient is lower than what would be observed at sea level. This pressure effect must be taken into account when simulating the radiational characteristics of the atmosphere.

From Fig. 2 one can obtain a physical picture as to what levels of the atmosphere are contributing to the signal detected by a ground-based radiometer. The transmittance, or ability of the radiation to penetrate the atmosphere, versus height in the atmosphere is presented for three different frequencies and for summer and winter conditions. For a vertically-pointing antenna, note that at 58 GHz almost all the radiation which reaches the THERMASONDE™ emanates from a height equal to or less than about 1 km, whereas at 54 GHz the radiation comes from considerable depth in the atmosphere. It can also be seen that these curves change very little due to large seasonal

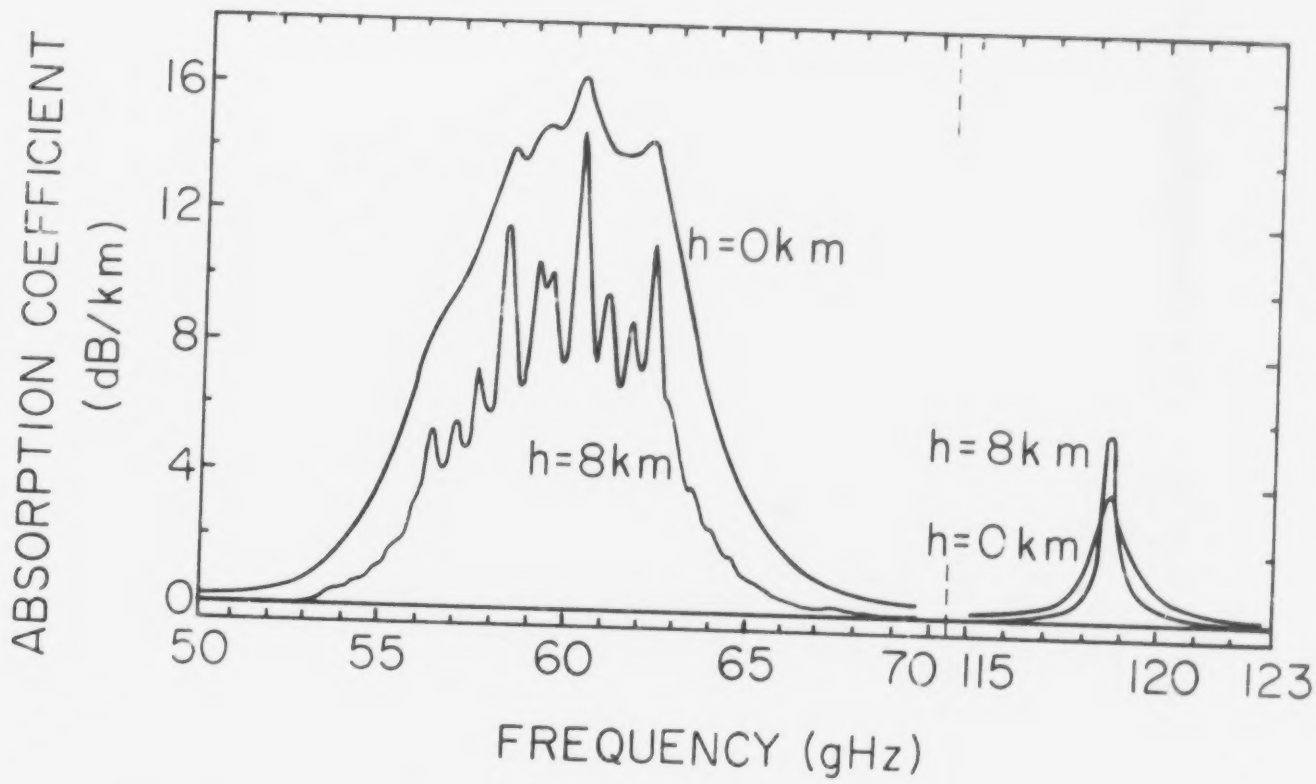

FIG. 1 Frequency and altitude dependence of atmospheric oxygen absorption.

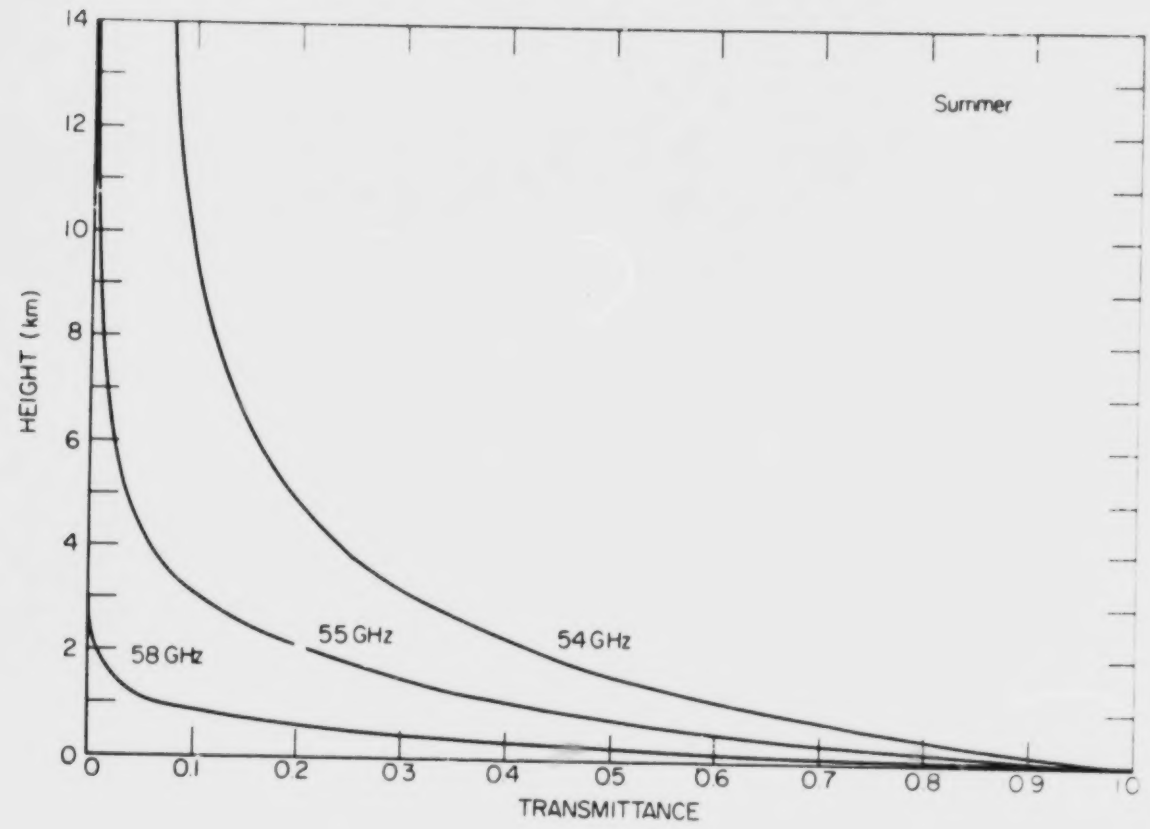

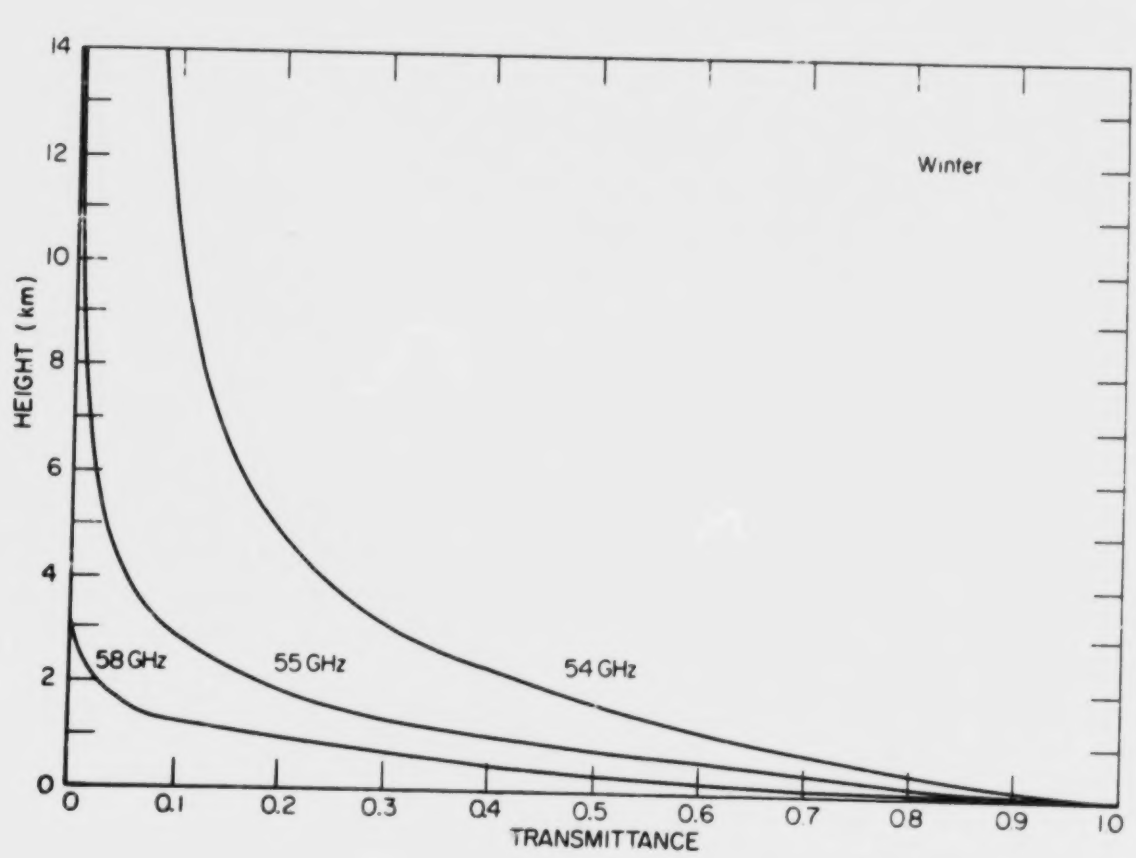

FIG. 2 Frequency and seasonal dependence of transmission function.

differences in atmospheric conditions. Therefore, it follows that by varying the frequency it is possible to obtain temperature information from different depths in the atmosphere.

There is another mode of operation which can be used to vary the depth in the atmosphere from which the radiation reaches the THERMASONDE™ antenna. In Fig. 3 it can be seen that by operating at 54 GHz and varying the elevation angle from 0° to 90° it is possible to receive radiation coming from different depths in the atmosphere. It can also be seen in the same figure that at 55 GHz the same principle applies, but the upper limit in the atmosphere above which little or no contribution is detected is much lower than when operating at 54 GHz. These two modes of operation, namely, fixed-angle frequency scanning and fixed-frequency angle scanning, place different requirements on the level of sophistication required in the instrumentation. For example, in the former mode of operation it is essential to have a radiometer that measures the absolute temperature at each frequency. In the latter mode, the equipment restrictions are far less, and one can deal with a relative temperature differential and construct a temperature profile of the atmosphere; however, since the frequency is fixed there is a restriction on the depth to which the atmosphere can be probed and the necessary assumption of a horizontally stratified atmosphere must be imposed. Since for boundary layer studies in the air-earth interface it is primarily the first mile of the atmosphere that is critically important, it appears that the fixed-frequency angle scanning mode can provide the necessary information throughout this most important region of the atmosphere.

A photograph of our research radiometer which is electronically tunable between 50 and 60 GHz is shown in Fig. 4. This Radiometric THERMASONDE™ (Mark 0) was developed and produced by our sister division, Sperry Microwave Electronics Division at Clearwater, Florida. In our experimental programs this research THERMASONDE™ was used in both modes of operation; however, most of the data were obtained by, and all those presented here are for, a fixed-frequency angle scan mode of operation. To the extent possible we attempted to obtain nearly simultaneous direct soundings of the lower level temperature structure using more than one system.

Figure 5 shows our kytoon, on which a modified radiosonde package was

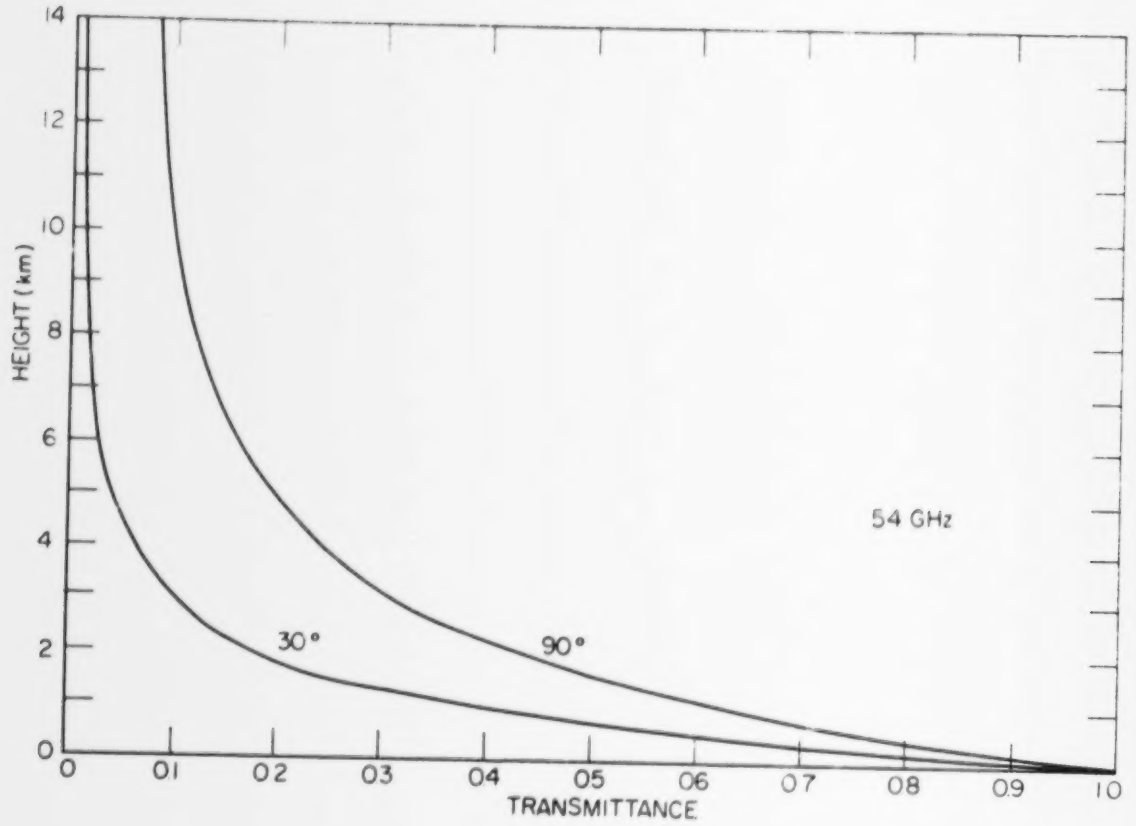

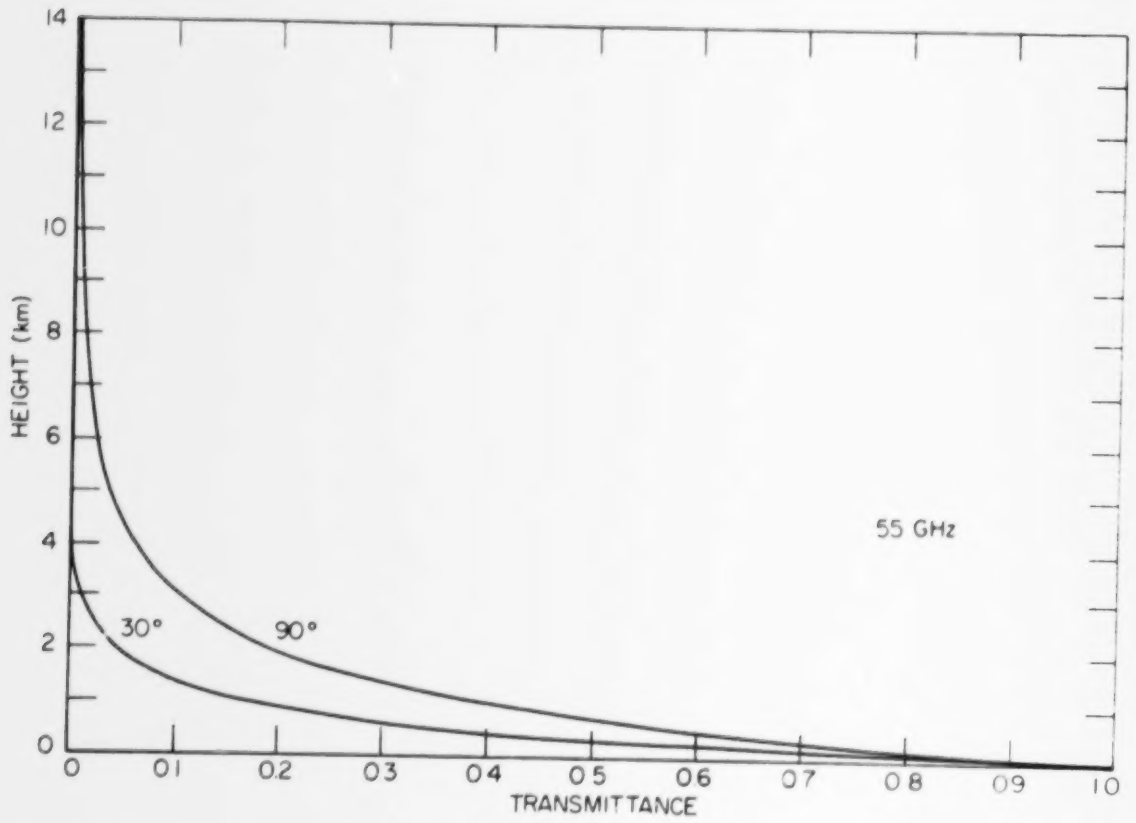

FIG. 3 Elevation angle dependence of transmission functions.

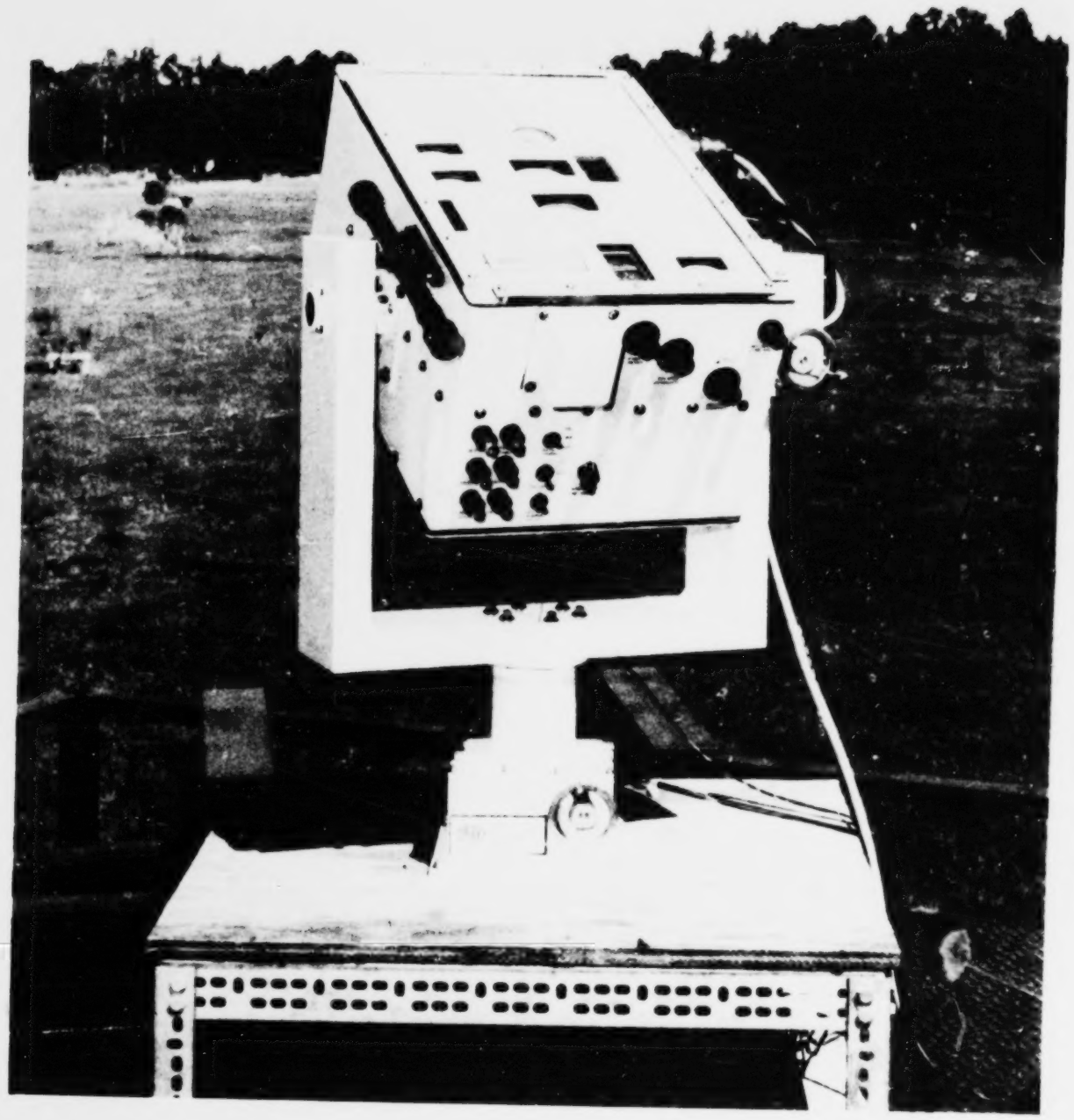

FIG. 4 Radiometric THERMASONDE^{TM}, Mark 0, research model.

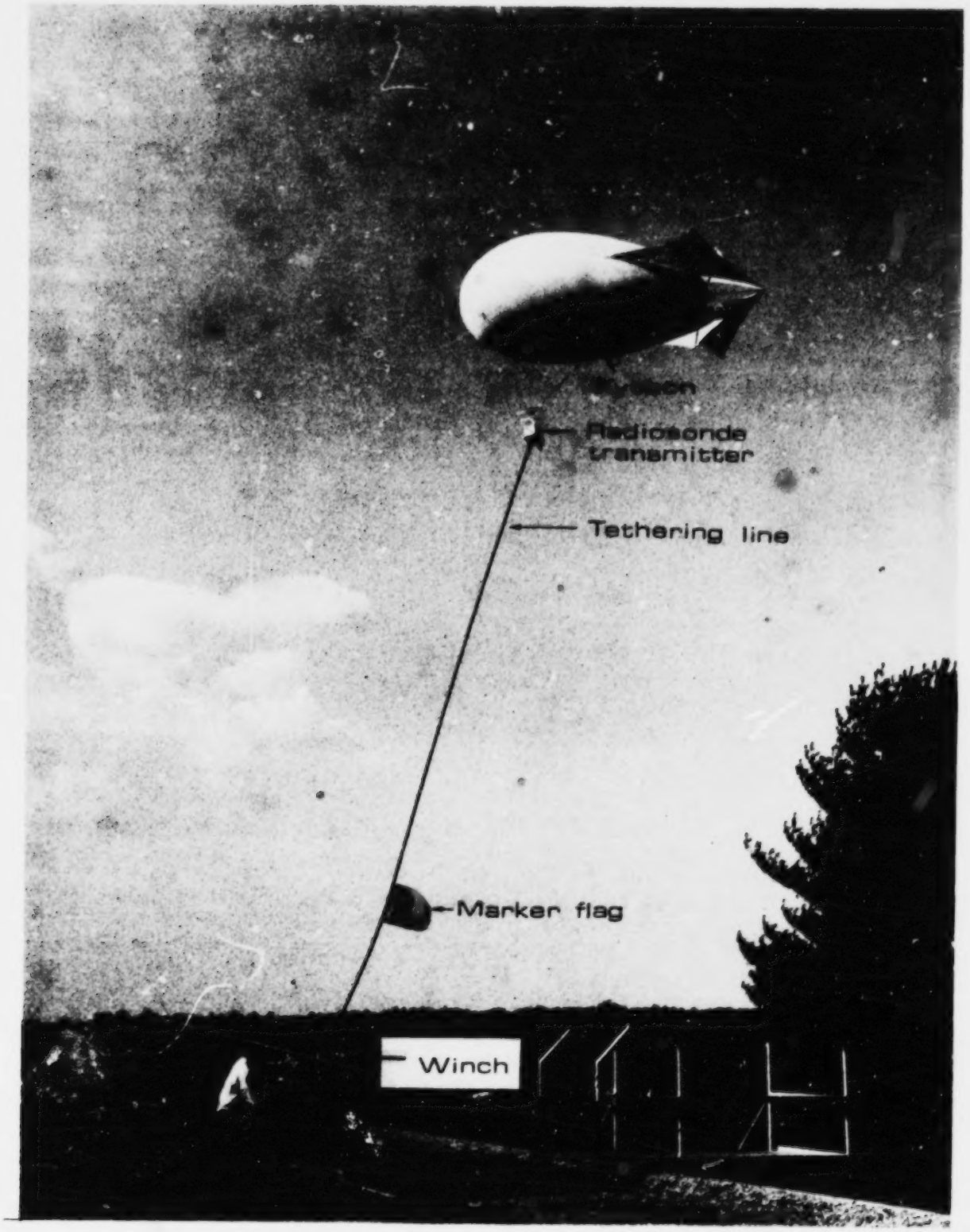

FIG. 5 Kytoon-borne modified radiosonde system for direct measurement of low-level temperature structure.

suspended, with a tethering line used to control the height. This is an extremely awkward and time-consuming way to obtain a direct measurement of the temperature structure. Since the kytoon was flown above 150 feet (actually up to altitudes of 3,000 feet), we had to comply with Federal Aviation Agency requirements that markers be placed every 50 feet on the tethering line. We used this method only as a last resort when no other direct observational device was available.

Figure 6 shows the highest meteorologically instrumented tower in the United States (WKY-TV), located outside of Oklahoma City. A number of on-site radiosonde and radiometric observations were taken here, along with simultaneously recorded tower sensor data. Figure 7 shows a photograph of the aerovane and aspirated thermometer located at each observational level on the tower, with the highest one at 1,455 feet. Radiosonde observations made at Tinker Air Force Base, approximately 12 miles removed from our site, were used along with on-site radiosonde observations for comparing the directly measured profiles with those measured passively and remotely with the Radiometric THERMASONDE™.

The physics of the radiational characteristics of the atmosphere are sufficiently well behaved and understood that computer models can be developed to simulate what a real THERMASONDE™ would measure. As an example, Fig. 8 shows a plot of a Tinker Air Force Base RAOB which was used as input data for the computer to derive radiometric brightness temperatures at 55 GHz as a function of elevation angle. These data are plotted along with the actually observed radiometric observations. It can be seen that there was close correspondence between the real and simulated data. These data are plotted as a function of height using what we refer to as the applicable height concept (see Appendix II). A set of applicable heights was computer-derived from a fictitious lapse profile typical of each station. For each frequency and elevation angle the height where the computed brightness temperature equaled the fictitious air temperature was called the applicable height. Thus for each frequency and elevation angle it is possible to derive under lapse conditions one and only one applicable height. The main advantage of this scheme is that it provides a way to obtain a real time output of the temperature

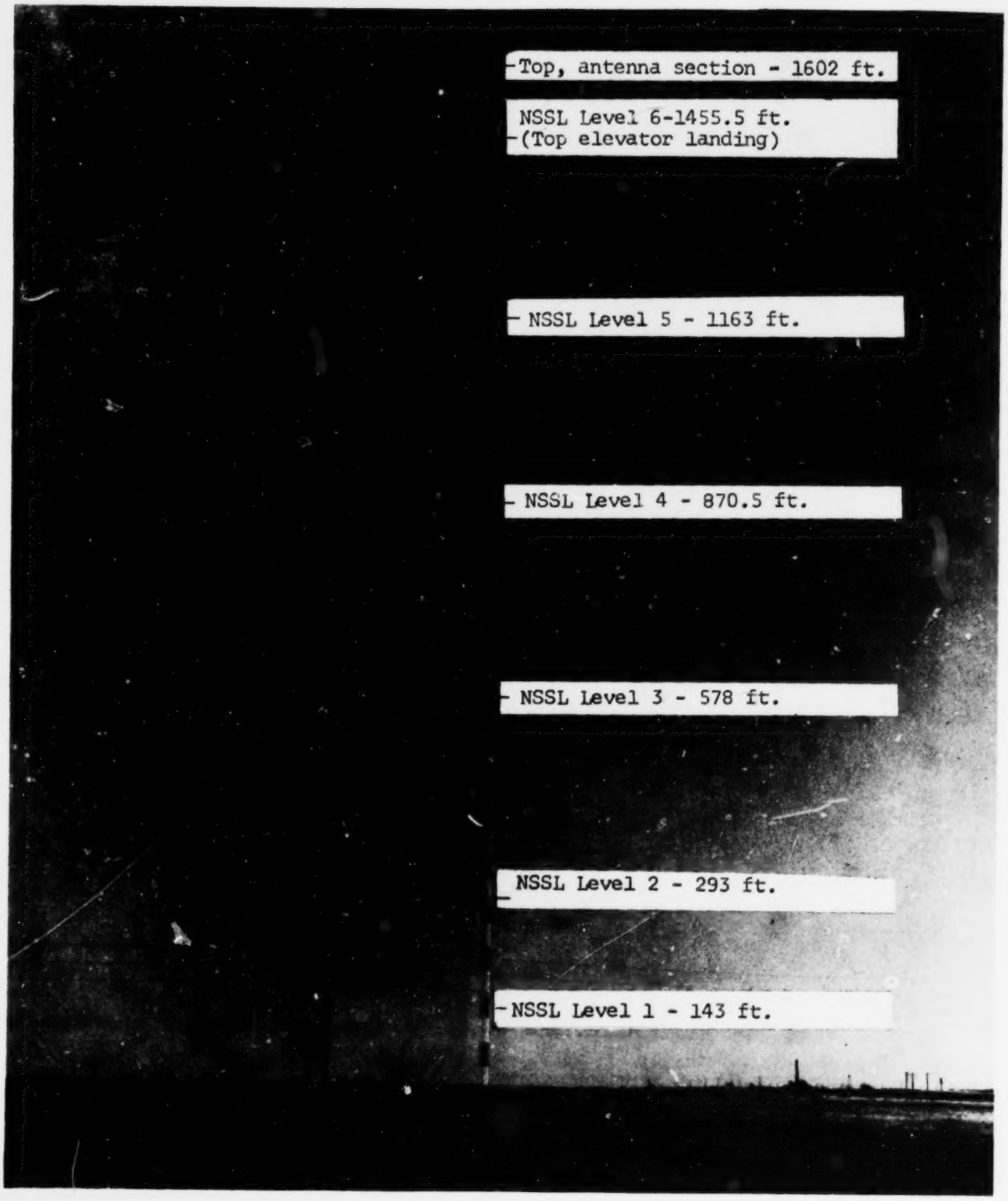
Top, antenna section - 1602 ft.
NSSL Level 6-1455.5 ft.
(Top elevator landing)
NSSL Level 5 - 1163 ft.
NSSL Level 4 - 870.5 ft.
NSSL Level 3 - 578 ft.
NSSL Level 2 - 293 ft.
NSSL Level 1 - 143 ft.

FIG. 6 Meteorologically instrumented tower, station WKY-TV outside Oklahoma City.

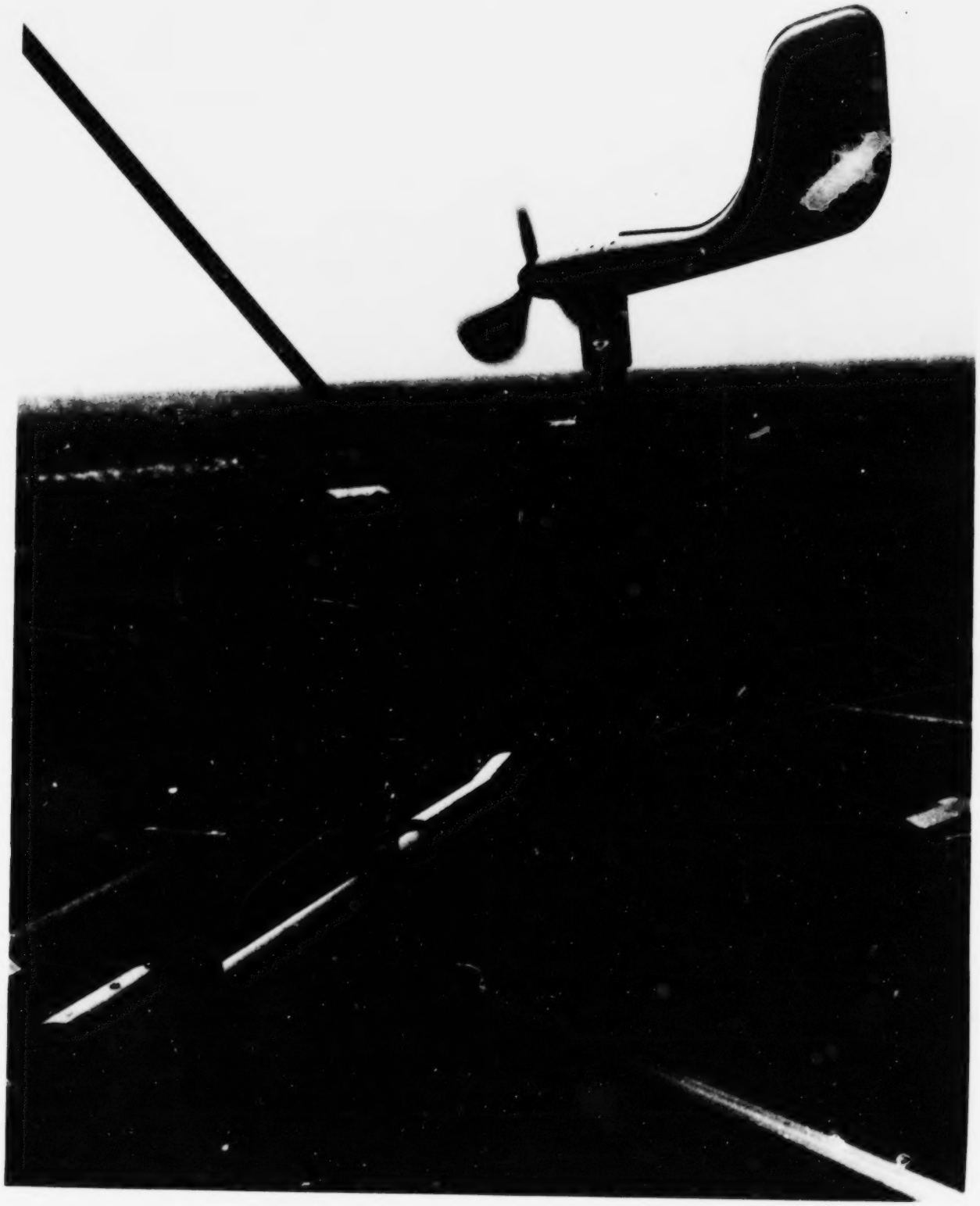

FIG. 7 Meteorological sensors on the WKY-TV tower.

profile. One of the main disadvantages is that it does not provide an optimum scheme for translating brightness temperatures to air temperature as a function of height. This is especially noticeable under inversion conditions and, as shown in Fig. 8, the scheme typically provides a smoothing of ground-based inversions. At this point no attempt has been made to correct for this systematic error, yet the significant effects and ability to detect the height of gound-based inversions can be seen in this and subsequent figures.

One of the most difficult conditions to be measured using the standard radiosonde is the highly turbulent superadiabatic lapse condition, as shown in Fig. 9. These conditions are prevalent in the lowest layers of the atmosphere, where ground heating of the air is very intense. The relatively slow response time and rather rapid ascent of the radiosondes result in the smoothing of these highly turbulent conditions. During the time in which we were operating adjacent to the 1500-foot instrumented tower, the Radiometric THERMASONDE™ detected the superadiabatic conditions that were also measured by the tower but not shown in the on-site RAOB data.

Figure 10 illustrates a large number of multiple soundings which, upon careful examination, depict some of the vast differences that can occur in the low-level stability conditions. For example, the Tinker RAOB which was taken about two hours after the other sounding shows a simple ground inversion, whereas the tower shows an elevated inversion. The first reliable data point from the on-site RAOB was not obtained until the radiosonde was above the top of the tower. Standard meteorological practice is to draw a straight line from the surface to that data point, which in this case indicates a ground inversion whose height is above that detected by both the tower and the Tinker data. The computer-simulated radiometric results using the Tinker sounding as input data show the height of the inversion corresponding approximately with that of the Tinker sounding, but with a characteristic decrease in the radiometer intensity of the inversion. The character of the THERMASONDE™ data corresponded most closely with that measured by the tower. This was not unusual, since the THERMASONDE™ often depicted the smaller scale structure in the lowest layers quite adequately.

Figure 11 shows an example of what can be expected under ground inversion

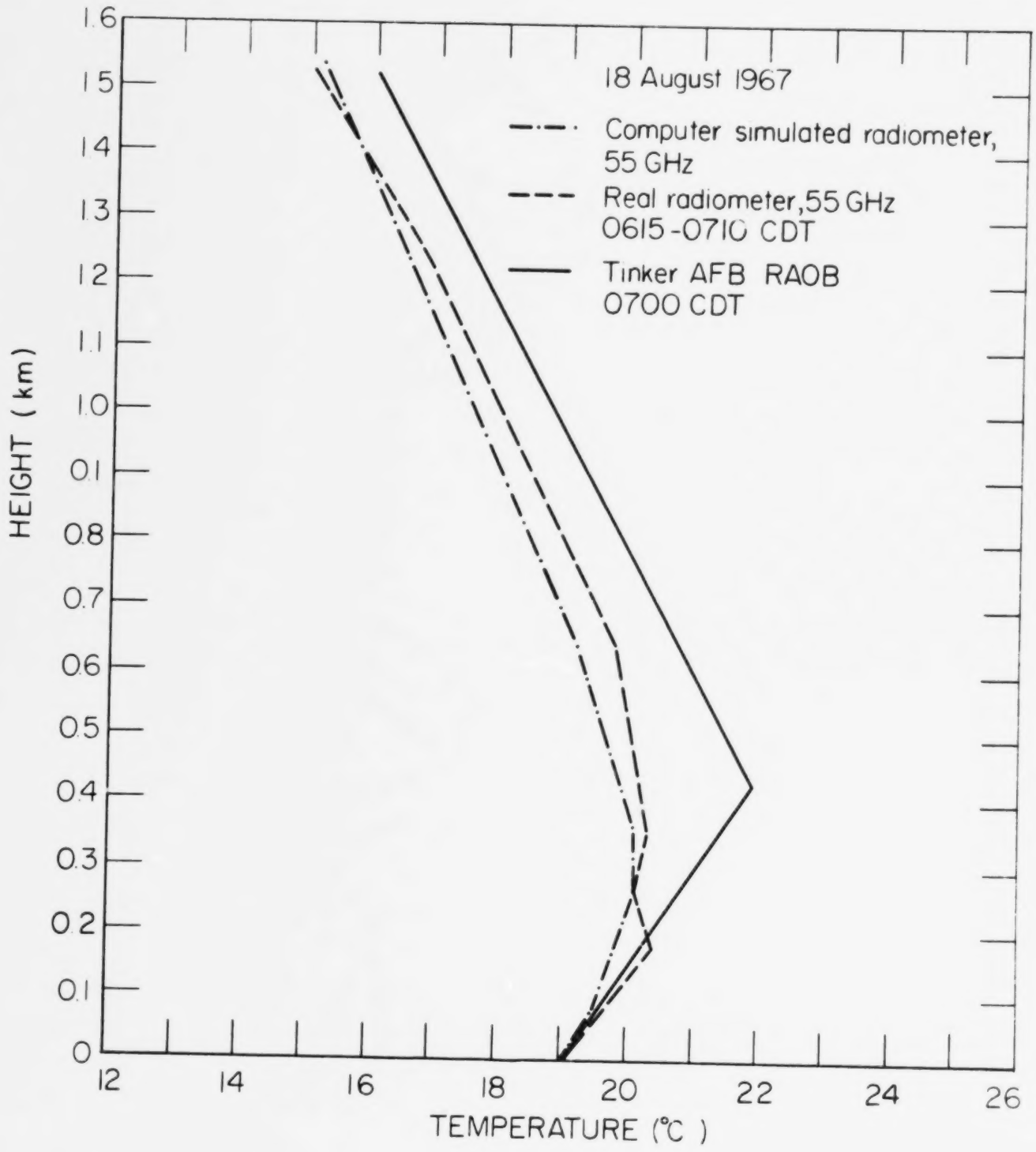

FIG. 8 Comparison of computer simulated and measured radiometric data.

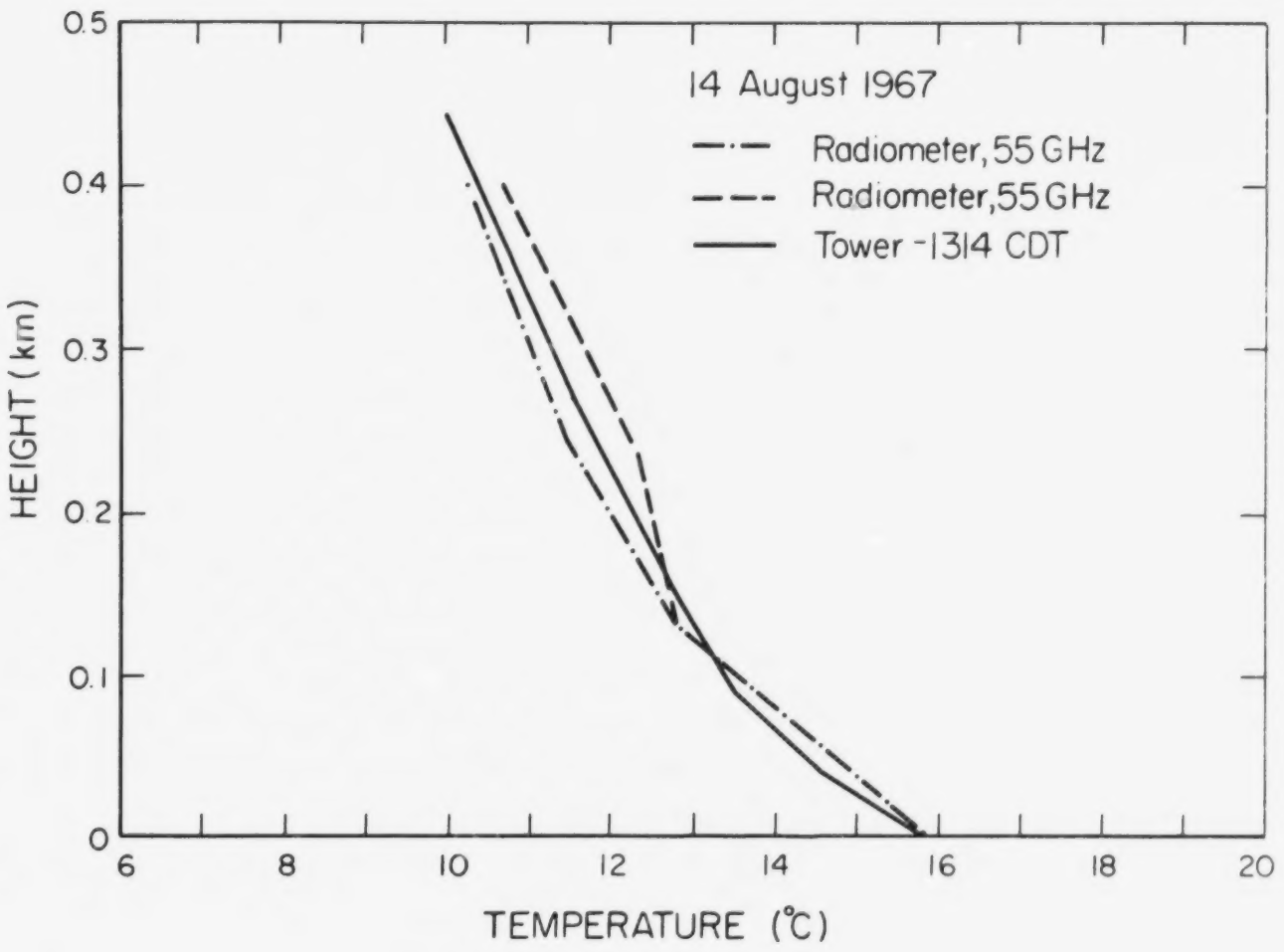

FIG. 9 Comparison of measured radiometric data with tower data during superadiabatic lapse conditions.

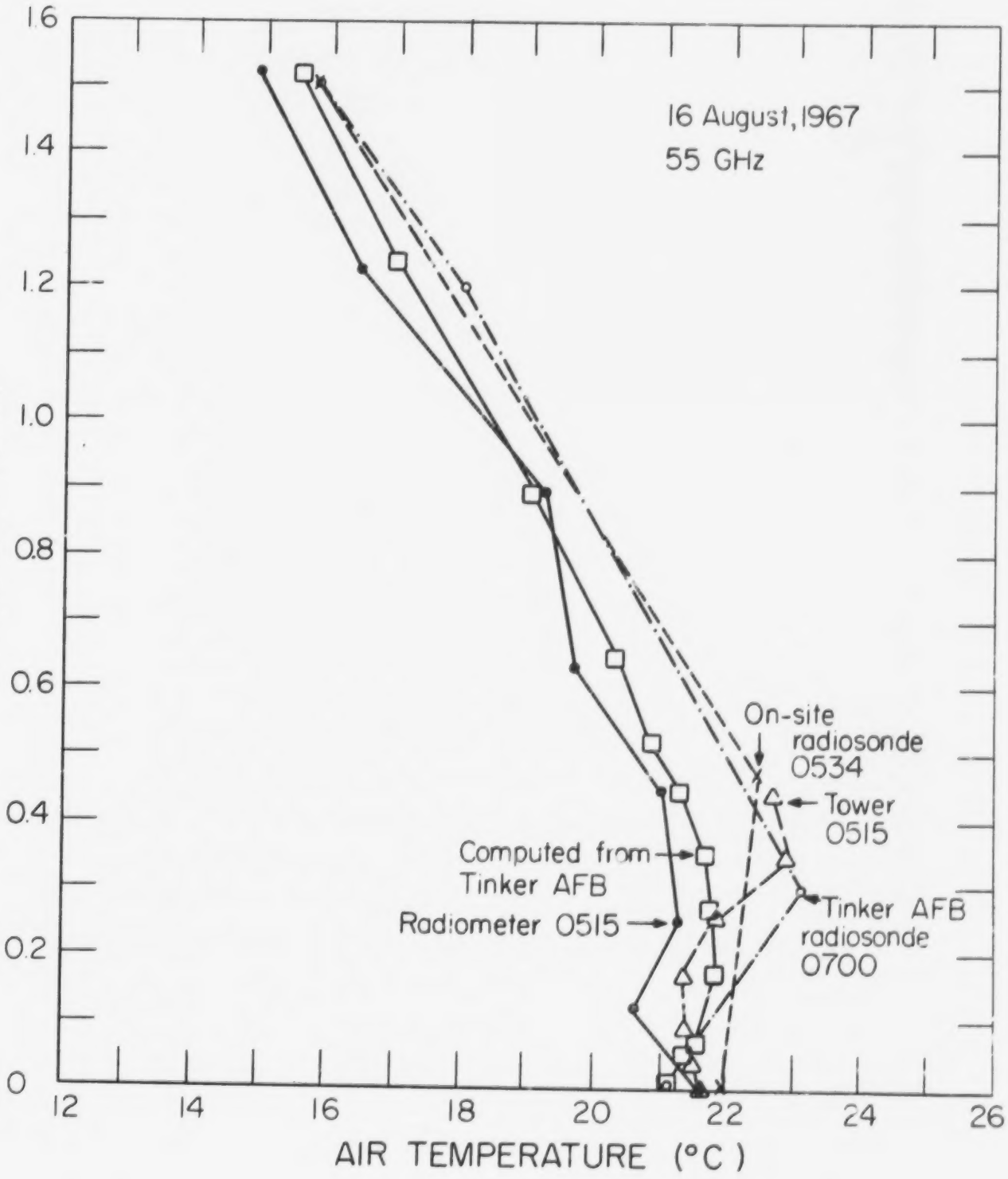

FIG. 10 Comparison of measured and computer simulated radiometric data with on-site radiosonde data, tower data, and RAOB data from nearby Tinker Air Force Base.

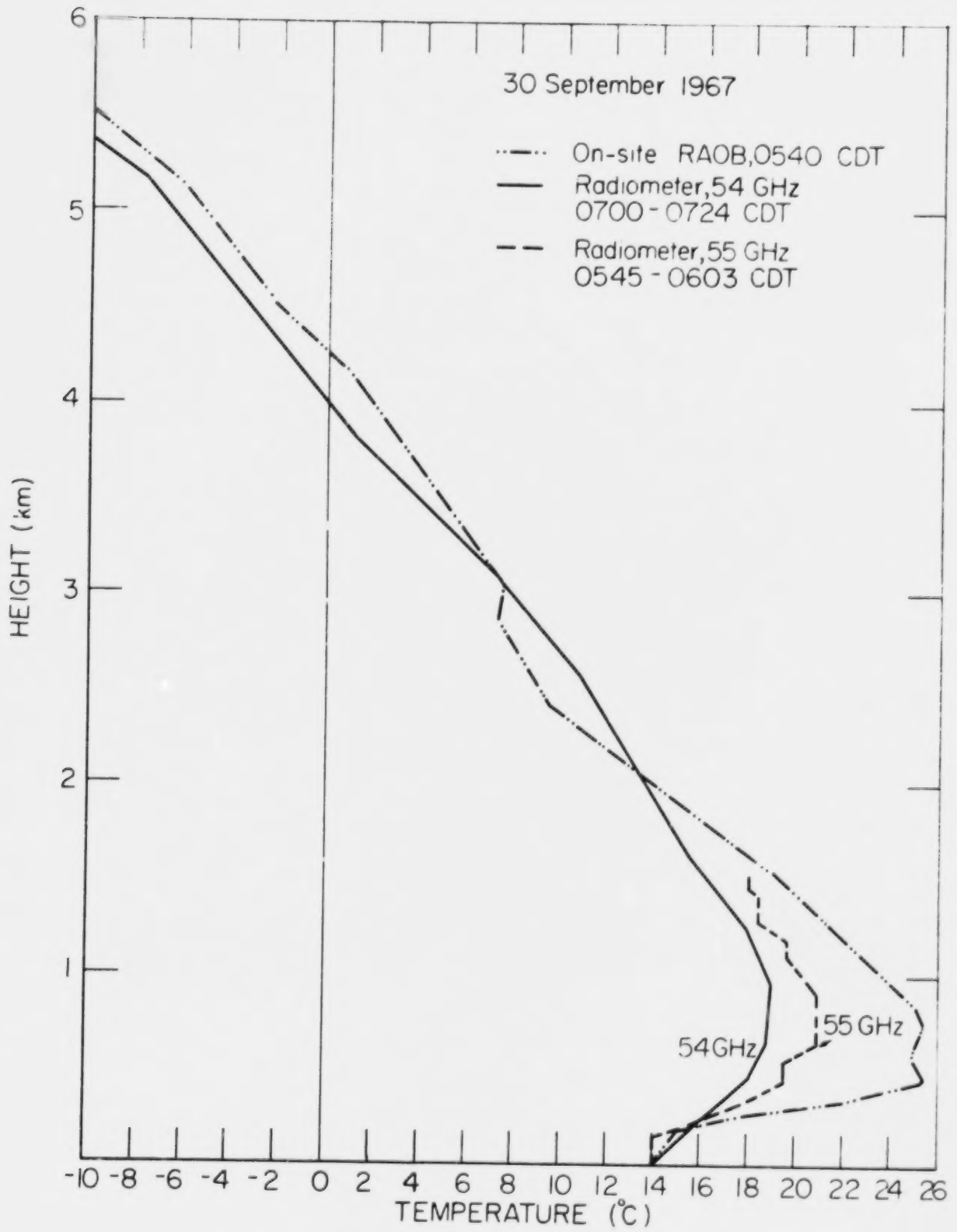

FIG. 11 Comparison of measured radiometric data at two different frequencies with on-site RAOB data during an intense ground inversion.

conditions when operating at two different frequencies. At 55 GHz the Radiometric THERMASONDE™ response to a ground inversion is greater than that at 54 GHz. Using the applicable height concept, it can be seen that the temperature structure of approximately the first mile (1.5 km) can be obtained using a fixed-frequency angle scan mode of operation at 55 GHz, whereas at 54 GHz it is possible to probe to about 5.5 km but with less response to the detail structure in the lowest layers. Thus the frequency selected must be dictated by the operational requirements.

The depth to which the atmosphere can be interrogated is also proportional to station surface pressure. To illustrate this feature the applicable heights for 90° elevation angle for two stations differing widely in height above sea level are shown in Table I. First, it can be seen that for Clearwater, Florida,

TABLE I

Surface Pressure Effects

Location	Surface Pressure	Applicable Height at 90° Elevation Angle	
		55 GHz	54 GHz
Clearwater, Florida (11 ft. above sea level)	1020 mb	1.40 km	5.13 km
	1000	1.45	5.42
	980	1.48	5.72
Salt Lake City, Utah (4277 ft. above sea level)	890 mb	1.80 km	6.46 km
	870	1.87	6.74
	850	1.95	7.02

(which is only a few feet above sea level) the atmospheric temperature structure can be obtained to only 1.4 km, whereas at Salt Lake City (which is nearly a mile high) for the same frequency the profile to 1.8 km (400 meters higher) can be obtained. This effect becomes more pronounced at lower frequencies with the height difference being about 1 km at 54 GHz. Note also for each station, as the surface pressure varies there is a corresponding variation in height to which the atmosphere can be probed. Thus any technique developed to translate

brightness temperatures to air temperature as a function of height must consider the altitude of the station and the surface pressure variability at that station.

Let us now consider a number of observations that were gathered at different geographical locations and under a variety of meteorological conditions. In Fig. 12, observations taken at three different frequencies correspond very closely with the RAOB data taken during lapse conditions. Since the technique for translating radiometric data was developed on lapse profiles, we should expect that it would perform best under these conditions, and it does.

In Fig. 13 there are, once again, large differences between two RAOBs taken close by. The on-site RAOBs were taken by Weather Bureau personnel under the adverse conditions usually encountered when operating in the field. Note that the first reliable data point was much higher than that obtained at the standard Weather Bureau RAOB station about a mile away. A vast difference is implied between these two RAOBs in measuring the height of the inversion. On the other hand, the THERMASONDE™ indicated a height of the inversion which corresponded closely to the official RAOB profile. When operating under field conditions, as is usually the case in air pollution work, it is not unreasonable to expect that trained radiosonde operators will miss the lowest-layer atmospheric observations critical to air pollution.

Figure 14 shows a case with nearly isothermal conditions in the lowest layers and lapse conditions above. The THERMASONDE™ results corresponded closely with those measured directly and, in general, this type of atmospheric stability condition presented no problem in remote probing.

Figure 15 shows what sometimes happens when there is a low-level elevated inversion and ground effects mask the lowest layer lapse conditions. Under these conditions and using a translation scheme based on lapse profile applicable heights, the THERMASONDE™ shows the lowest layers as being isothermal and indicates the height of the inversion to be slightly below that measured with the radiosonde.

Figure 16 shows that when an elevated inversion is at a much higher level

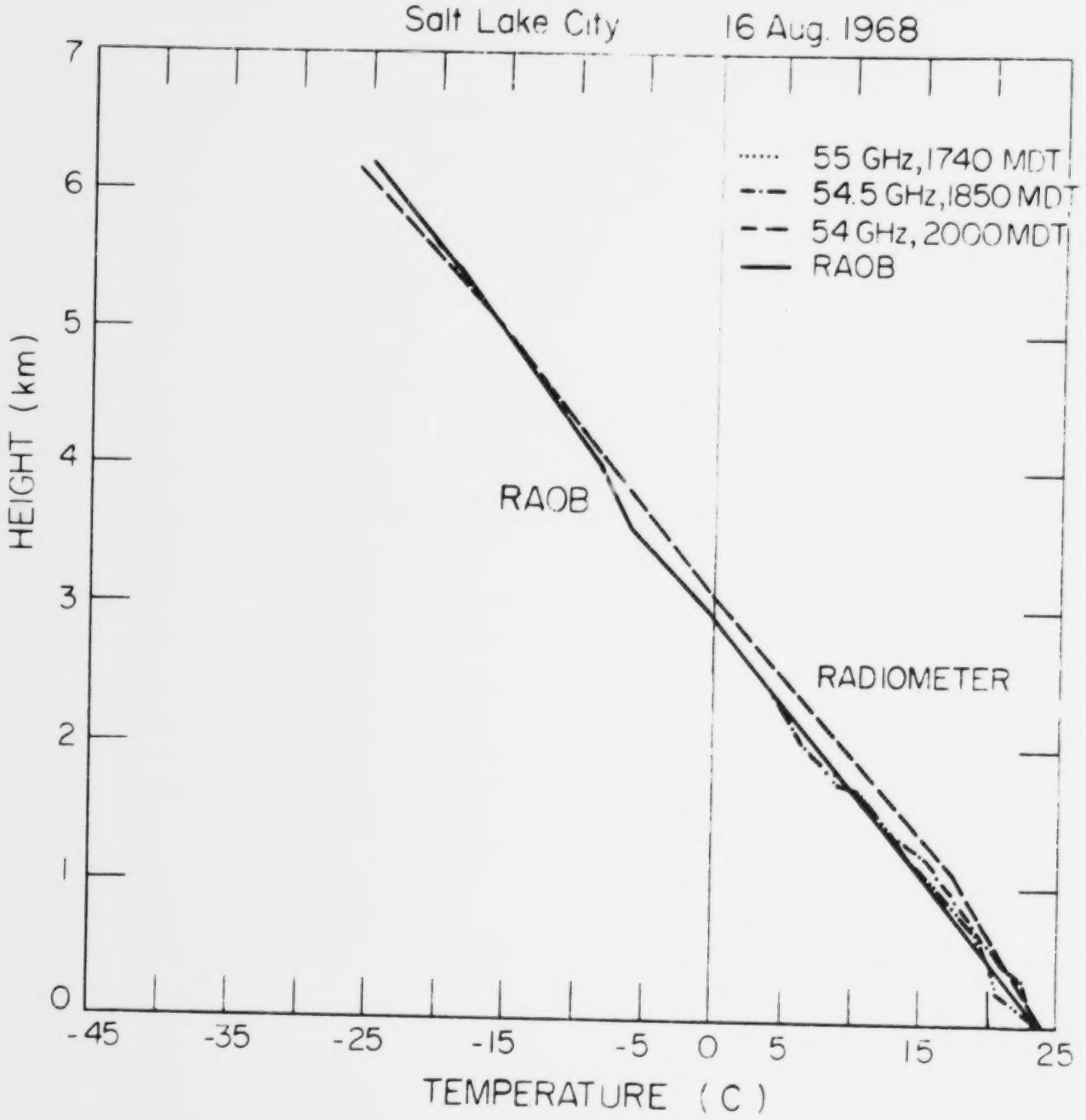

FIG. 12 Comparison of measured radiometric data at three frequencies with on-site RAOB data during lapse conditions.

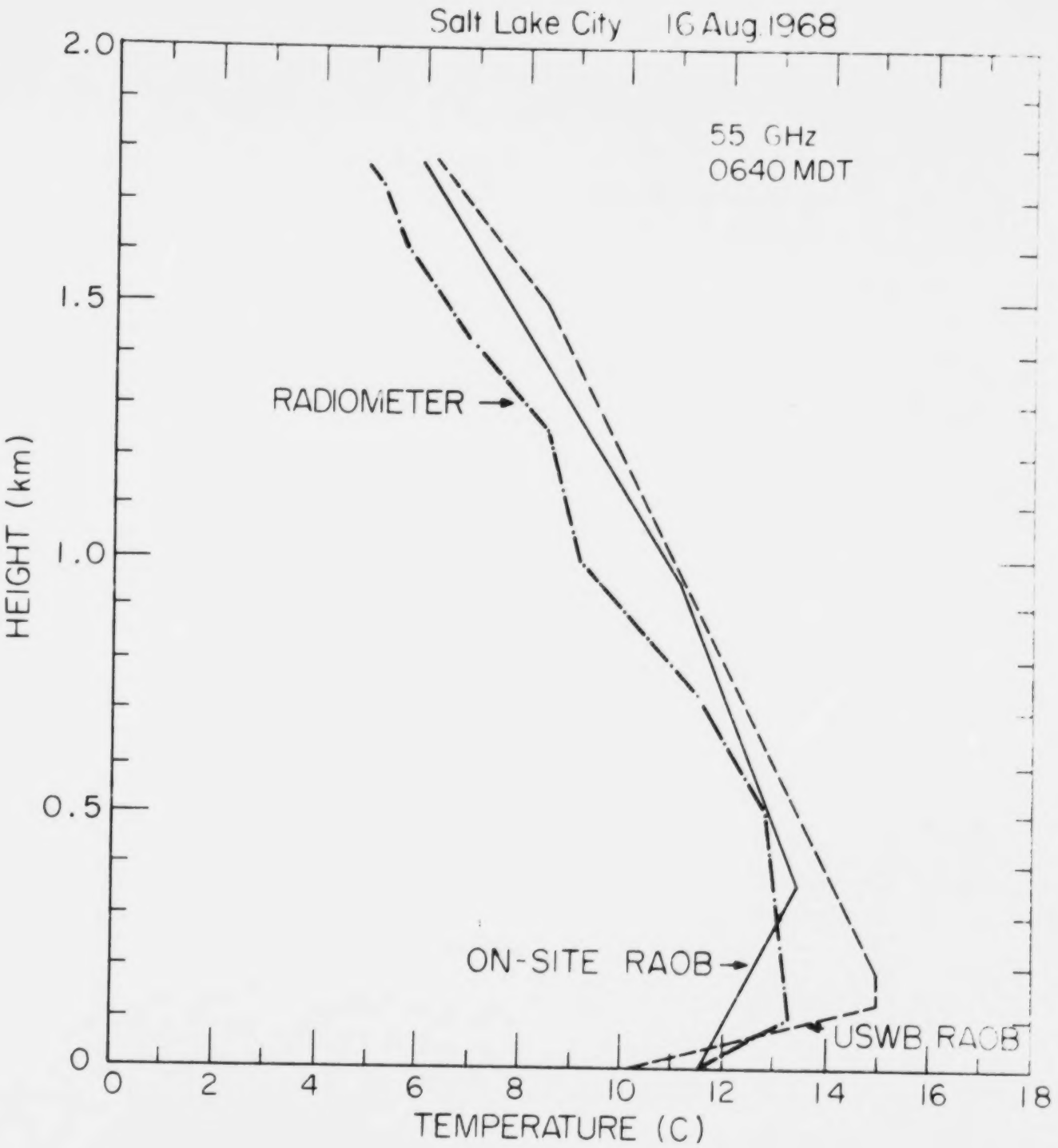

FIG. 13 Comparison of measured radiometric data with on-site and nearby USWB RAOB data during a ground inversion.

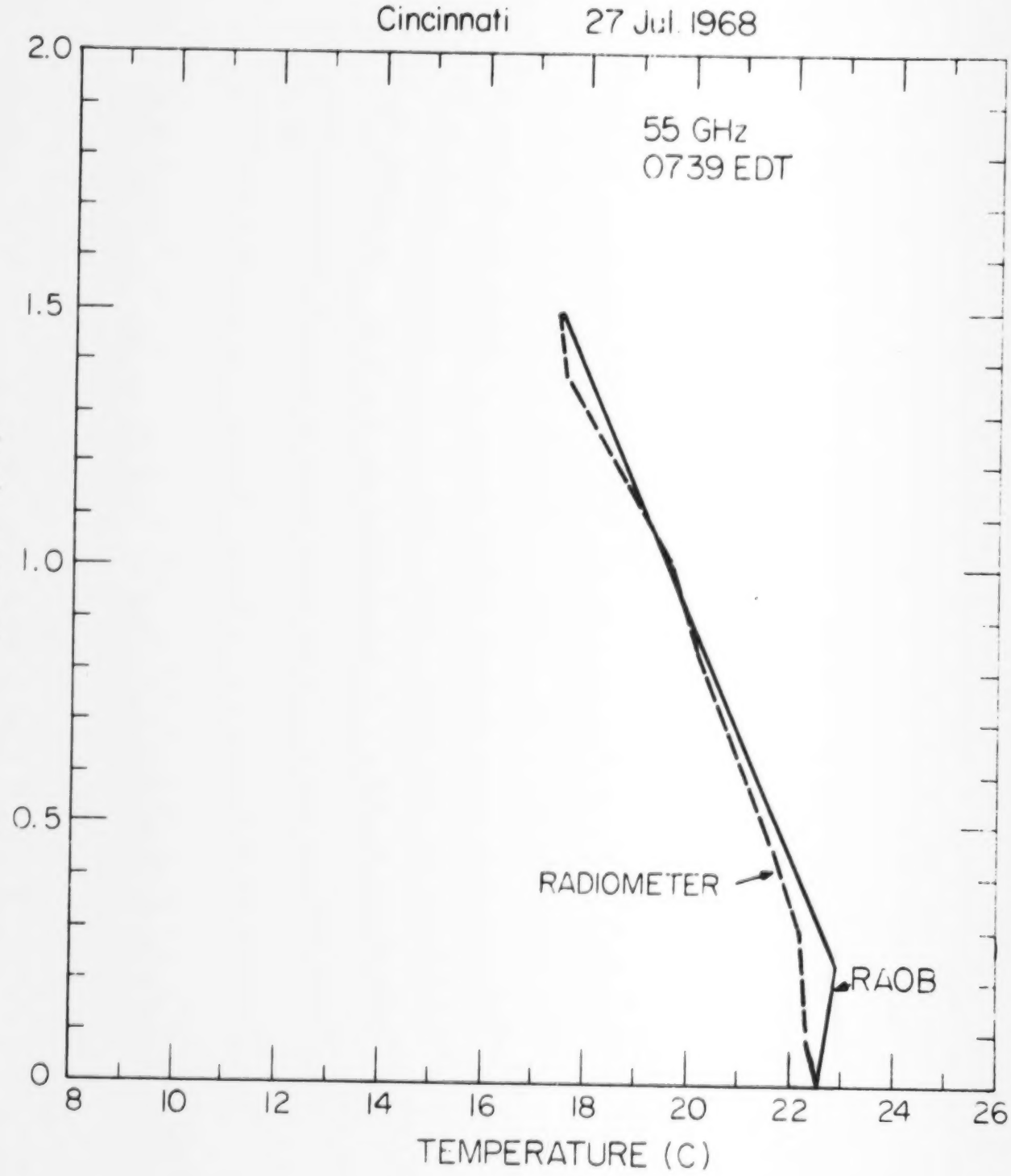

FIG. 14 Comparison of measured radiometric data with RAOB data during a nearly isothermal ground inversion.

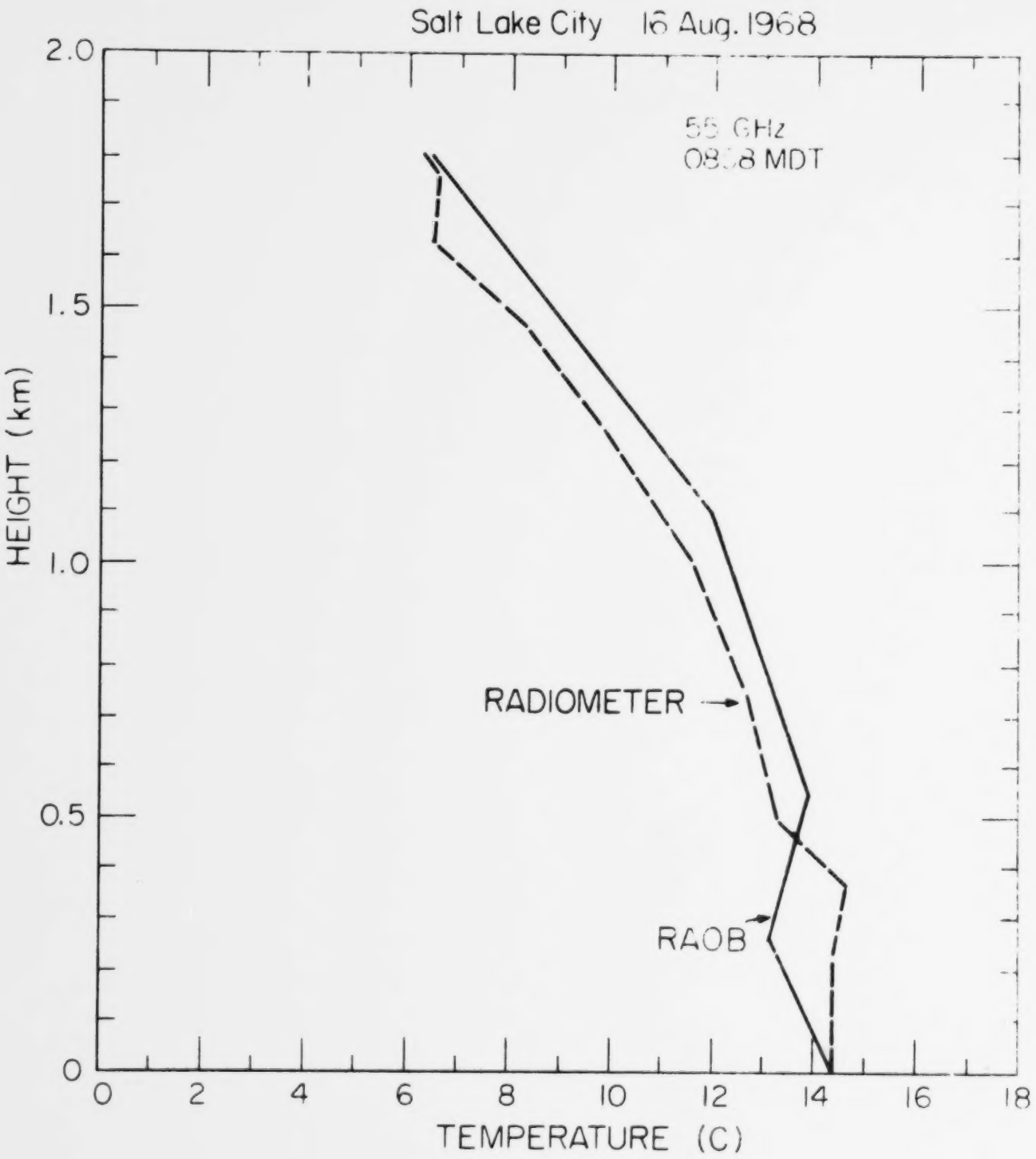

FIG. 15 Comparison of measured radiometric data with RAOB data during a low-elevated inversion when ground effects influence the radiometric signal.

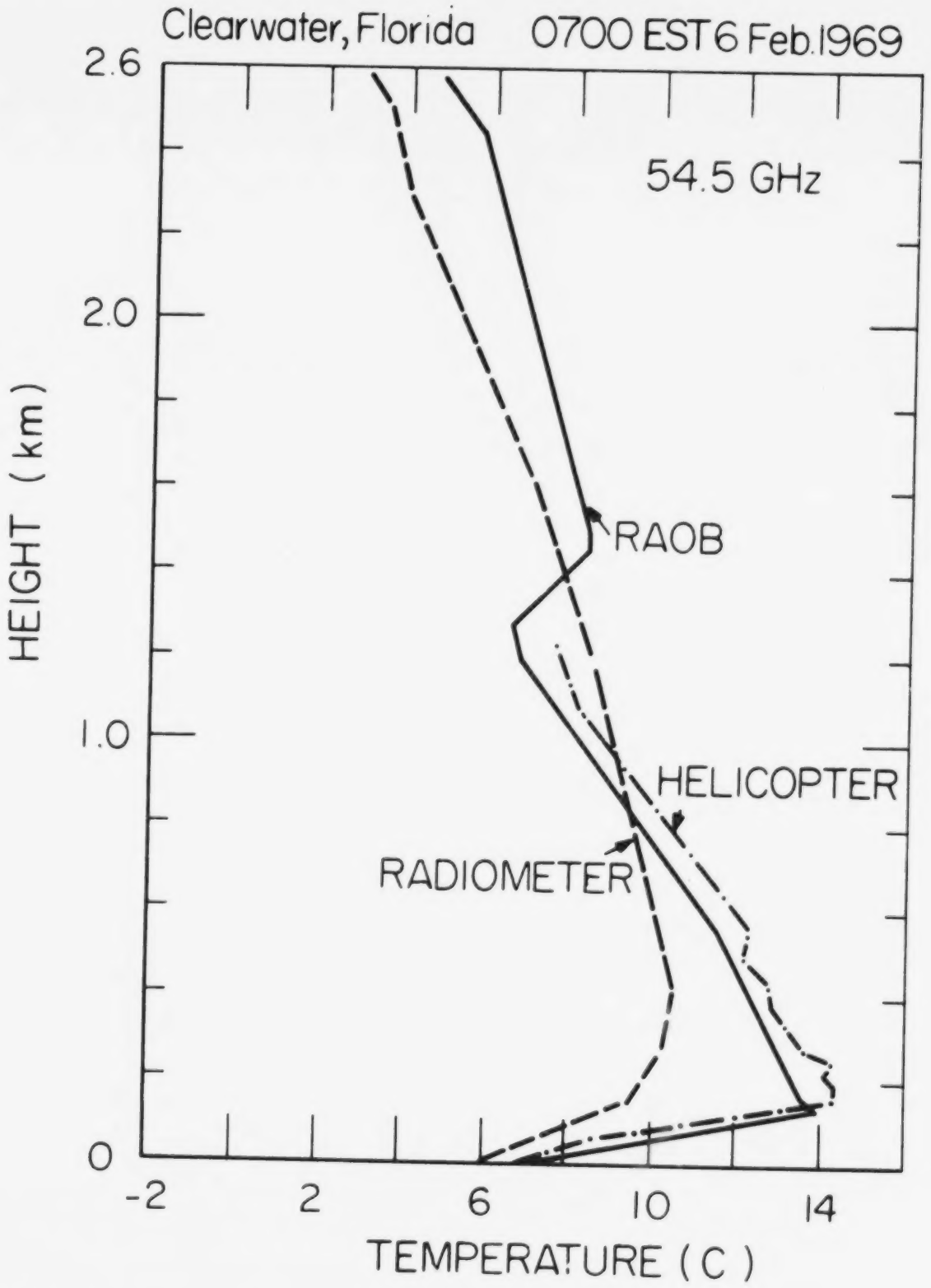

FIG. 16 Comparison of measured radiometric data with RAOB and helicopter data during both ground and elevated inversions.

(in this case about a mile high) this remote probing technique smooths out that elevated inversion, whereas the height of the ground inversion and the radiometric deflection corresponds with that measured by the RAOB and also by an instrumented helicopter.

Within the Radiometric THERMASONDE™ is an integrating circuit which smooths out the small-scale random noise fluctuations. This integrator has a time constant (or integrating time) which may be varied by the operator, but mostly a 60-second integration time was used in the fixed-frequency angle scan mode of operation. As a consequence of the angle scanning and comparatively long integration time, the information received at one angle is remembered, in a sense, by the integrator and carried forward, then outputted at a small finite time later, by which time the THERMASONDE™ is pointing at a new angle. This effect also introduces a certain amount of smoothing and displacement in the profile.

The effects of the integrating circuit can be seen in Fig. 17. A slow scan rate of about 2° per minute was made at 54.5 GHz, first in an upward, then in a downward direction. The colder brightness temperatures at higher elevation angles are carried downward and outputted in the downward scan, giving a colder profile than when scanning upward. This same effect tends to smooth the deflections associated with the low-level ground inversion. Thus it appears that the best THERMASONDE™ deflection and correspondence with the RAOB and helicopter profile can be obtained with an upward scanning mode of operation.

Another factor that enters into the quality of the output is the rate at which the antenna is scanned. Figure 18 shows the difference between a slow and a fast upward scan under the same conditions and, as was expected, the fast upward scan produced greater smoothing in the profile. We have found that a scan rate between 3° and 4° per minute could be used without a serious degradation due to smoothing, which means that it takes approximately 20 to 30 minutes to complete a sounding through 90 degrees of elevation. In principle, as the noise level in the equipment is reduced the integration time can be shortened and a more rapid observation cycle time is possible. Also, using a simple scheme for translating the Radiometric THERMASONDE™ data it is

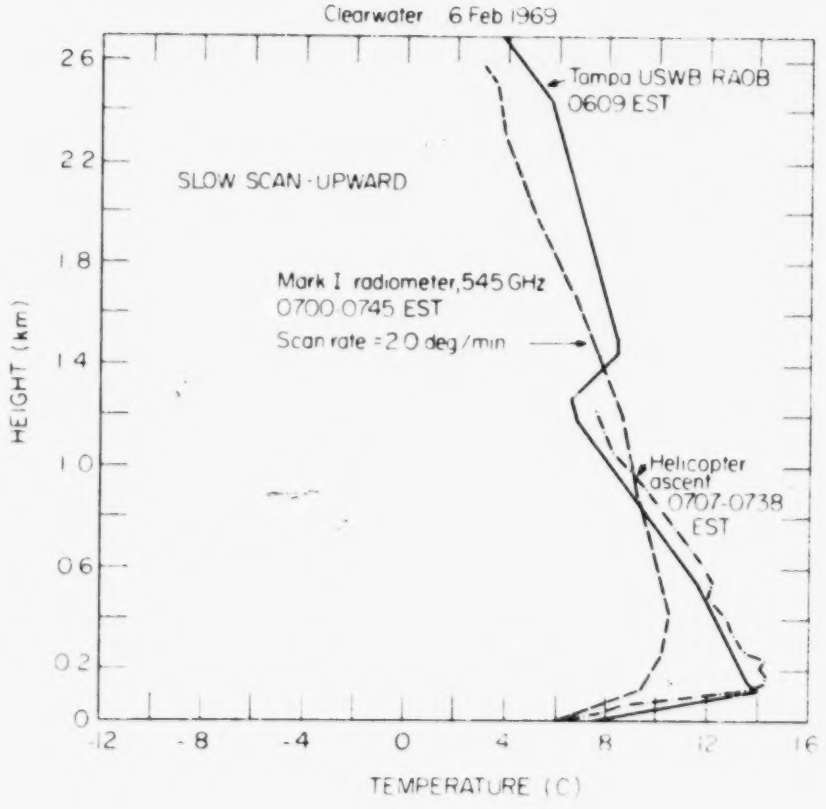

FIG. 17 Comparison of radiometric data obtained from upward and downward angle scans.

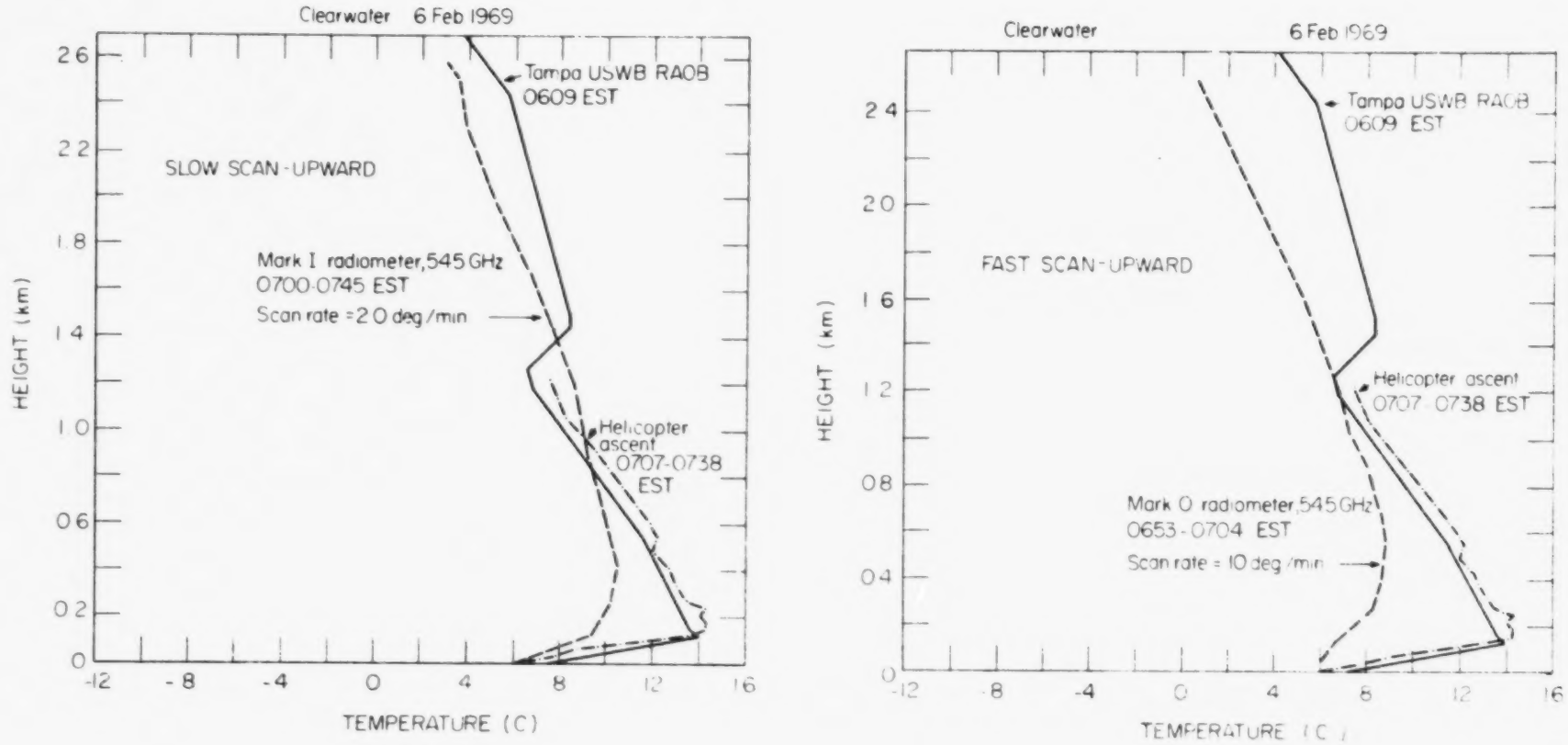

FIG. 18 Comparison of radiometric data obtained using fast and slow upward angle scanning rates.

possible to have an X-Y plotter continuously plot the temperature profile as the antenna scans from 0° to 90°.

Figure 19 shows a composite of three different profiles taken on three different days under 3 different stability conditions of the atmosphere. It can be clearly seen that the Radiometric THERMASONDE™ can distinguish between and provide for a good measure of unstable, neutral, and stable atmospheric conditions which are essential in the determination of the transport and flux characteristics within the air-earth interface.

Work is continuing in the development of both the hardware for obtaining the radiometric temperature data and the means for translating it into air temperature versus height, but it can be seen that even at this stage a great many operational requirements can be satisfied by the Radiometric THERMASONDE™ on nearly a real time basis.

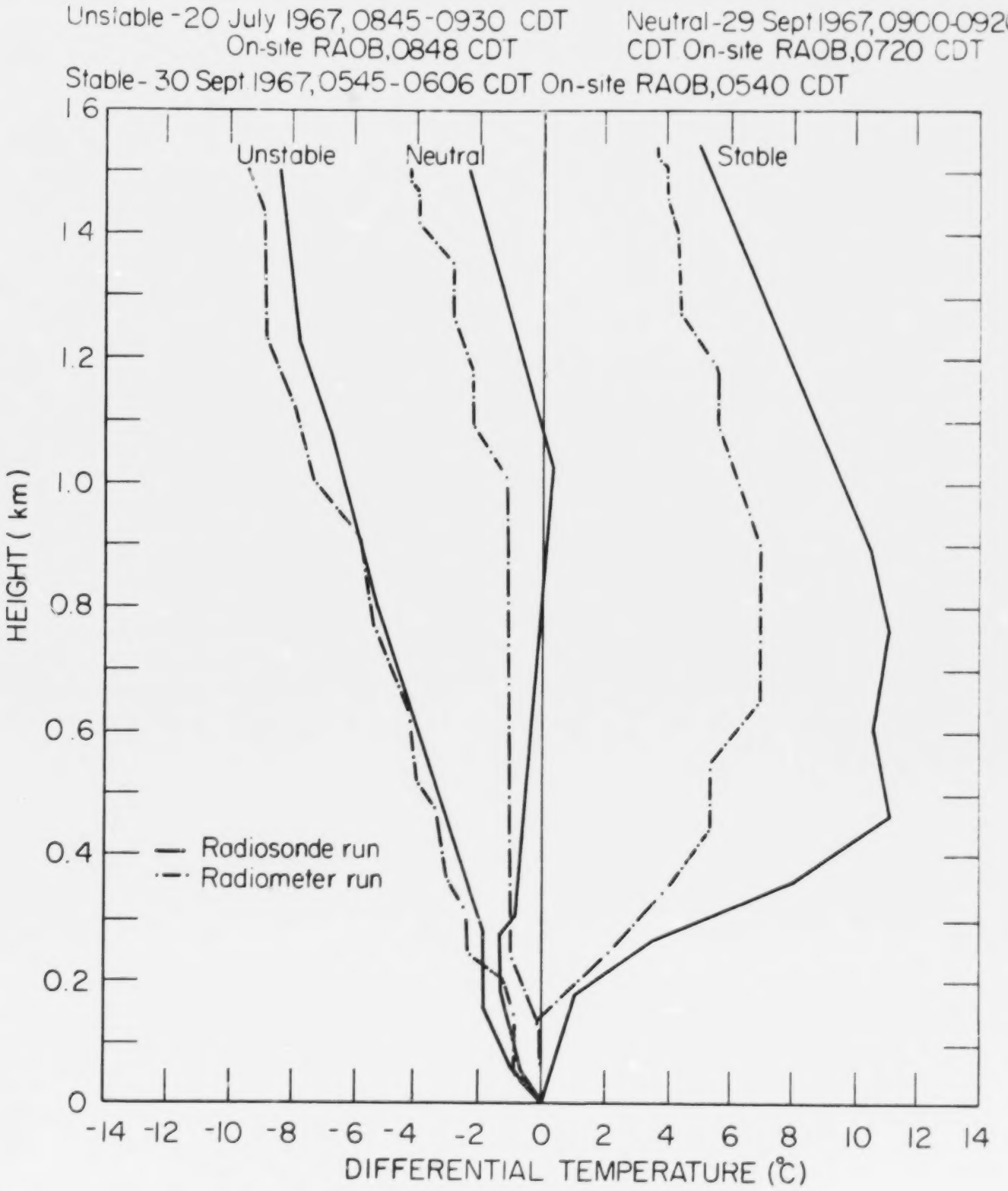

FIG. 19 Comparison of three different radiometric soundings with RAOB data taken during stable, unstable, and neutral or isothermal atmospheric conditions.

APPENDIX II

DEVELOPMENT OF APPLICABLE HEIGHT CONCEPT

BLANK PAGE

APPENDIX II

DEVELOPMENT OF APPLICABLE HEIGHT CONCEPT

The applicable height concept has been used throughout the report for directly translating radiometric brightness temperature observations into low-level temperature profile measurements. This appendix shows that the applicable height concept can be inferred from the radiometric brightness temperature equation if particular operational constraints are observed and some error tolerated in the resultant temperature profile. For a radiometer situated on the ground, operating in the millimeter wavelength region (5 mm) of the electromagnetic spectrum, the radiometric brightness temperature is given by

$$T_{B_\nu}(0) = \int_0^{s_e} T(s)\gamma_\nu(s) \exp\left[-\int_0^s \gamma_\nu(s')ds'\right] ds + T_c \exp\left[-\int_0^{s_e} \gamma_\nu(s)ds\right] \quad (1)$$

where

s = distance (km) along the axis of the antenna from the ground ($s=0$) to the end of the atmosphere ($s=s_e$).

$T(s)$ = ambient air temperature (K)

$\gamma_\nu(s)$ = absorption coefficient (Np/km)

ν = frequency

T_c = cold space temperature ($\approx$3 K)

Assuming that the atmosphere is horizontally stratified, then Eq. (1) can be expressed in terms of vertical temperatures and absorption coefficients as a function of elevation angle. Generally, the horizontal stratification is taken to be either spherical or planar, but for the present the particular choice of modeling need not be specified. Under the assumption of horizontal stratification, the radiometric brightness temperature is given by

$$T_{B_\nu}(\theta) = \int_0^{z_e} T(z)\gamma_\nu(z)\, g(\theta,z) \exp\left[-\int_0^z \gamma_\nu(z')\, g(\theta,z)dz'\right] dz$$

$$+ T_c \exp\left[-\int_0^{z_e} \gamma_\nu(z)\, g(\theta,z)dz\right] \qquad (2)$$

where

z = vertical height (km) measured from the ground ($z=0$) to the end of the atmosphere ($z=z_e$).

θ = elevation angle

$g(\theta,z)$ = functional relationship between vertical height and distance introduced under the assumption of horizontal stratification of the atmosphere.

The applicable height concept resulted from the investigation of the transmissivity function and its derivative, which are respectively given by

$$\tau_\nu(\theta,z) = \exp\left[-\int_0^{z} \gamma_\nu(z')\, g(\theta,z')dz\right] \qquad (3)$$

and

$$\frac{d\tau_\nu(\theta,z)}{dz} = -\gamma_\nu(z)\, g(\theta,z) \exp\left[-\int_0^{z} \gamma_\nu(z')\, g(\theta,z')dz'\right] \qquad (4)$$

where z is any height in the atmosphere and angle is considered a parameter. By substituting the above equations into Eq. (2), it is immediately seen that the derivative of the transmissivity function (often called weighting function) determines the contribution of the ambient air temperature at any height to the total radiometric brightness temperature observed at a given frequency and angle combination, vis

$$T_{B_\nu}(\theta) = \int_0^{z_e} T(z)\left(-\frac{d\tau_\nu(\theta,z)}{dz}\right)dz + T_c\,\tau_\nu(\theta,z_e)\,. \qquad (5)$$

For frequencies between 50 and 60 GHz, the above equation can be further simplified in that it is not necessary to integrate to the end of the atmos-

phere in order to obtain an accurate calculation of the radiometric brightness temperature. Table I shows the transmissivity values for frequencies between 50 and 60 GHz at an elevation angle of 90° for pressure values less than 10 mb. These transmissivity values were calculated for a summer, Salt Lake City profile where the surface pressure was 868 mb. This is pointed out because at most stations the surface pressure is generally higher and, therefore, the height of the pressure levels (also given in Table I) would be greater so that the transmissivity values would be even smaller (all other things (ν, T(z), etc.) being equal).

TABLE I

		TRANSMISSIVITY VALUES				
	Pres.(mb) =	10	5	1	.5	.1
	Height (Km) =	30.3	35.2	47.6	53.2	65.0
Freq. (GHz) =	50.0	.75487	.75482	.75480	.75480	.75480
	51.0	.68280	.68252	.68218	.68214	.68213
	52.0	.55610	.55570	.55545	.55544	.55544
	53.0	.33501	.33469	.33454	.33454	.33453
	54.0	.09370	.09355	.09349	.09349	.09349
	54.5	.03017	.03011	.03008	.03008	.03008
	55.0	.00598	.00596	.00596	.00596	.00596
	55.5	.00060	.00059	.00059	.00059	.00059
	56-60	.00000	.00000	.00000	.00000	.00000

From Table I it can be seen that the change in transmissivity over the 10 mb to .1 mb region is small; consequently, the contribution from this region of the atmosphere is negligible. For example, if the mean temperature were 250 K over this region, then the contribution to the total brightness temperature measured at 54.5 GHz would be

$$250(\tau_\nu(10)-\tau_\nu(.1)) = 250(.00009) = .022K$$

From this it is apparent that the upper limit in Eq. (5) can be considered as the height of the 10 mb layer and that the value of the transmissivity determining the cold space contribution (2nd term on r.h.s.) can be regarded as that value which occurs at the 10 mb level, i.e.,

$$z_e = z(10 \text{ mb})$$

and

$$\tau_\nu(\theta, z_e) = \tau_\nu(\theta, z(10))$$

for all frequencies between 50 and 60 GHz. Restricting attention to the higher frequencies allows the elimination of the cold space contribution from Eq. (5) and the radiometric brightness temperature is then given only by

$$T_{B_\nu}(\theta) = \int_0^{z_e} T(z) \left(- \frac{d\tau_\nu(\theta, z)}{dz} \right) dz \qquad (6)$$

Since the integral of the weighting function (Eq. (4)) is always less than unity, it follows from Eq. (6) that the radiometric brightness temperature is always less than the maximum temperature that occurred in the temperature profile. This is illustrated by the following inequality

$$T_{B_\nu}(\theta) < \int_0^{z_e} T_{max} \left(- \frac{d\tau_\nu(\theta, z)}{dz} \right) dz = T_{max} \int_0^{z_e} \left(- \frac{d\tau_\nu(\theta, z)}{dz} \right) dz < T_{max}$$

where

$$T_{max} = \max \{T(z)\}$$

For the higher frequencies,

$$\int_0^{z_e} \left(- \frac{d\tau_\nu(\theta, z)}{dz} \right) dz \approx 1 \qquad (7)$$

and since no temperature profile is isothermal up to 10 mb,

$$T_{B_\nu}(\theta) \sim \int_0^{z_e} T_{min} \left(- \frac{d\tau_\nu(\theta,z)}{dz} \right) dz = T_{min} \int_0^{z_e} \left(- \frac{d\tau_\nu(\theta,z)}{dz} \right) dz \approx T_{min}$$

where

$$T_{min} = \min \{T(z)\}$$

Since the temperature function generally decreases with height in the troposphere, it is the warmer temperatures which contribute most significantly to the radiometric brightness temperature. It has been determined that for all realistic temperature profiles, frequencies at least as low as 54 GHz always satisfy the inequalities presented above. Therefore, for the frequencies that have been considered, it is always true that

$$T_{min} < T_{B_\nu}(\theta) < T_{max} \qquad (8)$$

Combining the above statement with the fact that the temperature profile is continuous (at least piecewise), it can be stated that there always exists a height where $T_{B_\nu}(\theta) = T(z)$.

It is now established that the radiometric brightness temperature is indeed a measure of the ambient air temperature at some height in the atmosphere. No real significance can be attached to this result unless the height at which the radiometric brightness temperature applies has some degree of stability. In order to establish the stability of the applicable height, it is necessary first to establish the stability of the weighting function. Table II presents transmissivity values computed for two significantly different temperature profiles representing typical summer and winter conditions. The transmissivity values for these profiles are for a frequency of 54.5 GHz and angles of 90 and 30 degrees elevation. Both profiles had the same surface pressure, but the temperature profiles themselves were significantly different, as illustrated by the surface temperatures 297 K and 276 K, respectively, for summer and winter conditions. The transmissivity function is dependent upon

TABLE II

ν = 54.5 GHz	$\tau_\nu(90, z_i)$		$\tau_\nu(30, z_i)$	
HEIGHT (km)	WINTER	SUMMER	WINTER	SUMMER
0.0	1.0	1.0	1.0	1.0
.25	.8410	.8404	.7065	.7054
.50	.7108	.7096	.5050	.5029
.75	.6049	.6039	.3659	.3645
1.00	.5182	.516	.2687	.2672
1.50	.3871	.3858	.1605	.1497
2.00	.2964	.2941	.0899	.0868
2.50	.2318	.2284	.0051	.0527
3.00	.1844	.1807	.0346	.0341
4.00	.1222	.1208	.0152	.0150
5.00	.0867	.0840	.0077	.0072
8.00	.0401	.0386	.0016	.0015
12.00	.0230	.0211	.0005	.0005
17.00	.0172	.0153	.0003	.0002
23.00	.0156	.0137	.0003	.0002
30.00	.0153	.0133	.0002	.0002

temperature, since the absorption coefficient is; but from Table II it is apparent that large temperature differences cause only small differences in the transmissivity function.

It should be noted that the fluctuations in the transmissivity function are not entirely due to temperature changes, since the absorption coefficient is also dependent upon the water vapor profile. For the previous summer and winter profiles presented here, normal moisture distributions were used for their respective seasons. However, the water vapor contribution is only a small percentage of the total absorption at 54.5 GHz. Its effect on the radiometric brightness temperature is illustrated in Table III by computations using realistic, saturated, and totally dry moisture profiles corresponding to

the same temperature profile.

TABLE III

ν = 54.5 GHz	SATURATED	REALISTIC	DRY
$T_{B_\nu}(90)$	273.594	273.207	272.375
$T_{B_\nu}(30)$	283.069	282.972	282.611

It can be seen that at 54.5 GHz that the maximum difference in brightness temperature between a realistic water vapor profile and one that is either saturated or totally dry is less than 1 K. This error is even smaller for the higher frequencies.

Since it is actually the derivative of the transmissivity function that determines the contribution of the temperature profile over different height intervals, differential transmissivity values have been calculated from Table II and are presented in Table IV. This table shows that the percentage contribution from a height interval in the atmosphere is nearly constant for a given frequency and angle. These results establish that the weighting function is reasonably stable for significantly different temperature profiles. This result will now be used to establish the validity of the applicable height concept for lapse profiles.

TABLE IV

ν = 54.5 GHz Height Interval	$\tau_\nu(90,z_i) - \tau_\nu(90,z_{i+1})$		$\tau_\nu(30,z_1) - \tau_\nu(30,z_{i+1})$	
	WINTER	SUMMER	WINTER	SUMMER
0.0 - .25	.1590	.1596	.2935	.2946
.25 - .50	.1302	.1308	.2015	.2025
.50 - .75	.1059	.1057	.1391	.1384
.75 - 1.0	.0867	.0870	.0972	.0973
1.0 - 1.5	.1311	.1311	.1181	.1175
1.5 - 2.0	.0907	.0917	.0607	.0629
2.0 - 2.5	.0646	.0657	.0348	.0341
2.5 - 3.0	.0474	.0477	.0205	.0186
3.0 - 4.0	.0622	.0599	.0194	.0191
4.0 - 5.0	.0355	.0368	.0075	.0078
5.0 - 8.0	.0466	.0454	.0061	.0057
8.0 - 12.0	.0171	.0175	.0011	.0010
12.0 - 17.0	.0058	.0058	.0002	.0003
17.0 - 23.0	.0016	.0016	.0000	.0000
23.0 - 30.0	.0003	.0004	.0001	.0000

For a lapse profile, the temperature distribution can be defined as

$$T(z) = \begin{cases} mz+T_o & \text{for } 0 \le z \le z_1 \\ T(z) & \text{for } z_1 < z \le z_e \end{cases} \qquad (9)$$

where z_1 is the height of the tropopause, T_o is the surface temperature and m is the lapse rate. The temperature distribution between the height of the tropopause and 10 mb pressure level has not been specifically defined. Using Eq. (9) to define the temperature function in Eq. (6), the radiometric brightness temperature for this class of profiles would be given by

$$T_{B_\nu}(\theta) = \int_0^{z_1} (mz+T_o) \left(- \frac{d\tau_\nu(\theta,z)}{dz} \right) dz + \hat{T} \int_{z_1}^{z_e} \left(- \frac{d\tau_\nu(\theta,z)}{dz} \right) dz \qquad (10)$$

where the mean value theorem has been applied to the second term on the r.h.s. of the above equation. Expressing the mean value as a deviation from the surface temperature (i.e., $\hat{T} = T_o - A$) and simplifying, the above equation can be expressed as

$$T_{B_\nu}(\theta) = m \int_0^{z_1} z \left(- \frac{d\tau_\nu(\theta,z)}{dz} \right) dz + T_o \int_0^{z_e} \left(- \frac{d\tau_\nu(\theta,z)}{dz} \right) dz - A \int_{z_1}^{z_e} \left(- \frac{d\tau_\nu(\theta,z)}{dz} \right) dz \qquad (11)$$

The last two integrals can be evaluated directly; the first integral defines a weighted mean height $z_\nu(\theta)$ which depends upon the derivative of the transmittance function and satisfies $0 < z_\nu(\theta) < z_1$. Evaluating Eq. (11), the result is

$$T_{B_\nu}(\theta) = m\, z_\nu(\theta) + T_o - A \left[\tau_\nu(\theta,z_1) - \tau_\nu(\theta,z_e) \right] - T_o \tau_\nu(\theta,z_e) \qquad (12)$$

The last term in the above equation can either be eliminated, since the final transmissivity value is approximately zero for most angles, or considered a known quantity, since the final transmissivity value is nearly constant (for given frequency, angle, and surface pressure) and the surface temperature is known. It is apparent that Eq. (12) combined with Eq. (9) states

$$T_{B_\nu}(\theta) = T(z_\nu(\theta)) + \varepsilon_\nu(\theta) \qquad (13)$$

where

$$\varepsilon_\nu(\theta) = - A \left[\tau_\nu(\theta,z_1) - \tau_\nu(\theta,z_e) \right] \qquad (14)$$

The error term given in Eq. (14) is frequency-, angle-, and temperature-dependent. In order to estimate its value, it is necessary to decide upon a realistic value for A . If the average temperature between the height of the tropopause and the height of the 10 mb pressure level is about 230 K,

then the value of A is given by $A = T_o - 230$, since the mean temperature value $\hat{T}$ would be nearly equal to the average temperature in this linear region of the transmittance function. Choosing $A = 50$ K and the height of the tropopause as 12 km, the error term can be elevated from Table II for 54.5 GHz at both 90 and 30 degrees elevation

$$\varepsilon_\nu(90) = -50(\tau_\nu(90, 12) - \tau_\nu(90, 30))$$
$$= -50(.0230 - .0153) = -.385$$
$$\varepsilon_\nu(30) = -50(\tau_\nu(30, 12) - \tau_\nu(30, 30))$$
$$= -50(.0005 - .0002) = -.015$$

The above computations show that the errors are, in general, tolerable and that they are strongly dependent upon angle. It has now been established that for lapse conditions the radiometric brightness temperatures are reasonably accurate measures of the ambient air temperatures at specific heights; and since it has already been established that the weighting function is nearly invariant, it can be concluded that these heights are also nearly invariant. It is for this reason that they have been termed applicable heights.

The invariance of the weighting function and the applicable height has been established for a given frequency, angle, and surface pressure. If these parameters are varied, then there is an effect upon the applicable height. Section III discusses these effects as well as refinements to the basic technique introduced by considering the basic climatological differences which occur at various locations within a given season. Section III also discusses possible refinements to the applicable height concept when it is applied to other than lapse profiles.